UNESP - Universidade Estadual Paulista
"Júlio de Mesquita Filho"
Faculdade de Odontologia de Araraquara

Ester Alves Ferreira Bordini

Engenharia tecidual e biotecnologia aplicadas no desenvolvimento de scaffolds multifuncionais para estimular o reparo do complexo dentina-polpa

Araraquara
2021

UNESP - Universidade Estadual Paulista
"Júlio de Mesquita Filho"
Faculdade de Odontologia de Araraquara

Ester Alves Ferreira Bordini

Engenharia tecidual e biotecnologia aplicadas no desenvolvimento de scaffolds multifuncionais para estimular o reparo do complexo dentina-polpa

Tese apresentada ao Programa de Pós-graduação em Reabilitação Oral – Área de Prótese, da Faculdade de Odontologia de Araraquara, da Universidade Estadual Paulista, para obtenção do título de Doutor em Reabilitação Oral.

Orientador: Profa. Dra. Diana Gabriela Soares dos Passos

Araraquara
2021

B729e

Bordini, Ester Alves Ferreira
Engenharia tecidual e biotecnologia aplicadas no desenvolvimento de scaffolds multifuncionais para estimular o reparo do complexo dentina-polpa / Ester Alves Ferreira Bordini. -- Araraquara, 2021
115 p.

Tese (doutorado) - Universidade Estadual Paulista (Unesp), Faculdade de Odontologia, Araraquara
Orientadora: Diana Gabriela Soares dos Passos

1. Medicina Regenerativa. 2. Engenharia Tecidual. 3. Dentina. I. Título.

Sistema de geração automática de fichas catalográficas da Unesp. Biblioteca da Faculdade de Odontologia, Araraquara. Dados fornecidos pelo autor(a).

Ester Alves Ferreira Bordini

Engenharia tecidual e biotecnologia aplicadas no desenvolvimento de scaffolds multifuncionais para estimular o reparo do complexo dentina-polpa

Comissão Julgadora

Tese para obtenção do grau de Doutor

Presidente e Orientador: Profa. Dra. Diana Gabriela Soares dos Passos
2º Examinador: Prof. Dr. Carlos Alberto de Souza Costa
3º Examinador: Profa. Dra. Débora Lopes Salles Scheffel
4º Examinador: Prof. Dr. Juliano Milanezi de Almeida
5º Examinador: Prof. Dr. Rodrigo Cardoso de Oliveira

Araraquara, 02 de fevereiro de 2021.

DADOS CURRICULARES

Ester Alves Ferreira Bordini

NASCIMENTO	17 de maio de 1991 Taquaritinga – SP
FILIAÇÃO	Neuclair Bordini Júnior Alessandra Henriqueta Alves Ferreira
2009-2013	Graduação em Odontologia pela Faculdade de Odontologia de Araraquara – FOAr/Unesp
2014-2016	Mestrado em Odontologia, Área de concentração em Biociências, Biomateriais e Ciências Forenses pela Faculdade de Odontologia de Araraquara – FOAr/Unesp
2018-2019	Doutorado em Reabilitação oral, Área de concentração em Prótese com Período Sanduíche pela University of Michigan, School of Dentistry – UofM
2017-2017	Estágio de docência em Patologia Bucal pela Faculdade de Odontologia de Araraquara – FOAr/Unesp
2017-2017	Estágio de docência em Prótese Parcial Removível II pela Faculdade de Odontologia de Araraquara – FOAr/Unesp
2018-2018	Estágio de docência em Prótese Total II pela Faculdade de Odontologia de Araraquara – FOAr/Unesp
2018-2018	Colaborador docente junto à disciplina de Engenharia Tecidual Aplicada à Odontologia, oferecida no programa de Pós-graduação em Reabilitação Oral da Faculdade de Odontologia de Araraquara – FOAr/Unesp

DEDICO ESTE TRABALHO...

À Deus,

Por não me desamparar e sempre ser meu sustento e minha provisão. Por preparar todos os meus caminhos e colocar as pessoas certas ao meu lado para percorrer e concluir esta jornada com maestria. Obrigada meu Deus por me capacitar mesmo em meio as provações. Sem Ti eu nada sou.

"Ó SENHOR, tua é a grandeza, o poder, a glória, a vitória e a majestade, porque tudo quanto há no céu e na terra a ti pertence". ***I Crônicas 29:11***

À minha mãe,

Por ser minha amiga e maior incentivadora. Você mais do que ninguém sempre acreditou em mim e esteve ao meu lado, me apoiando e me ouvindo com paciência, dizendo palavras sábias para me encorajar a ser forte e continuar lutando por meus objetivos. Saber que eu tenho você em minha vida traz acalento e felicidade ao coração. A mulher e profissional que eu sou hoje, dedico a você que não mediu esforços para que eu alcançasse minhas vitórias. A você todo o meu amor.

"Um sonho sonhado sozinho é um sonho. Um sonho sonhado junto é realidade".
Yoko Ono

AGRADECIMENTOS ESPECIAIS...

À minha orientadora Profa. Dra. Diana Gabriela Soares,

Obrigada por ser tão presente, companheira e por ter acreditado em meu potencial, me dando a oportunidade e privilégio de desenvolver grandes trabalhos ao seu lado. Você é exemplo de Professora e Pesquisadora competente e apaixonada pelo que faz, sendo inspiração para todos a sua volta. Sua paciência, dedicação e humildade em me ensinar e me guiar nas melhores decisões para concluirmos este trabalho com êxito, foram fundamentais para o meu crescimento pessoal e profissional. A convivência com você me ensinou que ser forte, determinada e dedicada em nossa vida e trabalho, apenas nos faz colher bons frutos ao longo do caminho. A você minha eterna gratidão.

Ao querido Professor Carlos Alberto de Souza Costa,

Obrigada por ter me aberto as portas de seu laboratório, contribuindo não somente para minha formação profissional, mas também acadêmica. Através de você tive a oportunidade de iniciar uma das mais incríveis jornadas da minha fase como pesquisadora. Agradeço em especial por ter confiado a mim a coordenação de seu laboratório e o desenvolvimento do trabalho de pesquisa no LPEB. Com você aprendi muito sobre a responsabilidade que temos para com a comunidade científica e com nossos colegas de laboratório no desenvolvimento de um trabalho sério e honesto. Seus ensinamentos são fundamentais em minha vida. A você toda a minha admiração.

Ao Prof. Dr. Marco Cícero Bottino,

Obrigada por sua receptividade e acolhimento durante meu período de Doutorado Sanduíche realizado em seu laboratório. Seu apoio, colaboração, direcionamento e entusiasmo com a pesquisa, possibilitou o desenvolvimento de um trabalho extraordinário e inovador. A oportunidade que tive de trabalhar com você e seu grupo de pesquisa, foram sem dúvida uma das maiores experiências da minha vida. Obrigada por sua contribuição tão importante em minha vida como pesquisadora.

AGRADECIMENTOS...

A minha família,

Que sempre esteve ao meu lado, me trazendo bases sólidas para perseverar em meu caminho. Obrigada por estarem torcendo e vibrando comigo em cada passo e vitória alcançada. Sou muito feliz por ter todos vocês em minha vida.

Ao meu noivo Lucas,

Por cada gesto de carinho, amor e cuidado comigo. Independente da distância física que muitas vezes fomos submetidos, você sempre esteve ao meu lado para me apoiar e me trazer de volta a segurança que por vezes se ausentava. Em você encontrei meu porto seguro. Obrigada por ser esse companheiro incrível, amigo e especial, que faz dos meus dias mais felizes quando estou ao seu lado. Todo o seu apoio foi imprescindível para que eu finalizasse esta etapa da minha vida. Te amo!

A minha amiga Fernanda Balestrero Cassiano,

Obrigada pela oportunidade de te ajudar e contribuir para sua orientação como aluna de Iniciação científica e por agora podermos trabalhar juntas e dividirmos nossas experiências na área profissional. Tê-la junto a mim nestes anos auxiliou no meu amadurecimento e desenvolvimento como pessoa e pesquisadora. Obrigada também por sua amizade e companheirismo. Conte sempre comigo.

A Profa. Dra. Josimeri Hebling,

Por seus importantes posicionamentos e contribuições científicas que me incitaram a ter uma reflexão crítica durante o desenvolvimento desta Tese de Doutorado. Me considero felizarda por poder estar inserida no mesmo grupo de pesquisa desta exímia Pesquisadora. Obrigada por todo seu afeto e gentileza.

Ao Conselho Nacional de Desenvolvimento Científico e Tecnológico – CNPq,

Agradeço o apoio financeiro concedido por meio da Bolsa de Doutorado no período de Dezembro/2016 a Novembro/2017.

À FAPESP - Fundação de Amparo à Pesquisa do Estado de São Paulo,

Pelo apoio financeiro essencial para realização desta pesquisa por meio da concessão da Bolsa de Doutorado no período de Dezembro/2017 a Janeiro/2021 (Processo n. 2017/20181-0) e pela Bolsa Estágio de Pesquisa no Exterior-BEPE (Processo n. 2018/14257-7). Agradeço também pelo Auxílio à Pesquisa - Jovem Pesquisador (Processo n. 2016/15674-5), ao qual este trabalho está vinculado e que custeou todas as despesas para realização desta pesquisa.

À Faculdade de Odontologia de Araraquara, da Universidade Estadual Paulista "Júlio de Mesquita Filho" – Unesp,

Representada pelo digníssimo Diretor Prof. Dr. Edson Alves de Campos e pela Vice-Diretora Profa. Dra. Patrícia P. Nordi Sasso Garcia. Obrigada por desde a minha graduação terem feito da FOAr a minha casa. Todos estes anos nesta belíssima instituição trouxeram imenso aprendizado e crescimento. Meu muito obrigada!

À coordenação do Programa de Pós-graduação em Reabilitação Oral da Faculdade de Odontologia de Araraquara – Unesp,

Representada pela coordenadora Profa. Dra. Ana Cláudia Pavarina e vice-coordenadora Profa. Dra. Daniela Aparecida de Godoi Gonçalves. Gostaria de agradecer a vocês por todo apoio e auxílio sempre que necessário. Meu muito obrigada também a todos os professores do Programa, os quais foram essenciais para meu aprendizado e crescimento profissional.

Ao Departamento de Fisiologia e Patologia da Faculdade de Odontologia de Araraquara – Unesp,

Representado pelo chefe Prof. Dr. Eduardo Colombari e vice-chefe Prof. Dr. Carlos Alberto de Souza Costa, departamento no qual esta pesquisa foi desenvolvida.

Ao Laboratório de Patologia Experimental e Biomateriais, do Departamento de Fisiologia e Patologia da Faculdade de Odontologia de Araraquara – Unesp,

Representado pelo responsável Prof. Dr. Carlos Alberto de Souza Costa, cuja infraestrutura permitiu o desenvolvimento da maior parte das metodologias

empregadas nesta Tese de Doutorado, bem como meu desenvolvimento como pesquisadora.

Ao Assessor Renan César Palomino, do Escritório Regional de Apoio à Pesquisa e Internacionalização da Faculdade de Odontologia de Araraquara – Unesp,
Muito obrigada por sempre ser tão solícito, atencioso e disposto em sanar dúvidas e resolver as questões burocráticas envolvidas com as bolsas e auxílios da FAPESP. Sua ajuda foi fundamental.

Aos secretários José Alexandre Garcia e Cristiano Afonso Lamounier, da Sessão Técnica de Pós-graduação da Faculdade de Odontologia de Araraquara – Unesp,
Obrigada por serem tão prestativos em me atenderem e me ajudarem com muita atenção e dedicação.

À Profa. Dra. Débora Simões de Almeida Colombari, do Departamento de Fisiologia e Patologia, da Faculdade de Odontologia de Araraquara – Unesp,
Pela sua colaboração em disponibilizar o microscópio de fluorescência para realização de parte das análises que compõem esta Tese de Doutorado.

Aos técnicos José Antônio Sampaio Zuanon e Juliana Pirola Garcia, do Laboratório de Patologia do Departamento de Fisiologia e Patologia, da Faculdade de Odontologia de Araraquara – Unesp,
Por todo apoio em várias etapas para execução dessa pesquisa, sempre com muita alegria, paciência e disposição. A ajuda de vocês foi de extrema importância!

Aos colegas do Laboratório de Patologia Experimental e Biomateriais, da Faculdade de Odontologia de Araraquara – Unesp,
Agradeço pelos dias de convivência, trocas de experiências e muito companheirismo proporcionados por meus colegas Maria Luísa de Alencar e Silva Leite, Carla Caroline de Oliveira Duque, Uxua Ortecho Zuta, Giovana Anovazzi, Taísa Pansani, Fernanda Basso, Igor Soares, Rafael Antônio e Lays Gomes. Obrigada por tudo.

À Faculdade de Odontologia de Bauru, da Universidade de São Paulo – USP,
Representada pelo digníssimo Diretor Prof. Dr. Carlos Ferreira dos Santos e pelo Vice-Diretor Prof. Dr. Guilherme dos Reis Pereira Janson. Obrigada por terem aberto a porta desta incrível Instituição para que eu pudesse finalizar junto com a minha orientadora este trabalho.

Ao Laboratório de Cultura de Células e Engenharia Tecidual, do Centro Integrado de Pesquisas 3, da Faculdade de Odontologia de Bauru – USP,
Representado pela responsável Profa. Dra. Diana Gabriela Soares dos Passos, cuja organização da infraestrutura permitiu a finalização desta Tese de doutorado. Sem todo o seu apoio seria inviável a realização deste trabalho e a minha formação como pesquisadora.

Aos colegas do Laboratório de Cultura de Células e Engenharia Tecidual, da Faculdade de Odontologia de Bauru – USP,
Obrigada aos colegas de laboratório Fernanda Balestrero Cassiano, Marjorie de Oliveira Gallinari, Érika Bronze Uhle, Leandro Edgard Pacheco, Larissa Álamo e Camila Melo. A receptividade, alegria, amizade e leveza de vocês foram fundamentais para permitir a conclusão deste projeto. Obrigada pela convivência diária e momentos compartilhados. Vocês estão guardados em meu coração com muito carinho!

À todos,
Que direta ou indiretamente contribuíram para realização deste trabalho.

“O que vale na vida não é o ponto de partida e sim a caminhada. Caminhando e semeando, no fim terás o que colher”

Cora Coralina*

* Cora Coralina. Livro: Estrutura da língua Iatê, página 5. Autor: Geraldo Lapenda. Editora Universitária UFPE (278 páginas), 1965. ISBN-13: 978-8573152814.

Bordini EAF. Engenharia tecidual e biotecnologia aplicadas no desenvolvimento de scaffolds multifuncionais para estimular o reparo do complexo dentina-polpa [tese de doutorado]. Araraquara: Faculdade de Odontologia da UNESP; 2021.

RESUMO

Este trabalho teve por objetivo empregar diferentes técnicas de engenharia tecidual e biotecnologia para o desenvolvimento de scaffolds biomiméticos em associação com moléculas com reconhecido potencial osteogênico, visando seu emprego em estratégias cell-homing para reparo do complexo dentina-polpa. A primeira estratégia foi baseada na formulação de scaffolds de quitosana (CH) contendo hidróxido de cálcio (Ca) e beta-glicerofosfato de sódio (βGP), sendo realizada sua caracterização físico-química (MEV, EDS, FTIR, perda de massa, grau de porosidade) e biológica in vitro (ensaios de contato direto e extrato). O potencial cell-homing foi testado em um modelo experimental pulp-in-a-chip, onde os scaffolds sem células foram cultivados justapostos a uma cultura 3D das células pulpares humanas sob pressão intra-pulpar simulada. Viabilidade celular (Alamar blue e Live/Dead), adesão/espalhamento (F-actina), migração celular (transwell), deposição cálcio/matriz mineralizada (o-cresolftaleína/Alizarin red), atividade de ALP (ensaio ponto final) e expressão de DSP (imunofluorescência) foram avaliados (n=6; ANOVA/Tukey; α=5%). A partir da incorporação de Ca e βGP em uma formulação específica foi possível desenvolver um scaffold poroso de quitosana contendo nano-glóbulos de cálcio e fosfato depositados sobre sua superfície (CH-Ca-βGP), com grau de degradabilidade controlada. Este scaffold permitiu adequada interação com as células pulpares semeadas sobre os mesmos, apresentando efeito bioestimulador sobre a viabilidade e expressão de marcadores de diferenciação odontogênica (ALP e mineralização), bem como foi capaz de modular a quimiotaxia e diferenciação celular à distância, de forma significativamente superior às demais formulações. Finalmente, o ensaio pulp-in-a-chip demonstrou seu potencial em mobilizar células da cultura 3D para sua superfície, e induzir a expressão de DSP e matriz mineralizada na ausência de suplementação osteogênica. A segunda estratégia foi baseada na formulação de um hidrogel fotopolimerizável de gelatina e metacrilato de metila (GelMA), ao qual foram adicionados nanotubos de haloisita (HNT) contendo dexametasona (DEX), criando-se um sistema de liberação controlada. Estes hidrogéis foram caracterizados quanto a morfologia (MEV), composição física e química (MET/FTIR), degradação enzimática e resistência compressiva. A avaliação biológica foi realizada por meio do contato direto com células pulpares humanas de dentes decíduos (SHEDs), e em modelo de co-cultura a distância com transwells sob estímulo inflamatório (LPS). Foram realizadas análises de viabilidade celular (MTS), atividade de ALP (AnaSpec) e deposição de matriz mineralizada (Alizarin red). A biocompatibilidade foi avaliada por teste de implantação em subcutâneo de ratos, e o potencial bioativo em defeitos críticos em calvária (ANOVA Two-way/Tukey; α=5%). Foi possível desenvolver um hidrogel macro-poroso com adequado módulo de compressão e degradabilidade, capaz de promover liberação controlada da DEX. As células semeadas sobre a superfície do GelMA contendo 5% de HNT-DEX 10% e em modelo de co-cultura sob estímulo inflamatório apresentaram os maiores valores de atividade de ALP e deposição de matriz mineralizada. Este biomaterial não promoveu reação inflamatória tecidual, e foi capaz de aumentar intensamente a deposição óssea in vivo. A partir dos

resultados obtidos, podemos concluir que ambos os sistemas desenvolvidos são promissores para aplicação na regeneração dentinária, pois são capazes de interagir positivamente com as células pulpares e estimulam a expressão do fenótipo odontoblástico in vitro e in vivo.

Palavras-Chave: Medicina Regenerativa. Engenharia Tecidual. Dentina.

Bordini EAF. Tissue engineering and biotechnology applied to the development of multifunctional scaffolds to stimulate pulp-dentin complex repair [tese de doutorado]. Araraquara: Faculdade de Odontologia da UNESP; 2021.

ABSTRACT

The aim of this study was to apply tissue engineering and biotechnology techniques to develop biomimetic scaffolds in association with osteogenic molecules, as a cell-homing therapy for dentin regeneration. The first strategy was based on chitosan (CH) scaffolds containing calcium hydroxide (Ca) and beta-glycerophosphate (βGP). The scaffolds were subjected to physical-chemical (MEV, EDS, FTIR, degradation, porosity degree) and in vitro biological characterizations (direct contact and extract assay). Cell-homing potential was evaluated in a pulp-in-a-chip experimental model, in which cell-free scaffolds were cultivated in intimate contact with 3D cultures of dental pulp cells under simulated intra-pulpal pressure. Cell viability (Alamar blue and Live/Dead), adhesion/spread (F-actin), cell migration (transwell), calcium/mineralized matrix deposition (o-cresolftaleína/Alizarin red), ALP activity (end point assay) and DSP expression (immunofluorescence) were evaluated (n=6; ANOVA/Tukey; α=5%). The incorporation of Ca and βGP in a specific formulation created a stable porous chitosan scaffold containing calcium phosphate nano-globules on its surface (CH-Ca-βGP). This scaffold allowed adequate interaction with pulp cells and presented biostimulator effect on cell viability and odontogenic markers expression (ALP and mineralization) on cells seeded onto its surface and at distance, along with chemotactic potential. These cell effects were significantly higher than the other formulation. Finally, pulp-in-a-chip assay showed that CH-Ca-βGP mobilized cells from 3D culture to its surface, and induced DSP expression and mineralized matrix deposition in absence of osteogenic supplementation. In the second strategy, a photopolymerized hydrogel composed by gelatin and methyl metacrylate (GelMA) was associated with halloysite nanotubes (HNT) functionalized with dexamethasone (DEX), creating a drug delivery system. Hydrogel morphology (MEV), physical and chemical composition (MET, FTIR), enzymatic degradation and compressive strength were assessed. Biological analysis was performed by seeding stem cells from human exfoliated deciduous teeth (SHEDs) onto hydrogens, and by means of a co-culture model at distance using transwells under inflammatory stimulus (LPS). Cell viability (MTS), ALP activity (AnaSpec) and mineralized matrix deposition (Alizarin red) were determined. Hydrogel biocompatibility was evaluated after rat's subcutaneous implantation and the bioactive potential was investigated on critical calvarial defects (ANOVA Two-way/Tukey; α=5%). It was possible to create a porous hydrogel with adequate compressive modulus and degradability, capable to promote a controlled release of DEX. Cells seeded on GelMA surface containing 5% of HNT-DEX 10% and in co-culture model under inflammatory stimulus presented the highest values of ALP activity and mineralized matrix deposition. This biomaterial did not elicit inflammatory reaction and was capable to promote an intense increase on bone deposition in vivo. Based these results, it was possible conclude that both systems are promising for application in dentin regeneration, since they are capable to interact positively with pulp cells and also stimulate the odontoblastic phenotype expression in vitro and in vivo.

Keywords: Regenerative medicine. Tissue engineering. Dentin.

SUMÁRIO

1 INTRODUÇÃO.....17

2 PROPOSIÇÃO.....21

3 PUBLICAÇÕES.....22

3.1 Publicação 1 22

3.2 Publicação 2 68

4 CONSIDERAÇÕES FINAIS.....104

REFERÊNCIAS.....105

APÊNDICE A – SUPPLEMENTARY INFORMATION (PUBLICAÇÃO 2) 111

ANEXO A – COMPROVANTE ARTIGO EM REVISÃO NA DENTAL MATERIALS 113

ANEXO B – COMPROVANTE ARTIGO EM REVISÃO NA ACTA BIOMATERIALIA 114

ANEXO C – COMPROVANTE ARTIGO PUBLICADO CLINICAL ORAL INVESTIGATIONS.....115

1 INTRODUÇÃO

Há vários anos, diversos pesquisadores têm trabalhado no sentido de tentar compreender e então modular o processo de regeneração tecidual através do desenvolvimento de biomateriais que se adaptem ao microambiente biológico ao qual é inserido, de forma a induzir uma resposta celular específica e otimizar o processo de reparo local[1-3]. Assim, o emprego dos conceitos de Engenharia Tecidual e Biotecnologia têm apresentado amplo destaque dentro da Medicina e Odontologia contemporânea, sendo considerados como um campo multidisciplinar que integra princípios da ciência dos materiais, farmacologia, biologia celular e molecular, com o objetivo de solucionar problemas clínicos de forma mais efetiva[4-6]. Esta área de estudo baseia-se na interação de um biomaterial para atuar como substituto temporário da matriz extracelular (scaffold), células precursoras com potencial regenerativo e fatores biológicos para modulação da resposta celular[7-10].

A formulação de scaffolds biocompatíveis e bioativos, capazes de induzir a quimiotaxia das células tronco residentes do tecido pulpar (DPCs) para o sítio de regeneração, seguido de diferenciação odontoblástica e deposição de matriz extracelular mineralizada, é de grande interesse para a regeneração da dentina em casos de exposição pulpar em uma estratégia denominada cell-homing[11-13]. No capeamento pulpar direto (CPD), espera-se que a superfície do biomaterial em contato com a polpa participe efetivamente da formação de uma barreira de dentina por meio da indução do processo de regeneração tecidual mediado pelas DPCs. A estratégia cell-homing dentro da Engenharia Tecidual vem ganhando cada vez mais popularidade entre os pesquisadores devido aos aspectos éticos envolvidos, visto que esta terapia não envolve a implantação de células tronco em seres humanos, o que gera menor custo operacional e praticidade técnica, aproximando, assim, a experimentação laboratorial da aplicabilidade clínica[3,11,14]. Para tanto, o biomaterial a ser empregado nesta terapia deve promover quatro fenômenos biológicos básicos: 1) induzir a quimiotaxia das células precursoras; 2) permitir sua adesão e proliferação; 3) induzir sua diferenciação; e 4) ativar sua atividade secretória, resultando na deposição do novo tecido[11,15].

O processo de adesão e proliferação das células precursoras sobre a estrutura dos scaffolds pode ser otimizado por meio do controle da arquitetura e composição química dos biomateriais[16,17]. Dessa forma, os scaffolds formulados

devem apresentar composição química similar ao tecido alvo, e propriedades mecânicas adequadas, além de uma morfologia que estimule o espalhamento celular, com a consequente expressão de um fenótipo odontoblástico[18-20]. O emprego de polímeros naturais, como a quitosana e gelatina, tem ganhado popularidade devido a melhor biocompatibilidade com os tecidos circundantes desde que a composição química é similar à matriz extracelular in vivo[21-23]. A quitosana apresenta similaridade estrutural com as glicosaminoglicanas teciduais, o que proporciona integração com o tecido circundante, apresentando grupamentos amino e hidroxila que podem ser empregados para conjugação com drogas, fatores de crescimento e minerais de forma a aumentar sua bioatividade[24]. Já a gelatina é composta por colágeno desnaturado, o principal componente da matriz extracelular do tecido pulpar. Assim, scaffolds a base de gelatina são ricos em sequencias RGD (arginine-glycine-aspartic acid) aumentando as taxas de adesão e diferenciação celular[23,25,26].

A incorporação de fases minerais em scaffolds desenvolvidos para regeneração de tecidos mineralizados, tais como hidroxiapatita, beta-tri-calcio-fosfato, aluminato de cálcio, hidróxido de cálcio, dentre outros, aumenta a interação das células mesenquimais indiferenciadas com o substrato, devido à maior similaridade com a matriz extracelular natural, induzindo fortemente a expressão do fenótipo osteoblástico/odontoblástico, com consequente aumento na deposição de matriz mineralizada in vitro e in vivo[20,21,27-32,33]. Outra estratégia que apresenta resultados promissores é a associação destas fases minerais com moléculas empregadas na suplementação osteogênica in vitro, como o ácido ascórbico (AA) e o beta-glicero-fosfato (βGP), com o objetivo de criar um scaffold biomimético capaz de promover um microambiente pró-osteogênese. Estudos prévios demonstraram que esta associação leva a um aumento na diferenciação osteo/odontogênica e na deposição óssea in vivo, tendo sido demonstrado que o βGP em associação com cálcio aumenta de forma intensa o potencial mineralizador de scaffolds sintéticos e naturais[24-36]. Assim, o βGP tem sido considerado como uma molécula bioativa dentro da engenharia de tecidos mineralizados, com baixo custo, elevada estabilidade e efeito bioativo similar aos fatores de crescimento empregados para esta proposta terapêutica[36].

Outra forma de apresentação dos scaffolds com grande aplicabilidade para regeneração dentinária são os hidrogéis fotoativados, devido a sua fácil

manipulação e possibilidade de injeção direta na área de defeitos pequenos e irregulares. Dentre estes hidrogéis, o metacrilato de gelatina (GelMA) apresenta estrutura tridimensional macro-porosa rica em colágeno e sequências RGD (arginina-glicina-aspartato), o que proporciona maior adesão, espalhamento e proliferação celular sobre a estrutura do biomaterial[37]. Com a introdução de anidrido metacrílico à solução da gelatina, ocorre um aumento da estabilidade mecânica do hidrogel proporcionada por ligações moleculares insaturadas que se formam com os grupamentos amina livres presentes na molécula do polímero[22,38,39]. Além disso, este hidrogel pode ser polimerizado após a adição de fotoiniciadores, que quando ativados por luz UV ou LED se decompõe e produzem radicais livres que se ligam aos grupos metacrilatos, tornando-os materiais tridimensionalmente estáveis a temperatura ambiente[40]. Ainda, por ser um hidrogel composto por gelatina, quando submetido ao processo de hidrólise obtém-se como produto final o colágeno, principal componente da matriz extracelular da dentina[41]. Diversos estudos já demonstraram o potencial do GelMA como plataforma para proporcionar a regeneração óssea[42,43], do tecido pulpar[44,45] e de tecidos mineralizados vascularizados[37,46].

Outra versatilidade dos hidrogéis é a possibilidade de criar sistemas de liberação controlada de drogas, a partir da incorporação de componentes bioativos durante o processo de formulação dos biomateriais[37,42,45]. Assim, o uso de nanotubos torna-se promissor por estas estruturas proporcionarem um aumento na efetividade do sistema, devido à maior área de superfície, permitindo uma liberação lenta e gradual de baixas dosagens de drogas bioativas[47]. Dentre estas estruturas, os nanotubos de haloisita (HNTs) são interessantes desde que são oriundos de uma fonte natural e biocompatível, a argila[48]. Os HNTs são estruturas tubulares que ocorrem naturalmente, sendo formados internamente por lâminas de aluminosilicato de caulina, enroladas de 15 a 20 vezes gerando um diâmetro interno de cerca de 15 nm. Esta superfície interna constituída por alumina apresenta carga positiva, enquanto a superfície externa recoberta por sílica é carregada negativamente e apresenta diâmetros variando de 40-60 nm[47,49]. Esta morfologia e composição dos HNTs possibilita o carregamento de drogas distintas, com diferentes características de carga[50]. Devido ao seu comprimento (0.4-1.5 μm), suas partículas são facilmente dispersas em água ou polímeros polares, tornando-os um sistema altamente promissor para incorporação em hidrogéis, como o GelMA[51].

De acordo com a literatura, quando usados como sistema de liberação de drogas, os HNTs apresentam a habilidade de proteger a droga contra a degradação por enzimas, e proporcionam um aumento no tempo de liberação[47]. Diversos estudos já demonstraram que os HNTs não apresentam toxicidade sobre células humanas, apesar das mesmas serem capazes de penetrarem o ambiente intracelular. Além disso, esta característica se torna interessante por permitir o carregamento de drogas para o interior das células. A capacidade destas estruturas em promover a liberação de diversas drogas, aumentando a bioatividade de scaffolds já é bem consolidada na literatura[47,52-54].

Assim, surge o interesse em investigar o potencial dos HNTs funcionalizados com moléculas bioativas como uma estratégia para estimular a regeneração de tecidos mineralizados in situ. Dentro deste contexto, a dexametasona (DEX) apresenta-se como uma droga em potencial para regeneração de tecidos mineralizados, devido à mesma modular a expressão do fenótipo osteo/odontoblástico, promovendo aumento da deposição de matriz mineralizada[55-58]. A DEX é um corticosteroide sintético comumente utilizado no tratamento de condições inflamatórias, auxiliando no controle da dor e no direcionamento da resposta celular[55,58,59]. Entretanto, a administração local da DEX em altas concentrações pode ocasionar efeitos tóxicos sobre as células, interferindo negativamente na neo-formação tecidual[55]. Estudos prévios já demonstraram que é possível obter um padrão de liberação controlada da DEX por meio de sua incorporação no interior dos HNTs[60]; desta forma, o emprego desta tecnologia em combinação com GelMA surge como uma estratégia altamente interessante para a regeneração dentinária em casos de exposição pulpar.

Diante do exposto, o presente projeto de pesquisa propôs a aplicação de diferentes tecnologias no campo da engenharia tecidual para obter scaffolds bioativos com potencial para regeneração dentinária. Duas propostas foram abordadas visando a regeneração dentinária: (1) desenvolvimento de um scaffold poroso de quitosana em associação com hidróxido de cálcio e beta-glicerofosfato; e (2) formulação de um hidrogel fotopolimerizável de GelMA contendo um sistema de liberação controlada de dexametasona à base de HNTs. Desta forma, esta Tese de Doutorado será dividida em dois capítulos, de forma a abordar separadamente as duas estratégias desenvolvidas.

2 PROPOSIÇÃO

O objetivo do presente trabalho foi desenvolver biomateriais com potencial de aplicação para a reparação do complexo dentina-polpa dentro da estratégia cell-homing, por meio da associação de polímeros de origem natural (quitosana e gelatina) com fatores osteogênicos (hidróxido de cálcio, β-glicerofosfato e dexametasona).

2.1 Objetivos Específicos

Desenvolver um scaffold poroso de quitosana em associação com hidróxido de cálcio e β-glicerofosfato capaz de modular a quimiotaxia e diferenciação odontogênica de células pulpares humanas, levando a um aumento na sua capacidade de deposição de matriz mineralizada.

Desenvolver um hidrogel fotopolimerizável à base de metacrilato de gelatina associado a um sistema de liberação controlada de dexametasona, com potencial bioativo sobre células pulpares humanas de dentes decíduos em condição normal e sob estímulo inflamatório.

3 PUBLICAÇÕES

Esta tese de Doutorado foi dividida em duas publicações. A primeira foi resultante dos experimentos desenvolvidos no Brasil, sob orientação da Profa. Dra. Diana Soares (Processo FAPESP n. 2017/20181-0). A segunda publicação foi resultante dos experimentos desenvolvidos na Universidade de Michigan, sob orientação do Prof. Dr. Marco Bottino (Processo FAPESP n. 2018/14257-7).

3.1 Publicação 1

Chitosan in association with osteogenic factors as a cell-homing platform for dentin regeneration: analysis in a pulp-in-a-chip model

Bordini EAF[1]; Cassiano FB[2]; Bronze-Uhle ES[2]; Álamo L[2]; Hebling J[3]; de Souza Costa CA[1]; Soares DG[2].

[1]Department of Physiology and Pathology, Univ. Estadual Paulista – UNESP, Araraquara School of Dentistry, Araraquara, SP, Brazil. Humaitá Street, 1680, Araraquara, SP, Brazil. Postal code: 14801-903.

[2]Department of Operative Dentistry, Endodontics and Dental Materials, Sao Paulo University – USP, Bauru School of Dentistry, Bauru, SP, Brazil. Al. Dr. Octávio Pinheiro Brizola, 9-75, Bauru, SP, Brazil. Postal code: 17012-901.

[3]Department of Orthodontics and Pediatric Dentistry, Univ. Estadual Paulista – UNESP, Araraquara School of Dentistry, Araraquara, SP, Brazil. Humaitá Street, 1680, Araraquara, SP, Brazil. Postal code: 14801-903.

Corresponding Author:

Prof. Dr. Diana Gabriela Soares

Department of Operative Dentistry, Endodontics and Dental Materials

Sao Paulo University – USP, Bauru School of Dentistry - FOB

Al. Dr. Octavio Pinheiro Brizola, 9-75, Bauru, SP, Brazil. Zip code: 17012-901.

e-mail: soares.dg@usp.br

Artigo submetido na Dental Materials. Bordini EAF, Cassiano FB, Bronze-Uhle ES, Álamo L, Hebling J de Souza Costa CA, Soares DG. Chitosan in association with osteogenic factors as a cell-homing platform for dentin regeneration: analysis in a pulp-in-a-chip model. Dent. Mater. 2021. ANEXO A. (With Editor)

* Artigo formatado segundo as normas da Dental Materials

CHITOSAN IN ASSOCIATION WITH OSTEOGENIC FACTORS AS A CELL-HOMING PLATFORM FOR DENTIN REGENERATION: ANALYSIS IN A PULP-IN-A-CHIP MODEL

ABSTRACT

Objective: In this paper we proposed the association of β-glycrophosphate (βGP) and calcium-hydroxide with chitosan (CH), to formulate a porous bioactive scaffold suitable as a cell-homing platform for dentin regeneration.

Methods: Calcium hydroxide and βGP solutions were incorporated to chitosan to modulate scaffold architecture and composition by phase separation technique. Architecture, chemical composition and degradability were evaluated. Biological characterizations were performed by seeding dental pulp cells (DPCs) onto scaffolds, or by cultivating them in contact with the leachable components (extracts), to determinate cytocompatibility, and odontoblastic differentiation. Then, cell-free scaffolds were positioned in intimate contact with a 3D culture of DPCs in a pulp-in-a-chip platform under simulated pulp pressure. Cell mobilization and odontoblastic markers expression were evaluated. Deposition of mineralized matrix was assessed in direct contact with dentin, in absence of osteogenic factors.

Results: Incorporation of calcium hydroxide e βGP generated a stable porous chitosan scaffold containing Ca-P nanoglobular topography (CH-Ca-βGP), that favored cell viability, alkaline phosphatase activity and mineralized matrix deposition by cells seeded onto scaffold structure and at distance. Pulp-in-a-chip assay denoted its chemotactic and bioactive potential, as dentin sialoprotein positive DPCs from 3D culture adhered onto CH-Ca-βGP in a higher amount than plain chitosan. Higher deposition of mineralized matrix onto scaffold and surrounding dentin was also observed.

Conclusions: CH-Ca-βGP scaffold creates a microenvironment capable to mobilize DPCs migration towards its structure, harnessing the odontogenic potential and culminating with the expression of a highly mineralizing phenotype, key factors for cell-homing strategy.

1. INTRODUCTION

The advances on Regenerative Dentistry field have led to considerable research interest on development of innovative therapeutic strategies based on Tissue Engineering triad, that involves the presence of stem/progenitor cells, biomimetic scaffolds and signaling molecules [1,2,3]. Among the proposed strategies, stem cell-based therapy relies on the growth of exogenous stem cells onto scaffolds in laboratory atmosphere, followed by construct transplantation to stimulate local tissue genesis [3,4,5]. Nevertheless, the high cost, potential contamination, risks of immunogenicity and mutagenicity, raises concern for clinical translation [6,7,8]. Considering the self-renewal and multilineage ability of dental pulp stem cells, scaffold-based therapy offers new insights to achieve tissue reconstruction, as this strategy proposes application of cell-free scaffolds associated with bioactive signaling molecules capable to mobilize endogenous stem cells, in a process denominated cell-homing [9,5,10,11].

Our group has been proposed the use of chitosan as a suitable biopolymer to fabricate porous scaffolds for dentin cell-homing mediated regeneration. [12-16]. Chitosan has several biological and chemical properties that allows simplistic and low-cost methods to fabricate scaffolds with variable forms, like porous sponges, biomembranes, nanofibers, and hydrogels [12,17-20]. Also, the amino and hydroxyl groups from chitosan allow conjugation with drugs, growth factors and minerals, creating effective release systems and biomimetic structures [21,16]. The structural similarity with glycosaminoglycans (GAGs) favors wound healing with minimal immune response, attracting host proteoglycans for tissue interaction [22]. The cationic nature has been related with interesting biological functions, as hemostasis, antimicrobial activity, mucoadhesiveness and osteoconductiveness [23]. Finally,

chitosan is degradable by lysozyme, leaching mostly amino sugars that exerts no toxicity and are incorporated into metabolic pathways [24]. Biological compatibility of chitosan in different architectures and formulations with dental pulp cells has been widely demonstrated by in vitro and in vivo studies [25-27,16,28].

Incorporation of inorganic particles, such as calcium and phosphate, on chitosan composition has been proposed as bioactive cue to promote cell mobilization and activation towards an osteo/odontoblastic phenotype [29,30]. Therefore, mineral-rich scaffolds would play a pivotal role to harness the differentiation potential of cells to ensure the success of in situ biomineralization with no need of growth factors [31,32]. Previously work have demonstrated that incorporation of a mineral phase on scaffold structure can also modulate tree-dimensional architecture and surface topography, depending on fabrication rote [33,12,14,16]. Soares et al. [16] described a strategy to modulate chitosan scaffolds porosity degree and pore interconnectivity by calcium-hydroxide dispersion incorporation on chitosan solution under vigorous stirring and gradual freezing, leading to a 3D micro-environment that allowed for cell mobilization throughout its structure, along with a controlled calcium release at bioactive dosages due to complexation into chitosan structure.

β-Glycerophosphate salt (βGP) has been used as osteogenic inductor, and as a modulator of chitosan-based hydrogel thermo-responsive gelation process [34]. Several studies have been carried out with chitosan-βGP thermo responsive hydrogels for several applications, including bone and dentin tissue engineering, in which βGP has been used to promote gelation process of chitosan at 37 ^{o}C [35-37]. More recently, incorporation of βGP on scaffolds has been considered as a leading strategy for mineralized tissue regeneration, since it would be possible to create an

osteogenic microenvironment capable to provide osteoconductive and osteoinductive signals, as it is used in vitro to formulate osteogenic medium [38-42]. Therefore, in this paper we proposed the association of βGP and calcium-hydroxide with chitosan, to formulate a porous biomaterial containing a precipitate of calcium and phosphate nanoglobules, capable of recapitulate the mechanisms related with in vivo dentinogeneses, as a cell-homing strategy for dentin regeneration.

2. MATERIALS AND METHODS

2.1 Selecting scaffolds composition

2.1.1 Scaffolds formulation

Chitosan powder of high molecular weight (CH; >75% deacetylated, 310-375 kDa, Sigma-Aldrich, St. Louis, MO, USA) was dissolved at room temperature in 2% (v/v) acetic acid solution (Labsynth, Diadema, SP, Brazil) to obtain a 1% (w/v) CH solution. Then, calcium hydroxide suspension (Ca; Labsynth) was prepared at 1% (w/v) in distilled water, followed by gradual incorporation in CH solution (1:2) remaining under magnetic stirring for 5 min (CH-Ca solution). This technique performed to organize porous architecture by bubbling effect, as described by Soares et al. [16]. Afterwards, highly concentrated β-glycerophosphate disodium aqueous solution (56 wt%; βGP, Sigma-Aldrich) was incorporated into CH and CH-Ca solution in different ratios (1:5 or 1:10) to induce precipitation of calcium and phosphate on chitosan surface. βGP concentration was based on previously formulations of thermo-responsive chitosan hydrogels which demonstrated cytocompatibility with dental pulp cells [35,37]. Phase separation technique was performed to get the foam scaffolds after casting prepared solutions in acrylic molds (25-mm diameter), and submitting then to gradual freeze at -20 °C for 4 h, -80 °C

overnight, followed by immersion in liquid nitrogen at -198 °C for 30 min. Finally, formulations were freeze-dried (Liotop L101, Liobras, São Carlos, SP, Brazil) overnight at -56 °C. Altogether, six groups were obtained at this phase: CH (control), CH-Ca, CH-βGP (5:1), CH-βGP (10:1), CH-Ca-βGP (5:1) and CH-Ca-βGP (10:1).

2.1.2. Scaffold cross-linker treatment and disinfection process

Cross-linking with glutaraldehyde vapor was performed to improve scaffolds stability and maintain architectural porosity as previously stablished [16]. Subsequently, scaffolds were immersed in 70% ethanol and submitted to vacuum for 30 min to remove internal air bubbles and to proceed the disinfection process. Then, biomaterials were distributed in 48-well plate (Corning®, New York, NY, USA) containing phosphate buffered saline (PBS; pH 7.4, Gibco®, Invitrogen™, Carlsbad, CA, USA) and they were washed twice to remove residual ethanol from samples. Scaffolds were incubated overnight at 37 °C and 5% CO_2 in α-MEM supplemented with 10% (v/v) fetal bovine serum, 1% penicillin-streptomycin and L-glutamine (Gibco®) in order to prepare the samples for in vitro biological analysis.

2.1.3 Cell viability

Dental pulp cells (DPCs) used in this study were obtained by enzymatic digestion from impacted third molars (male donor, 18-years old) as previously described by Soares et al. [13]. All procedures were in agreement with the Ethical Committee of Araraquara School of Dentistry, University Estadual Paulista – UNESP (CAAE 65455516.0.0000.5416). To evaluate the cytocompatibility of formulated materials, $1x10^5$ cells were seeded onto sterilized scaffolds [16] in 5 µl of medium, followed by incubation for 30 min at 37 °C and 5% CO_2 to allow cell adhesion in scaffolds

structures. The sets (scaffolds-DPCs) were then cultivated for 24 h in 500 µL α-MEM medium to perform the cell viability assay using Live/dead kit (Live/Dead® Viability/Cytotoxicity Kit; Invitrogen™). For this, biomaterials were washed with PBS (Gibco®) to neutralize the esterase activity from culture medium supplementation and were incubated for 30 min at room temperature in non-serum α-MEM containing 4 mM calcein AM (green fluorescence emission, viable cells) and 2 mM ethidium homodimer-1 (Eth-1; red fluorescence emission, dead cells). The presence of viable cells on scaffolds surface were examined in fluorescence microscope (EVOS FLoid Cell Imaging Station; Invitrogen™).

2.1.4 Structural scaffold evaluation

The morphology of scaffolds surfaces was assessed by scanning electron microscopy (SEM; JMS-6610V Scanning Microscope; JEOL, Tokyo, Japan). For this, samples were mounted on stubs with carbon tape and sputter-coated with gold. The analyzes were accomplished at an accelerating voltage of 15kV and magnifications from 200x and 1000x.

2.2 Physical/chemical scaffold characterization

2.2.1 Energy-dispersive X-ray spectroscopy (EDS)

The elemental composition of formulated scaffolds was evaluated by EDS analysis (FEI, Hillsboro, OR, USA) with samples mounted on stubs and sputter-coated with gold. The images were obtained at 15kV accelerating voltage and 1000x magnification. The dimensions of structures precipitated onto scaffolds surface was measured using the straight toolset from ImageJ software (National Institutes of Health - NIH; Bethesda, MD, USA).

2.2.2 Fourier-transform infrared spectroscopy (FTIR)

Chemical interactions between calcium hydroxide and βGP incorporated in chitosan polymeric structure were evaluated by FTIR spectroscopy analysis (Shimadzu FT-IR-8300, Shimadzu Corporation, Kyoto, Honshu, Japan). The samples were adapted in a diamond crystal (ATR - Smart Miracle™, Pike Technologies, Madison, WI, USA) and 32 scans were performed in a range spectral between 4000 a 400 cm^{-1} at spectral resolution of 4 cm^{-1}.

2.2.3 Physical characteristics of scaffold surface

Porosity degree and pore diameter was quantified on SEM images from scaffold surface by using threshold and straight tools of software ImageJ software (NIH). A total of 20 images of each scaffold were randomically selected (n=5), at 100x magnification.

2.2.4 In vitro degradation profile

In this experimental section, the in vitro degradability degree of crosslinked and non-crosslinked of selected formulations was carried out by weight loss measurement overtime. Samples (n=6) were distributed in 24-well plate (Corning®) and incubated in 1.5 mL of PBS (Gibco®) for 1 h. After this period, baseline wet weight was recorded. New measurements were performed once a week until complete 35 days, in an analytical scale (Mettler Toledo XS105 DualRange; Columbus, OH, USA). Scaffolds degradation pattern was calculated considering baseline as 100% wet mass.

2.3 In vitro effect of cell/scaffolds constructs – Direct contact assay

2.3.1 Cell culture morphology

The attachment of DPCs directly cultivated onto cross-linked CH, CH-Ca, CH-βGP, and CH-Ca-βGP scaffolds was evaluated up to 14 days by Live/dead staining (n=4). Also, cytoskeletal cell morphology was observed by F-actin fluorescence images. Cell/scaffold constructs (n=4) were fixed with 4% paraformaldehyde (PFA; Dinâmica, Indaiatuba, SP, Brazil), followed by PBS washing, cell membrane permeabilization with 0.1% Triton X-100 (Sigma-Aldrich) and 30-minute incubation with ActinRed™ 555 ReadyProbes™ Reagent (Invitrogen™) prepared in 2% bovine albumin serum (BSA; 1:40). The nuclei of cells were stained with SlowFade™ Diamond Antifade Mountant with DAPI (Invitrogen™) and images were acquired at 1, 7, and 14 days of cell culture (EVOS FLoid Cell Imaging Station; Invitrogen™).

2.3.2 Cell viability measurement

The cytocompatibility of scaffolds was investigated after 1, 7, 14 and 21 days of cells/scaffolds growth in complete basal α-MEM. At each time point, the analyzes were performed by fluorescence method, diluting Alamar blue reagent (Invitrogen™) in α-MEM serum-free (1:10) with consecutive sets of incubation for 3 h at 37 °C and 5% CO_2. Afterwards, the collected supernatants were submitted to a fluorescence microscope reader (540 nm excitation - 590 nm emission; Synergy H1, BioTek Instruments, Winooski, VT, USA). Data was normalized at 100% of cell viability for CH group (control) at each time-point.

2.3.3 Odontogenic potential of scaffolds

To evaluate the potential of scaffolds to induce the odontogenic differentiation of DPCs seeded onto material's surface, the cells/scaffolds constructs (n=8) were cultivated up to 21 days in osteogenic medium (complete α-MEM; 50 mM ascorbic acid; 10 mM β-glycerophosphate; Sigma-Aldrich). For alkaline phosphatase assay (ALP), cells were submitted to 0.1% sodium lauryl sulphate lysis buffer and then a colorimetric kit (Labtest, Lagoa Santa, MG, Brazil) containing monophosphate thymolphthalein was incorporated in the cell lysate and incubated for 15 min at 37 °C to detect the cell enzymatic activity by absorbance reader (Synergy H1) at 590 nm. In the same samples, total protein concentrations were obtained by Lowry/Folin-Ciocalteau reagent (Sigma-Aldrich) and calculated by a standard curve, which allowed the normalization of ALP activity results. The CH group was determined as 100% of ALP activity in each time-point.

Also, Alizarin red staining was used to confirm the potential of scaffolds to stimulate the differentiation of DPCs by deposition of mineralized matrix. The cells/scaffolds constructs (n=8) cultivated in osteogenic medium were washed with PBS, fixed in 70 % ethanol at 4 °C for 1 h, followed by PBS washing, and incubation for 15 min with Alizarin Red S staining solution (40 mM, pH 4.2; Sigma-Aldrich). Samples were washed with water to remove the overflow dye and were transferred to a tube containing cetylpyridinium chloride 10% (Sigma-Aldrich). Absorbance was measured at 570 nm (Synergy H1) and mineralized matrix deposition was calculated considering CH as 100% upon background extraction (scaffolds with no cells) from each sample.

2.4 In vitro cell response at distance – Extract assay

2.4.1 Indirect cytocompatibility of scaffolds constituents' compounds

To evaluate the effects of compounds released from scaffolds at distance, the scaffolds CH, CH-Ca, CH-βGP, and CH-Ca-βGP were incubated in complete α-MEM at 37 °C and 5% CO_2 up to 14 days to obtain the conditioned medium (extracts; n=6). DPCs (1.5 x 10^3 cells/well) were cultivated in 96-well plates (Corning®) and cultured in complete α-MEM at 37 °C and 5% CO_2 for 24 h. After that, basal medium of cells was replaced with the 24 h extracts and the medium was refreshed every 48 h to get new extracts applications. At 1, 3, 7 and 14 days, cell viability was determined by Alamar blue assay.

2.4.2 Calcium deposition

Calcium liquiform reagent (Labtest Diagnóstica, Lagoa Santa, MG, Brazil) was applied to detect the amount of calcium deposited by cells following 14 days treatment with extracts. Cells (n=6) were incubated overnight at 4 °C with hydrochloric acid 1N (HCl; Labsynth). The samples were homogenized and work reagent containing phthalein purple was added to interact with calcium released that was detected in a plate reader (Synergy H1) at 570 nm. Calcium concentration was calculated by means of a standard curve, and CH group was considered as 100% of calcium deposition.

2.4.3 Scaffolds chemotactic potential

Transwell assay was chosen to assess the potential of different scaffolds formulations to induce cell migration. For this, 24-well plates transwells (n=4; polyethylene membrane, 8-µm micropore; Corning®) were incubated with complete α-MEM at 37 °C for 2 h, and DPCs (2×10^4 cells/transwell) were seeded onto the upper compartment. After a 1-hour incubation period at 37 °C and 5% CO_2, the scaffolds were disposed in plate bottom followed by 24- and 48-hour incubation

period in 1mL of culture medium. The membranes were fixed in 70% ethanol, washed in deionized water, and cotton swabs were carefully applied in the upper transwell chamber to remove the non-migrated cells. DAPI reagent (Invitrogen™) was used to stain the nuclei of migrating cells on lower compartment and a fluorescence microscope (EVOS FLoid Cell Imaging Station; Invitrogen™) was used to acquire a total of 6 images *per* membrane (20x objective). The number of stained cells were counted using threshold tool of ImageJ software (NIH) and the mean values were submitted for statistical analysis.

2.5 Biomimetic assays

2.5.1 Pulp-in-a-chip system with simulated intra-pulpal pressure

The purpose of this experimental section was to mimic the application of cell-free scaffolds in direct contact with pulp tissue in the laboratory condition. For this, a tri-dimensional (3D) cell culture of DPCs was formulated with type I collagen (Corning®) dissolved in a basal α-MEM 10x concentrated (4:1) and neutralized with sodium hydroxide (5M; Labsynth) to reach pH 7.2. After incubation for 30 min at 37 °C and 5% CO_2, 1x10^5 DPCs were cultured onto the polymerized collagen matrix (6-mm diameter) and the set was cultivated for 48 h corresponding to cell growth period. Plain CH and CH-Ca-βGP scaffolds were adapted in the bottom of an acrylic mini-chamber (6 mm in diameter, 12 mm in height, and 250 µL in volume; 3DKube™, Kiyatec, Greenville, SC, USA) and 3D cell culture was overlapped in direct contact with materials. To simulate the intra-pulpal pressure, the chamber was closed, and the end tubing of the device was connected to a liquid column reservoir (15 cm.H_2O, i.e. 11 mmHg). Five milliliters of complete α-MEM were circulated every day in the system with the aim to promote cell oxygenation. The circuit was

cultivated at 37 °C and 5% CO_2 up to 14 days. Surfaces in inner contact with scaffolds and 3D culture were analyzed with respect to cell viability by Live/dead (scaffold and 3D culture) and Alamar blue (3D culture), such as previously described. The number of migrating cells in the scaffolds was counted 14 days after fixing the biomaterial in PFA 4% (Sigma-Aldrich) and incubating it with DAPI (Invitrogen™) for 15 min (ImageJ software - 4 images for each sample, n=4). Immunofluorescence staining was performed in scaffolds after fixing in PFA at 4 °C overnight and then incubating with the conjugated goat polyclonal DSP primary antibody (Santa Cruz Biotechnology; Dallas, TX, USA) at 1:50 dilution at 4 °C overnight. Thereafter, the samples were incubated for 1 h at room temperature with mouse anti-goat secondary antibody (Santa Cruz Biotechnology) at 1:1000 dilution, followed by DAPI nuclei staining (Invitrogen™) and fluorescence image capturing in EVOS FLoid microscope (Invitrogen™) with a 20x objective.

2.5.2 In situ dentin disc assay

Human dentin discs (1-mm thick and 8-mm diameter) were obtained from third molars (after consent approval from Ethical Committee of Araraquara School of Dentistry - CAAE 65455516.0.0000.5416). Then, a central perforation (1-mm thick and 5-mm diameter) was created with diamond bur and CH and CH-Ca-βGP scaffolds (1-mm thick and 6-mm diameter) were adapted. Thereafter, $1x10^5$ cells were seeded onto scaffolds, as previously described, and the set was incubated in basal α-MEM medium for 14 days. Deposition of mineralized matrix onto scaffold and dentin surfaces were quantified by Alizarin red assay.

2.6 Statistical analysis

The experiments were performed in triplicate in distinct moments. Data obtained were analyzed in Prism 8 software (GraphPad; San Diego, CA, USA) with t-student, One- or Two-way ANOVA followed by Tukey post hoc test to determine significant differences between groups. P-values of < 0.05 were considered statistically significant.

3. RESULTS

3.1 Scaffolds characterization and cell viability determination of initial formulations

SEM images revealed that incorporation of calcium hydroxide and βGP promoted alteration on surface topography and overall architecture of chitosan scaffolds, which affected the viability of DPCs seeded onto material´s surface (Figure 1a). Plain CH scaffolds presented a lamellar pore structure, whereas CH-Ca scaffold featured round and well distributed pore network. Both CH and CH-Ca scaffolds had a smooth surface and allowed the establishment of clusters of viable DPCs 24 h after cell seeding.

When βGP solution was added in CH and CH-Ca, it was possible to note pore disorganization. Irregular needle-like structures were observed on CH-βGP, and globular deposits were detected on CH-Ca-βGP. For both, CH and CH-Ca, incorporating βGP in a 5:1 ration caused more intense pore collapse, and also noticeable reduction on the number of viable cells clusters adhered to its surface. Therefore 10:1 CH/CH-Ca to βGP was selected for scaffolds formulation.

3.2 Physical/chemical characterization of selected scaffolds

3.2.1 Analysis of scaffolds chemical composition

High magnification SEM images and EDS graphs from each formulation are presented on Figure 1b. Plain CH scaffolds were essentially composed by carbon (C) and oxygen (O) elements, while in CH-Ca group occurred the addition of calcium (Ca). βGP incorporated CH and CH-Ca scaffolds displayed sodium and phosphate ions in its surface. Needle-like structures on CH-βGP had an average size of 6,18 μm. The Ca-P precipitate observed on CH-Ca-βGP was in around of 57 nm, being described as nanoglobules.

3.2.2 FTIR analysis

Figure 2a represents the FTIR spectra of CH, CH-Ca, CH-βGP and CH-Ca-βGP scaffolds. CH had the following characteristic bands, located at specific wavelengths at approximately: 3500-3100 cm^{-1} (-OH and –NH stretching), 2917 and 2871 cm^{-1} (asymmetric and symmetrical stretching of -C–H), 1654 cm^{-1} (relative to C=O stretching of amide I groups), 1637 and 1550 cm^{-1} (angular vibrations of -NH2 groups relative to amide II) and 1319 cm^{-1} (relative to -C-N stretching bands of amide III), 1404 and 1317cm^{-1} (assigned to -C-H and -OH deformations), 1377 cm^{-1} (-C-H angular deformations), 1058 - 1026 cm^{-1} (relative to symmetrical and asymmetric stretching vibrations of -C–O groups [(C–O–C)] and 983 cm^{-1} characteristic of the saccharide structure of chitosan. FTIR CH-Ca spectrum show marked displacement in the position and intensity change of characteristic chitosan bands. Significant changes in displacement are observed at 1637 cm^{-1} to 1603 cm^{-1}, 1550 cm^{-1} to 1529 cm^{-1} and on bands at 1408-1423 cm^{-1}, indicate alterations on relative stretching and bending vibrations of amides and amines chitosan scaffold. Also, the appearance of new absorption bands located in 1463 cm^{-1}, 1446 cm^{-1} and 1423 cm^{-1} and the reduction of bands in 1377 cm^{-1} and 1317 cm^{-1} confirming the complexation of

calcium ions in the amine (-NH2) and hydroxyl groups of chitosan structure, which are confirmed by the presence of bands related to the Ca-O and Ca-N bonds stretching located in the region of 670 -644 cm^{-1}.

βGP addition also causes major changes in the characteristic chitosan scaffold bands. FTIR spectrum of CH-βGP showed a strong decrease in the intensity of the bands referring to -CH2 groups stretching of chitosan located at 2920 cm^{-1} and 2868 cm^{-1}. In addition, a strong suppression of the characteristic amides I, II and III, related to symmetrical and asymmetric stretching of -NH2, -NHC=O and -C-N, located at 1690-1200 cm^{-1} and changes in the regions of 1100-700 cm^{-1}, referent to symmetrical and asymmetric stretching vibrations of -C–O groups. Bands with low intensity are observed at 1643 cm^{-1}, 1564 cm^{-1} and 1406 cm^{-1} wavelengths. Characteristic bands localized at 1075 cm^{-1} (relatives to P-O-C stretching), 1050 cm^{-1} (relatives to -PO4-2 stretching), 980 cm^{-1}, 937 cm^{-1}, 870 cm^{-1}, 780-750 cm^{-1} (relatives to -HPO4-2 presence and aliphatic stretching of P-O-C groups). The CH-Ca-βGP spectrum presents similar alterations observed in CH-βGP (10:1) FTIR, at same wavelength shift region.

3.2.3 Physical characterization of scaffolds

As showed in Figure 2b, there was no significant difference related with porosity degree among the scaffolds, except for CH-βGP, which featured the lowest porosity degree (34.8%). The highest pore diameter was found for CH-Ca (120.7 μm) e CH-Ca-βGP (85.2 μm), being significantly higher than the other groups (Figure 2c).

3.2.4 In vitro degradation profile

The percentage of scaffold weight loss after 35 days of incubation is demonstrated in Table 1. Non-crosslinked CH and CH-Ca scaffolds (G-) demonstrated high degradation at day 1 of incubation, with a mass lost in around of 52.7% and 63.3%, respectively. After 35 days, complete degradation occurred for both scaffolds. Slow and controlled degradation in the first 7 days of incubation occurred for CH-βGP and CH-Ca-βGP (G-), with mass loss of 40.1% and 60.7%, respectively, being detected from 14 days.

Crosslinked CH (G+) remaining stable throughout 35 days, with mass loss of 12%. The CH-Ca (G+) group featured mass loss in around of 50%, 75% and 91% at 21, 28 and 35 days. CH-βGP (G+) scaffold demonstrated a constant weight in the first 14 days, with 36% mass loss at 21 days, keeping a stable mass up to 28 days (59%). Consistent degradation for CH-Ca-βGP (G+) was observed at 21 days, with a degradability degree around 30.3%, 38.5% and 76% in the respective 21, 28 and 35 days.

3.3 In vitro biological characterization of cells seeded onto scaffolds

Live/dead (Figure 3a) and F-actin (Figure 3b) assays were performed to determine cell viability and adhesion/spread potential of DPCs cultivated onto scaffolds surfaces. Images obtained from each group were submitted to qualitative analysis that allowed to observe an increase in the number of viable cells (green staining) overtime (up to 14 days) for the groups CH, CH-Ca and CH-Ca-βGP. Minimal number of dead cells (red staining) at 14 days were detected in these scaffolds. Cells were able to stretch onto these biomaterials, exhibiting an elongated cytoskeleton. In contrast, less attachment and viability were observed for DPCs seeded on CH-βGP surface at all periods of analysis. Also, F-actin images exhibited

DPCs organized in small clusters with low amounts of cells spreading on the biomaterial structure.

Alamar blue assay (Figure 3c) revealed increase on cell viability values for CH-Ca in comparison to CH, from 1 to 14 days. An increase on 52.6 and 20.4% on cell viability was observed for CH-Ca-βGP at 14 and 21 days, respectively. CH-βGP promoted a reduction in DPCs viability at 1, 7, 14 and 21 days, with approximately values of 50.4%, 57.5%, 73.7% and 77.7%, respectively, which indicated the low cytocompatibility of this formulation. Increased values of ALP activity were detected at all time-points (20.7%, 32.8% and 83.3%, at 7, 14 and 21 days respectively) for CH-Ca-βGP, whereas CH-Ca had increases only at 7 days (37.5%) (Figure 3d). CH-Ca scaffolds stimulated deposition of mineralized matrix around 1.5 times and 2.5 times, in comparison to CH, whereas DPCs cultivated onto CH-Ca-βGP deposited 3.2 times and 3.8 times increase amounts of mineralized matrix at 14 and 21 days of incubation (Figure 3e).

3.4 Effect of scaffolds conditioned medium in cell response

Increase on cell viability values was detected for cells cultivated in contact with extracts from CH-Ca, CH- βGP, and CH-Ca-βGP at 3 and 7 days, with CH-Ca-βGP presenting the highest values with significant difference from CH at both periods (Figure 4a). This group also lead to expressive increase in calcium deposition after 14 days of cultivation, being two times higher in comparison with CH (Figure 4b). Transwell assay demonstrated a significant increase on the number of migrating cells in comparison to CH only for CH-Ca-βGP, denoting the chemoattractant potential of this formulation (Figure 4c and 4d).

3.5 In vitro bioactivity potential of CH and CH-Ca-βGP scaffolds as cell-free tissue engineering system

Schematic representation and representative image of pulp-in-a-chip model is presented on Figure 5a and 5b. Chemotactic potential of CH and CH-Ca-βGP was observed by Live/dead (Figure 5c) images. Both formulations stimulated the migration of DPCs cultivated on 3D cultures to the scaffolds surfaces from 3 days in the pulp-in-a-chip model. Nevertheless, a higher number of migrating cells was detected on CH-Ca-βGP, as detected by cell counting at 7 and 14 days (Figure 5d and 5e). Immunofluorescence staining for DSP detect few positive cells onto CH-Ca-βGP scaffold (Figure 5f).

It is important to note that cells remained viable and were capable to spread on 3D culture throughout the entire experimental period (Figure 6a), validating the experimental pulp-in-a-chip model under simulated pulp pressure proposed here. The cells in 3D culture were capable to proliferate through time, as demonstrated by the cell viability increase on CH and CH-Ca-βGP (Figure 6b).

Finally, dentin disc assay also demonstrated the potential of CH-Ca-βGP to induce mineralized matrix deposition in absence of osteogenic supplementation, and in an environment surrounded by dentin, as a significant increase on alizarin red staining was detected. Mineralized matrix deposition was also noted on dentin discs surface with no significant difference between both groups for this parameter (Figure 6c).

4. DISCUSSION

Development of scaffolds to stimulate in situ neo-tissue formation is a challenge in the context of Regenerative Dentistry. These materials should present bioactivity to stimulate precursor cell mobilization, proliferation and odontoblastic

differentiation to achieve dentin regeneration. Selecting natural polymers, such as chitosan, to fabricate the scaffolds allows for a biologically compatible structure capable to mimic host extracellular matrix and improve mesenchymal stem cells interaction, increasing cell recognition, activity, and differentiation [36]. In the present investigation, we proposed the fabrication of chitosan scaffolds in association with calcium hydroxide and βGP to create a chemotactic and bioactive microenvironment capable to boost dentin neo-genesis. Collective results demonstrated that a specific formulation and fabrication rote resulted in a porous chitosan scaffold containing Ca-P nanoglobules at pore wall, which was defined as CH-Ca-βGP scaffold. This scaffold was capable to increase DPCs proliferation, differentiation and mineralized matrix deposition in direct contact and at distance, being an interesting alternative as a cell-homing platform for dentin regeneration.

Fabrication rote was based in a method developed by our group, in which calcium hydroxide dispersion is incorporated to chitosan solution under vigorous stirring, leading to a bubbling effect resulting from calcium hydroxide carbonation and CO_2 release upon calcium carbonate reaction with acetic acid. Gradual freezing allows for bubbles expansion leading to a highly organized and interconnected porous network on chitosan structure. Additionally, calcium is complexed to chitosan creating a sustained release of bioactive dosages capable to improve the odontoblastic differentiation of DPCs seeded onto its structure [16]. The positive effect of calcium hydroxide on the porous architecture of chitosan can be observed on SEM images, leading to a significant increase on pore size, from 56.4 μm on plain chitosan, to 120.7 μm on CH-Ca. Thereafter, we incorporated βGP solution to chitosan and chitosan-calcium-hydroxide solution and subjected to gradual freezing protocol and freeze drying. Nevertheless, βGP interfered with porous distribution on

chitosan-calcium-hydroxide formulations, leading also to a slight reduction on pore size (85.7 μm). According to Ghavimi et al. [43], incorporation of phosphate on chitosan reduces porosity degree due to an increase in the chemical molecular bonds among the constituent's compounds, in the inner scaffold structure. An adequate microenvironment to support the process of tissue regeneration requires stable and interconnected porous matrix to allow cell infiltration and proliferation, and also to facilitate local vascularization and increase the delivery of oxygen and nutrients throughout the entire structure of the biomaterial [44,45]. Previously studies recommended a pore range from 75–250 μm for dentin regeneration, as it allows increase on proliferation rates and favor odontogenic differentiation of DPCs, allowing secretion and mineralization of extracellular matrix in large amounts [46,44,16].

FTIR data confirmed Ca complexation to chitosan by the appearance of new bands at 1463 cm^{-1}, 1446 cm^{-1} and 1423 cm^{-1}, referent of protonated amine ($-NH_2$) and hydroxyl vibration groups [47,16]. The presence of βGP was indicated by interaction of phosphorous and phosphate groups in the chemical structure of chitosan in the frequency region of 1075 cm^{-1} and 1050 cm^{-1}, respectively [48]. Changes in the FTIR spectra shown that chemical interactions can occur through hydrogen bonds between C=O groups of chitosan and -OH groups of βGP and/or through electrostatic interactions between -NH groups of chitosan (positively charged) and -P-OH phosphate groups (negatively charged) from βGP, and Ca-O (negatively charged) from calcium hydroxide, corroborating the insertion and interaction of these compounds in the chemical structure of chitosan scaffolds. The incorporation of βGP on chitosan and chitosan-calcium-hydroxide scaffolds reduced degradability degree, regardless of chemical crosslinking by glutaraldehyde. This

matrix stabilization is a consequence of electrostatic cross-linking mediated by βGP phosphate groups and chitosan amino groups [49]. Therefore, more resistant three-dimensional structures could be assembled, allowing for a stable matrix to allow adequate cell interaction, with degradability starting at 21 days in a controllable manner.

βGP incorporation on CH-Ca also led to precipitation of Ca-P nanoglobules onto chitosan surface. In absence of calcium hydroxide, incorporation of βGP resulted in an irregular surface topography which was defined as needle-like shape. Similarly, Dessì et al. [50] observed the presence of rod-like shape nano-sized crystal agglomerates (15-20 nm) on chitosan-βGP hydrogels in the presence of beta-tricalcium-phosphate (β-TCP). Precipitation of Ca-P is based on addition of phosphate groups to suspensions containing Ca^{2+} ions, that can be performed from different sources. This effect is highly dependent on pH of solution, as increase on pH reduces the solubility of phosphate-rich phase, leading to precipitation [51]. Calcium hydroxide in association with phosphate sources, such as phosphoric and orthophosphoric acid, has been used to precipitate Ca-P of nanometric size in a basic environment. The reaction occurs between PO_4^{3-} anions and Ca^{2+} ions. To further create hydroxyapatite, there is a need for high temperatures to create a crystalline phase [52]. Therefore, we believe that Ca-P nanoglobules observed on chitosan surface occurred due to interaction between Ca^{2+} ions released on calcium hydroxide suspension, and PO_4^{3-} anions from βGP, followed by precipitation of nano-agglomerates, as pH of CH-Ca solution was less acidic. However, the composition of Ca-P phase was not identified in this study. Nevertheless, in absence of calcium hydroxide, this precipitation did not occur, as observed for CH-βGP scaffold. In this case, an irregular surface topography was achieved. According to Saravanan et al.

[34], incorporation of βGP to chitosan reduces electrostatic repulsion and increase hydrogen bonding between chitosan chains, increase the electrostatic interactions between βGP phosphate groups and chitosan amino groups, and enhance chitosan-chitosan hydrophobic interactions. This effect is used to promote a thermogelling characteristic on chitosan hydrogels mediated by βGP, as at low temperature chitosan acquires a coiled configuration due to intramolecular hydrogen bonds. Altogether, these interactions may have interfered in the rheological behavior of CH-βGP solution during phase-separation at low temperatures, leading to a disrupted surface topography and a low porosity degree. The SEM images of chitosan-βGP hydrogel subjected to freeze-drying, performed by Gholizadeh et al. [36], in a very similar composition, also denoted the disruption of porosity and surface topography in comparison to plain chitosan.

According to live/dead and F-actin assay of cells seeded directly onto selected scaffolds surface, the needle-shape surface of CH-βGP interfered cell adhesion and spread, leading to reduced cell proliferation over time, whereas the other formulations allowed for a similar number of viable cells on scaffold surface, with cells being able to stretch over its structure over time. A higher proliferative rate at initial periods (7 days) was observed for CH-Ca, which may be a consequence of the higher pore size, with cells achieving similar parameters at late periods on CH, CH-Ca and CH-Ca-βGP. Several studies demonstrated that surface nano-topography has a direct relationship with an effective adhesion, spread, proliferation and cell differentiation [53-56]. Depending on the size of the irregularities on biomaterial surface, the interaction between cells and substrate can be impaired, reducing cell adhesion due to limited action of integrins, inducing apoptosis [57,58]. CH-Ca-βGP also featured the best results for odontoblastic differentiation, achieving

the highest values of ALP activity and mineralized matrix deposition. Both CH-Ca and CH-Ca-βGP lead to increase in ALP activity in around of 37.5-32.8% at 7 days in comparison to CH (control), with CH-Ca-βGP maintaining a higher ALP activity at 21 days (183.3%), whereas CH-Ca reduced this expression. An intense increase on mineralized matrix deposition was also observed for CH-Ca-βGP, being in around of 318.1% and 381.3% at 14 and 21 days, respectively, whereas CH-Ca achieved 142.8% and 248.7% on these same periods.

βGP has been widely used as a osteogenic inductor in vitro, as it provides inorganic phosphate under the activity of ALP, and also play a positive role on collagen expression and mineralization [59,60]. Therefore, βGP has been proposed as a bioactive small molecule in several scaffolds' composition, in substitution to growth factors, such as BMP-2, which have high costs, structural integrity requirements, and unwanted immunogenic responses, that reduce their potential clinical applications [40]. Hosseini et al., [42] proved that synthetic scaffolds content βGP improved dental pulp cells recognition, exerting positive effects on the proliferation rate, and had great osteoinductive potential even when other osteogenic factors are absent. Li et al. [40] demonstrated that a nanofibrous gelatin scaffolds containing osteogenic inducers ascorbic acid (AA) and βGP allowed for the creation of a pro-osteogenic microenvironment that was critical for bone regeneration. A huge increase on critical calvaria defect was observed for the matrices incorporated with βGP and AA/βGP, denoting that a biomimetic microenvironment which provides osteoconductive and osteoinductive signals is essential for mineralized tissue regeneration. He et al. [41] observed that the presence of GP-Ca on PCL matrixes in combination with hydroxyapatite (HA) caused a huge increase on osteoblastic differentiation of mesenchymal stem cells in comparison to PCL-HA and those

incorporated with GP-Na, and lead to the higher amount of bone regeneration in vivo. GP-Ca promoted osteogenic differentiation even in absence of osteogenic supplementation in the culture medium. According to the authors, the GP-Ca allows for a microenvironment rich in available organic phosphate and calcium ions, that are critical for cell-mediated biomineralization.

Based on a cell-homing strategy, it is essential that the biomaterial would be able to modulate a series of the biological events to guide the homing of dental pulp stem cells to the damage dentin site [61-63]. In this way, to improve the reparative dentin formation and achieve the success of local tissue reconstruction, these scaffolds should provide biochemical signals to delivery chemoattractive compounds to regulate cell function and drive DPCs migration [58,64]. Therefore, we performed two distinct approaches to test the scaffolds as a cell-free platform for dentin regeneration. Firstly, the released components of scaffolds immersed in culture medium were collected (extracts) and applied to cultured DPCs to evaluate if the formulations would be able to stimulate the cells at distance. It was possible to observe that calcium hydroxide and βGP incorporation were capable to increase cell viability at early cultivation periods. Nevertheless, CH-Ca-βGP was the only formulation capable to increase mineralized matrix deposition and induce the chemotaxis in comparison to plain chitosan scaffold. Therefore, CH and CH-Ca-βGP were tested in a pulp-in-a-chip model, in which cell-free scaffold was placed in intimate contact with a 3D culture of DPCs into a micro-chip system coupled to a liquid column to simulate pulpal pressure in 11 mmHg. This experimental model reproduced in vitro the direct application of pulp capping agents in clinical pulp exposure. Both scaffolds allowed cell migration from 3D culture to material's surface, with a higher number of cells being observed on CH-Ca-βGP. It was possible to

observe DSP positive cells at scaffold and 3D culture surfaces on CH-Ca-βGP group, even in absence of osteogenic supplementation on the culture medium, demonstrating the potential of this formulation as an inductive platform for local dentin regeneration. The mineralizing potential was further confirmed by dentin disc assay, which represents an *in situ* environment similar as in vivo, since dentin possess several growth factors that favor odontoblastic differentiation. We observed that the presence of calcium hydroxide and βGP in scaffold composition enhanced the mineralized matrix deposition in the scaffolds surface and around dentin discs, even in absence of osteogenic supplementation.

These positive effects can be explained by the release of βGP from chitosan polymer creating a local microenvironment capable to modulate mineralized tissue regeneration [65,66]. After release, βGP will be subjected to hydrolysis process to promote further release of high concentrations of inorganic phosphate compound that will act in the intracellular level regulating the expression of ERK signaling pathway [67,36,68]. The activation of this pathway will stimulate the recruitment, migration, proliferation and deposition of collagen in the early differentiation stages of cell differentiation [69]. This pathway will consequently improve the odontogenic phenotype of DPCs by an increase in BMP2 expression leading to deposition of mineralized matrix containing large amount of mineral crystalline structures, similar to hydroxyapatite [69,70]. Also, the combination of chitosan, βGP and calcium hydroxide allows the creation of an effective carrier and delivery vehicle of bioactive Ca^{2+} dosages, improving the osteo/odontogenic differentiation of mesenchymal stem cells by its intrinsic osteoinduction property, due to similarity composition with mineralized tissue [43,71]. In a study performed by Daculsi et al. [72], the authors suggested that the interaction between calcium and phosphate ions released from

biphasic calcium phosphate (BCP) ceramics incorporated on chitosan matrix, precipitated carbonate hydroxyapatite at biomaterial/bone interface and stimulated cell migration, adhesion and bone formation both in vitro and in vivo after implantation in rabbit femoral epiphysis. In addition, the material applied in rabbits was almost completely reabsorbed and substituted by cancellous bone after 3 weeks of implantation.

Therefore, the present investigation demonstrates a simplistic fabrication route to create porous chitosan scaffolds with adequate degradability degree, containing a Ca-P nanoglobules covered surface that allows for adequate cell interaction and improves odontoblastic differentiation. Thereafter, the leachable components of this scaffold are also capable to modulate odontoblastic phenotype at distance, as well as pulp cells chemotaxis. Direct interaction of pulp cells in a 3D matrix simulating clinical pulp exposure situation also revealed that the microenvironment created by this innovative scaffold is capable to mobilize the cells to its surface and induce odontoblastic differentiation, even in absence of osteogenic medium supplementation, along with stimulation of mineralized matrix deposition in an environment surrounded by dentin. Our work highlights the possibility of using simple and low-cost strategies to develop effective scaffolds for dentin tissue engineering application.

CONCLUSION

Collective results found in the present investigation demonstrates that association of chitosan with inexpensive osteogenic factors calcium hydroxide and bGP is a very interesting alternative to create a cell-responsive microenvironment capable to mobilize DPCs migration towards its structure, harnessing the odontogenic potential

and culminating with the expression of a highly mineralizing phenotype, key factors for cell-homing strategy.

ACKNOWLEDGMENTS

This work was supported by the São Paulo Research Foundation – FAPESP (grants # 2017/20181-0, 2016/15674-5, and 2018/09378-0), and by the Coordenação de Aperfeiçoamento de Pessoal de Nível Superior - CAPES – (Finance Code 001).

REFERENCES

1. Reed JA, Patarca R. Regenerative dental medicine: stem cells and tissue engineering in dentistry. J Environ Pathol Toxicol Oncol. 2006;25(3):537-69.

2. Li Y, Liang Q, Lin C, Li X, Chen X, Hu Q. Facile synthesis and characterization of novel rapid-setting spherical sub-micron bioactive glasses cements and their biocompatibility in vitro. Mater Sci Eng C Mater Biol Appl. 2017;75:646-652.

3. Mangione F, EzEldeen M, Bardet C, Lesieur J, Bonneau M, Decup F, Salmon B, Jacobs R, Chaussain C, Opsahl-Vital S. Implanted Dental Pulp Cells Fail to Induce Regeneration in Partial Pulpotomies. J Dent Res. 2017;96(12):1406-1413.

4. Fujii Y, Kawase-Koga Y, Hojo H, Yano F, Sato M, Chung UI, Ohba S, Chikazu D. Bone regeneration by human dental pulp stem cells using a helioxanthin derivative and cell-sheet technology. Stem Cell Res Ther. 2018;9(1):24.

5. Aziz NS, Yusop N, Ahmad A. Importance of Stem Cell Migration and Angiogenesis Study for Regenerative Cell-based Therapy: A Review. Curr Stem Cell Res Ther. 2020;15(3):284-299.

6. Casagrande L, Cordeiro MM, Nör SA, Nör JE. Dental pulp stem cells in regenerative dentistry. Odontology. 2011;99(1):1-7.

7. Galler KM, Eidt A, Schmalz G. Cell-free approaches for dental pulp tissue engineering. J Endod. 2014;40(4 Suppl):S41-5.

8. Abou Neel EA, Chrzanowski W, Salih VM, Kim HW, Knowles JC. Tissue engineering in dentistry. J Dent. 2014 Aug;42(8):915-28.

9. Chen F, Wu L, Zhang M, Zhang R, Sun H. Homing of endogenous stem/progenitor cells for in situ tissue regeneration: Promises, strategies, and translational perspectives. Biomaterials . 2011;32(12):3189-209.

10. Galler KM, Widbiller M. Cell-Free Approaches for Dental Pulp Tissue Engineering. J Endod. 2020 Sep;46(9S):S143-S149.

11. Tsutsui TW. Dental Pulp Stem Cells: Advances to Applications. Stem Cells Cloning. 2020;13:33-42.

12. Soares DG, Rosseto HL, Scheffel DS, Basso FG, Huck C, Hebling J, de Souza Costa CA. Odontogenic differentiation potential of human dental pulp cells cultured on a calcium-aluminate enriched chitosan-collagen scaffold. Clin Oral Investig. 2017;21(9):2827-2839.

13. Soares DG, Anovazzi G, Bordini EAF, Zuta UO, Silva Leite MLA, Basso FG, Hebling J, de Souza Costa CA. Biological Analysis of Simvastatin-releasing Chitosan Scaffold as a Cell-free System for Pulp-dentin Regeneration. J Endod. 2018;44(6):971-976.e1.

14. Bordini EAF, Cassiano FB, Silva ISP, Usberti FR, Anovazzi G, Pacheco LE, Pansani TN, Leite ML, Hebling J, de Souza Costa CA, Soares DG. Synergistic potential of 1α,25-dihydroxyvitamin D3 and calcium-aluminate-chitosan scaffolds with dental pulp cells. Clin Oral Investig. 2020;24(2):663-674.

15. Cassiano FB, Soares DG, Bordini EAF, Anovazzi G, Hebling J, Costa CAS. Simvastatin-Enriched Macro-Porous Chitosan-Calcium-Aluminate Scaffold for Mineralized Tissue Regeneration. Braz Dent J. 2020;31(4):385-391.

16. Soares DG, Bordini EAF, Cassiano FB, Bronze-Uhle ES, Pacheco LE, Zabeo G, Hebling J, Lisboa-Filho PN, Bottino MC, de Souza Costa CA. Characterization of novel calcium hydroxide-mediated highly porous chitosan-calcium scaffolds for potential application in dentin tissue engineering. J Biomed Mater Res B Appl Biomater. 2020;108(6):2546-2559.

17. Choudhary P, Ramalingam B, Das SK. Fabrication of Chitosan-Reinforced Multifunctional Graphene Nanocomposite as Antibacterial Scaffolds for Hemorrhage Control and Wound-Healing Application. ACS Biomater Sci Eng. 2020;6(10):5911-5929.

18. Patel DK, Dutta SD, Ganguly K, Lim KT. Multifunctional bioactive chitosan/cellulose nanocrystal scaffolds eradicate bacterial growth and sustain drug delivery. Int J Biol Macromol. 2020;170:178-188.

19. Sedghi R, Shaabani A, Sayyari N. Electrospun triazole-based chitosan nanofibers as a novel scaffolds for bone tissue repair and regeneration Carbohydr Polym. 2020;230:115707.

20. Zarei M, Samimi A, Khorram M, Abdi MM, Golestaneh SI. Fabrication and characterization of conductive polypyrrole/chitosan/collagen electrospun nanofiber scaffold for tissue engineering application. Int J Biol Macromol. 2020;168:175-186.

21. Zhang J, Xia W, Liu P, Cheng Q, Tahirou T, Gu W, Li B. Chitosan modification and pharmaceutical/biomedical applications. Mar Drugs. 2010;8(7):1962-87.

22. Venkatesan J, Kim SK. Chitosan composites for bone tissue engineering--an overview. Mar Drugs. 2010 Aug 2;8(8):2252-66.

23. Jiang T, James R, Kumbar SG, Laurencin CT. Chapter 5 - chitosan as a biomaterial: structure, properties, and applications in tissue engineering and drug delivery. Natural and Synthetic Biomedical Polymers, Elsevier, Oxford (2014), pp. 91-113

24. Kean T, Thanou M. Biodegradation, biodistribution and toxicity of chitosan. Adv Drug Deliv Rev. 2010;62(1):3-11.

25. Bakopoulou A, Georgopoulou A, Grivas I, Bekiari C, Prymak O, Loza K, Epple M, Papadopoulos GC, Koidis P, Chatzinikolaidou M. Dental pulp stem cells in

chitosan/gelatin scaffolds for enhanced orofacial bone regeneration. Dent Mater. 2019;35(2):310-327.

26. Amiryaghoubi N, Noroozi Pesyan N, Fathi M, Omidi Y. Injectable thermosensitive hybrid hydrogel containing graphene oxide and chitosan as dental pulp stem cells scaffold for bone tissue engineering. Int J Biol Macromol. 2020;162:1338-1357.

27. Talaat W, Aryal Ac S, Al Kawas S, Samsudin ABR, Kandile NG, Harding DRK, Ghoneim MM, Zeiada W, Jagal J, Aboelnaga A, Haider M. Nanoscale Thermosensitive Hydrogel Scaffolds Promote the Chondrogenic Differentiation of Dental Pulp Stem and Progenitor Cells: A Minimally Invasive Approach for Cartilage Regeneration. Int J Nanomedicine. 2020;15:7775-7789.

28. Vagropoulou G, Trentsiou M, Georgopoulou A, Papachristou E, Prymak O, Kritis A, Epple M, Chatzinikolaidou M, Bakopoulou A, Koidis P. Hybrid chitosan/gelatin/nanohydroxyapatite scaffolds promote odontogenic differentiation of dental pulp stem cells and in vitro biomineralization. Dent Mater. 2021;37(1):e23-e36.

29. Jeong JE, Park SY, Shin JY, Seok JM, Byun JH, Oh SH, Kim WD, Lee JH, Park WH, Park SA. 3D Printing of Bone-Mimetic Scaffold Composed of Gelatin/beta-Tri-Calcium Phosphate for Bone Tissue Engineering. Macromol Biosci. 2020;20(12):e2000256.

30. Sokolova V, Kostka K, Shalumon KT, Prymak O, Chen JP, Epple M. Synthesis and characterization of PLGA/HAP scaffolds with DNA-functionalised calcium phosphate nanoparticles for bone tissue engineering. J Mater Sci Mater Med. 2020;31(11):102.

31. Zhang J, Eyisoylu H, Qin XH, Rubert M, Müller R. 3D bioprinting of graphene oxide-incorporated cell-laden bone mimicking scaffolds for promoting scaffold fidelity, osteogenic differentiation and mineralization. Acta Biomater. 2020;14:S1742-7061(20)30740-6.

32. Björkenheim R, Jämsen E, Eriksson E, Uppstu P, Aalto-Setälä L, Hupa L, Eklund KK, Ainola M, Lindfors NC, Pajarinen J. Sintered S53P4 bioactive glass scaffolds have anti-inflammatory properties and stimulate osteogenesis in vitro. Eur Cell Mater. 2021;41:15-30.

33. Kim G, Park Y, Lee S, El-Fiqi A, Kim J, Lee E, Kim H, Kim E. Odontogenic stimulation of human dental pulp cells with bioactive nanocomposite fiber. J Biomater Appl. 2015;29(6):854-66.

34. Saravanan S, Vimalraj S, Thanikaivelan P, Banudevi S, Manivasagam G. A review on injectable chitosan/beta glycerophosphate hydrogels for bone tissue regeneration. Int J Biol Macromol. 2019;121:38-54.

35. Chen Y, Zhang F, Fu Q, Liu Y, Wang Z, Qi N. In vitro proliferation and osteogenic differentiation of human dental pulp stem cells in injectable thermo-sensitive chitosan/β-glycerophosphate/hydroxyapatite hydrogel. J Biomater Appl. 2016;31(3):317-27.

36. Gholizadeh S, Moztarzadeh F, Haghighipour N, Ghazizadeh L, Baghbani F, Shokrgozar MA, Allahyari Z. Preparation and characterization of novel functionalized multiwalled carbon nanotubes/chitosan/β-Glycerophosphate scaffolds for bone tissue engineering. Int J Biol Macromol. 2017;97:365-372.

37. Liu T, Li J, Shao Z, Ma K, Zhang Z, Wang B, Zhang Y. Encapsulation of mesenchymal stem cells in chitosan/β-glycerophosphate hydrogel for seeding on a novel calcium phosphate cement scaffold. Med Eng Phys. 2018;56:9-15.

38. Lotfi M, Bagherzadeh R, Naderi-Meshkin H, Mahdipour E, Mafinezhad A, Sadeghnia HR, Esmaily H, Maleki M, Hasssanzadeh H, Ghayaour-Mobarhan M, Bidkhori HR, Bahrami AR. Hybrid chitosan-ß-glycerol phosphate-gelatin nano-/micro fibrous scaffolds with suitable mechanical and biological properties for tissue engineering. Biopolymers. 2016;105(3):163-75.

39. Wang C, Cao X, Zhang Y. A novel bioactive osteogenesis scaffold delivers ascorbic acid, beta-glycerophosphate, and dexamethasone in vivo to promote bone regeneration. Oncotarget. 2017 May 9;8(19):31612-31625.

40. Li Y, Liu Y, Xun X, Zhang W, Xu Y, Gu D. Three-Dimensional Porous Scaffolds with Biomimetic Microarchitecture and Bioactivity for Cartilage Tissue Engineering. ACS Appl Mater Interfaces. 2019;11(40):36359-36370.

41. He Y, Li Q, Ma C, Xie D, Li L, Zhao Y, Shan D, Chomos SK, Dong C, Tierney JW, Sun L, Lu D, Gui L, Yang J. Development of osteopromotive poly (octamethylene citrate glycerophosphate) for enhanced bone regeneration. Acta Biomater. 2019;93:180-191.

42. Hosseini FS, Enderami SE, Hadian A, Abazari MF, Ardeshirylajimi A, Saburi E, Soleimanifar F, Nazemisalman B. Efficient osteogenic differentiation of the dental pulp stem cells on β-glycerophosphate loaded polycaprolactone/polyethylene oxide blend nanofibers. J Cell Physiol. 2019;234(8):13951-13958.

43. Ghavimi SAA, Lungren ES, Stromsdorfer JL, Darkow BT, Nguyen JA, Sun Y, Pfieffer FM, Goldstein CL, Wan C, Ulery BD. Effect of Dibasic Calcium Phosphate Incorporation on Cellulose Nanocrystal/Chitosan Hydrogel Properties for the Treatment of Vertebral Compression Fractures. AAPS J. 2019;21(3):41.

44. Gupte MJ, Swanson WB, Hu J, Jin X, Ma H, Zhang Z, Liu Z, Feng K, Feng G, Xiao G, Hatch N, Mishina Y, Ma PX. Pore size directs bone marrow stromal cell fate

and tissue regeneration in nanofibrous macroporous scaffolds by mediating vascularization. Acta Biomater. 2018;82:1-11.

45. Dissanayaka WL, Zhang C. Scaffold-based and scaffold-free strategies in dental pulp regeneration. J Endod. 2020;46(9S):S81-S89.

46. Chen X, Fan H, Deng X, Wu L, Yi T, Gu L, Zhou C, Fan Y, Zhang X. Scaffold Structural Microenvironmental Cues to Guide Tissue Regeneration in Bone Tissue Applications. Nanomaterials (Basel). 2018;8(11):960.

47. Yuan Q, Shah J, Hein S, Misra RDK. Controlled and extended drug release behavior of chitosan-based nanoparticle carrier. Acta Biomater. 2010;6(3):1140-8.

48. Vijaya Y, Popuri SR, Boddu VM, Krishnaiah A. Modified chitosan and calcium alginate biopolymer sorbents for removal of nickel (II) through adsorption. Carbohydr Polym. 2008; 72(2): 261-271.

49. Chan BP, Leong KW. Scaffolding in tissue engineering: general approaches and tissue-specific considerations. Eur Spine J. 2008;17 Suppl 4(Suppl 4):467-79.

50. Dessì M, Borzacchiello A, Mohamed TH, Abdel-Fattah WI, Ambrosio L. Novel biomimetic thermosensitive β-tricalcium phosphate/chitosan-based hydrogels for bone tissue engineering. J Biomed Mater Res A. 2013;101(10):2984-93.

51. Recillas S, Rodríguez-Lugoc V, Monterod ML, Viquez-Canoc S, Hernandeze L, Castañoa VM. Studies on the precipitation behavior of calcium phosphate solutions. J. Cer. Process. Res. 2012; 13(1):5-10.

52. Jalali F, Oveisi H, Meshkini A. Enhanced osteogenesis properties of titanium implant materials by highly uniform mesoporous thin films of hydroxyapatite and titania intermediate layer. J Mater Sci Mater Med. 2020;31(12):114.

53. Liu X, Holzwarth JM, Ma PX. Functionalized synthetic biodegradable polymer scaffolds for tissue engineering. Macromol Biosci. 2012;12(7):911-9.

54. BaoLin G, Ma PX. Synthetic biodegradable functional polymers for tissue engineering: a brief review. Sci China Chem. 2014;57(4):490-500.

55. Pilipchuk SP, Monje A, Jiao Y, Hao J, Kruger L, Flanagan CL, Hollister SJ, Giannobile WV. Integration of 3D Printed and Micropatterned Polycaprolactone Scaffolds for Guidance of Oriented Collagenous Tissue Formation In Vivo. Adv Healthc Mater. 2016;5(6):676-87.

56. Lim SS, Chai CY, Loh H. In vitro evaluation of osteoblast adhesion, proliferation and differentiation on chitosan-TiO 2 nanotubes scaffolds with Ca 2+ ions. Mater Sci Eng C Mater Biol Appl. 2017;76:144-152.

57. Beke S, Kőrösi L, Scarpellini A, Anjum F, Brandi F. Titanate nanotube coatings on biodegradable photopolymer scaffolds. Mater Sci Eng C Mater Biol Appl. 2013;33(4):2460-3.

58. García-Sánchez D, Fernández D, Rodríguez-Rey JC, Pérez-Campo FM. Enhancing survival, engraftment, and osteogenic potential of mesenchymal stem cells. World J Stem Cells. 2019;11(10):748-763.

59. Beck GR Jr, Zerler B, Moran E. Phosphate is a specific signal for induction of osteopontin gene expression. Proc Natl Acad Sci U S A. 2000 Jul 18;97(15):8352-7.

60. Beck GR Jr, Knecht N. Osteopontin regulation by inorganic phosphate is ERK1/2-, protein kinase C-, and proteasome-dependent. J Biol Chem. 2003 Oct 24;278(43):41921-9.

61. Tjäderhane L, Carrilho MR, Breschi L, Tay FR, Pashley DH. Dentin basic structure and composition—an overview. Endodontic topics – dentin: Part I. 2012; 20(1): 3-29.

62. Athirasala A, Lins F, Tahayeri A, Hinds M, Smith AJ, Sedgley C, Ferracane J, Bertassoni LE. A Novel Strategy to Engineer Pre-Vascularized Full-Length Dental

Pulp-like Tissue Constructs. Sci Rep. 2017;7(1):3323. doi: 10.1038/s41598-017-02532-3.

63. Campodoni E, Dozio SM, Panseri S, Montesi M, Tampieri A, Sandri M. Mimicking Natural Microenvironments: Design of 3D-Aligned Hybrid Scaffold for Dentin Regeneration. Front Bioeng Biotechnol. 2020;8:836.

64. Won JE, Lee YS, Park JH, Lee JH, Shin YS, Kim CH, Knowles JC, Kim HW. Hierarchical microchanneled scaffolds modulate multiple tissue-regenerative processes of immune-responses, angiogenesis, and stem cell homing. Biomaterials. 2020;227:119548.

65. Ke X, Li M, Wang X, Liang J, Wang X, Wu S, Long M, Hu C. An injectable chitosan/dextran/beta -glycerophosphate hydrogel as cell delivery carrier for therapy of myocardial infarction. Carbohydr Polym. 2020;229:115516.

66. Wasupalli GK, Verma D. Injectable and thermosensitive nanofibrous hydrogel for bone tissue engineering. Mater Sci Eng C Mater Biol Appl. 2020;107:110343.

67. Langenbach F, Handschel J. Effects of dexamethasone, ascorbic acid and beta-glycerophosphate on the osteogenic differentiation of stem cells in vitro. Stem Cell Res Ther. 2013;4(5):117.

68. Hatt LP, Thompson K, Müller WEG, Stoddart MJ, Armiento AR. Calcium polyphosphate nanoparticles act as an effective inorganic phosphate source during osteogenic differentiation of human mesenchymal stem cells. Int J Mol Sci. 2019;20(22):5801.

69. Franceschi RT, Ge C, Xiao G, Roca H, Jiang D: Transcriptional regulation of osteoblasts. Cells Tissues Organs. 2009, 189: 144-152.

70. Bonewald LF, Harris SE, Rosser J, Dallas MR, Dallas SL, Camacho NP, Boyan B, Boskey A: Von Kossa staining alone is not sufficient to confirm that

mineralization in vitro represents bone formation. Calcif Tissue Int. 2003, 72: 537-547.

71. Wu S, Zhou Y, Yu Y, Zhou X, Du W, Wan M, Fan Y, Zhou X, Xu X, Zheng L. Evaluation of Chitosan Hydrogel for Sustained Delivery of VEGF for Odontogenic Differentiation of Dental Pulp Stem Cells. Stem Cells Int. 2019;2019:1515040.

72. Daculsi G, Laboux O, Malard O, Weiss P. Current state of the art of biphasic calcium phosphate bioceramics. J Mater Sci Mater Med. 2003;14(3):195-200.

FIGURES

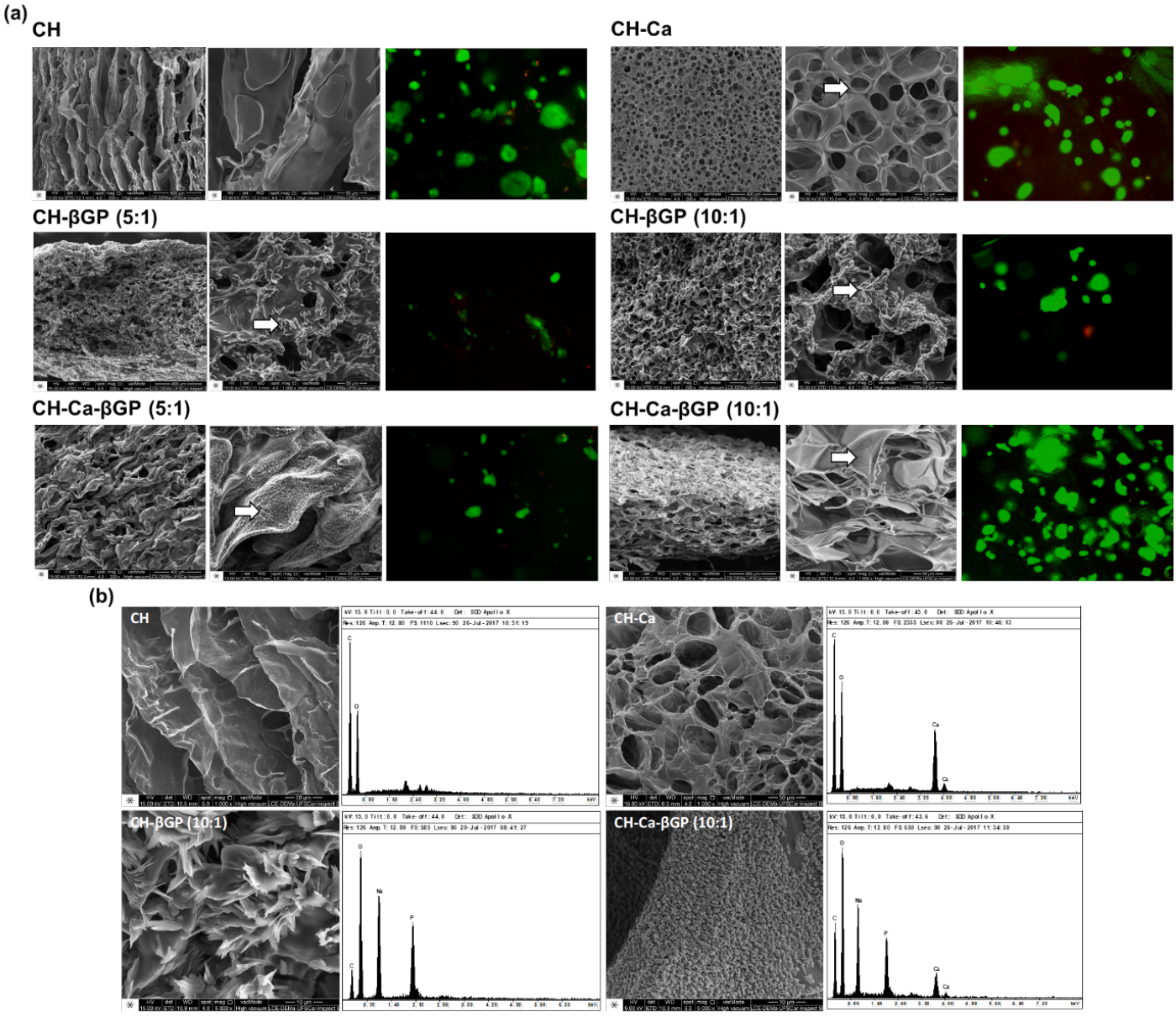

Figure 1. Morphological, biological and chemical characterizations of porous chitosan (CH) scaffolds conjugated with calcium hydroxide and/or β-Glycerophosphate (βGP) in different ratios (5:1 or 10:1). **(a)** Scanning electron microscopy (SEM) images of formulated scaffolds surfaces (200x and 1000x). Note the needle-like and nanoglobular structures on CH-βGP and CH-Ca-βGP, respectively (arrows). Representative images of Live/Dead assay to determine the cytocompatibility of DPCs cultivated on scaffolds. Green fluorescence indicates live cells. Red fluorescence indicates dead cells. **(b)** EDS spectrum obtained by SEM images (1000x) confirmed the incorporation of calcium, sodium and phosphate elements in scaffolds composition.

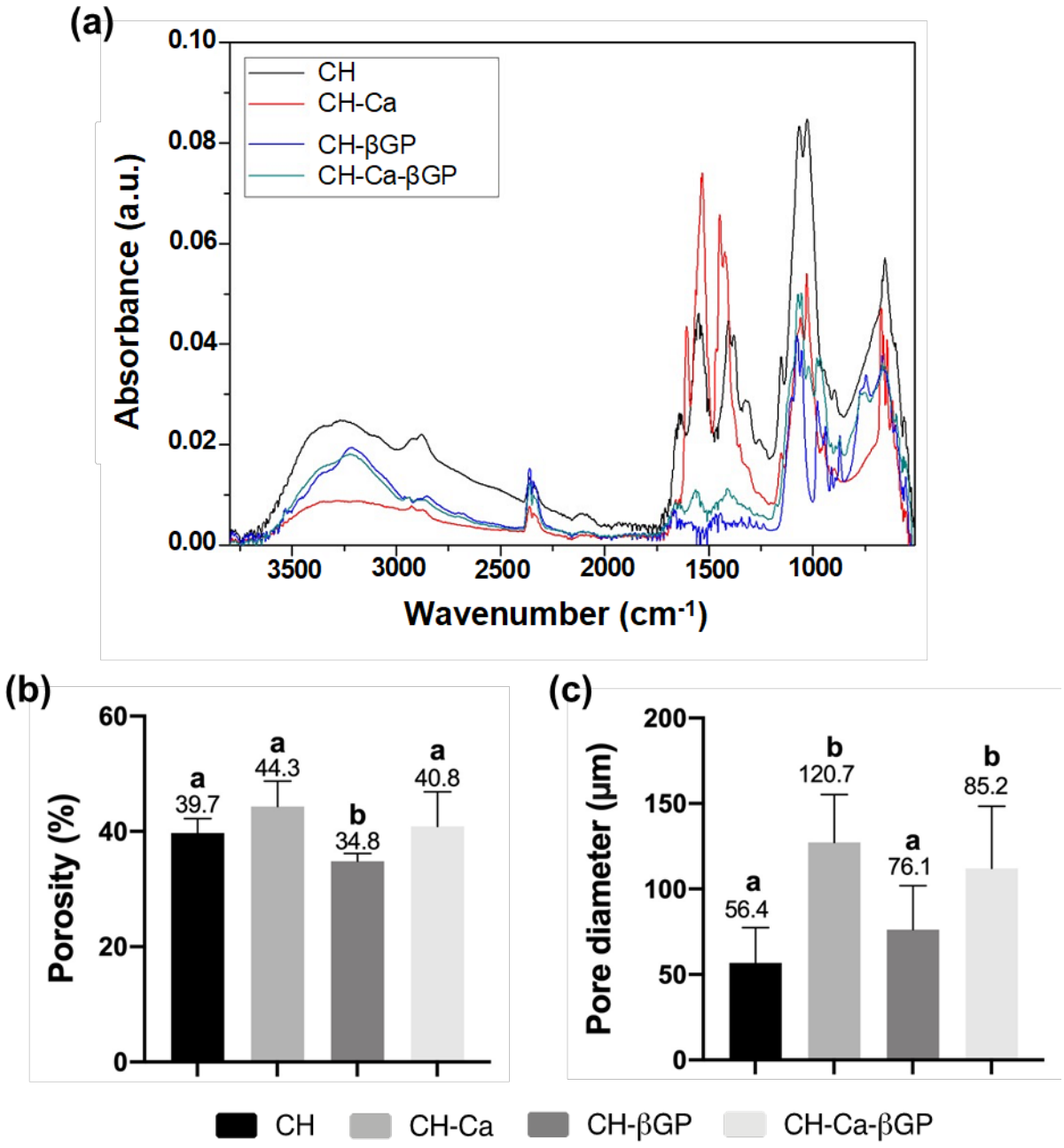

Figure 2. Chemical analysis and characterization of pore structure of scaffolds. **(a)** FTIR spectrum comparing characteristic bands of CH, CH-Ca, CH-βGP and CH-Ca-βGP scaffolds. **(b)** Porosity and pore diameter graphs from different scaffolds formulations. Bar graphs representing the average ± SD of porosity (%) and pore diameter (μm). Different letters indicate significant difference between the groups (ANOVA/Tukey test; α=5%).

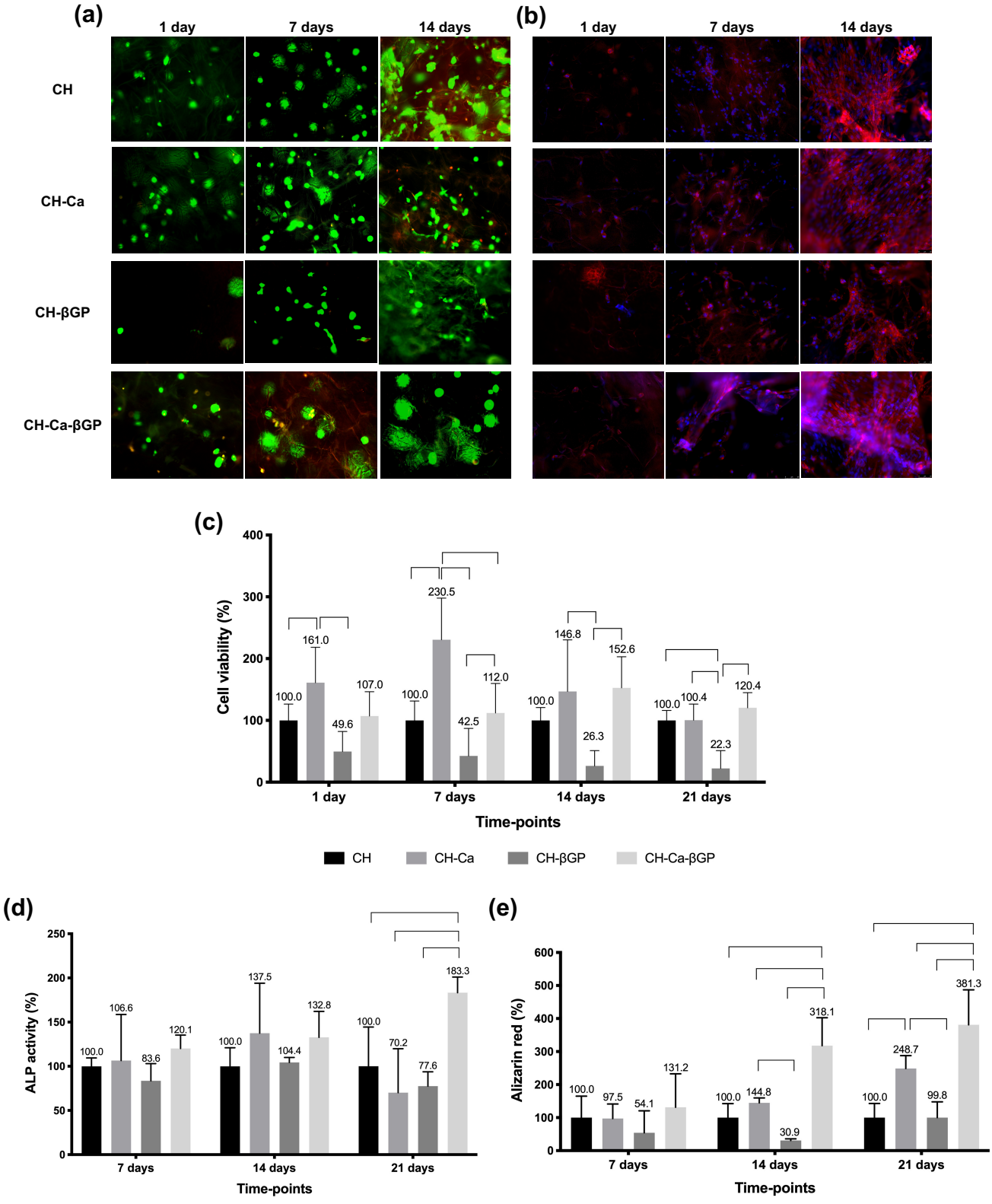

Figure 3. Biological characterization of cells seeded onto formulated scaffolds. **(a)** Representative Live/dead images of scaffolds surface for all experimental groups in both periods of analysis (20x). Green fluorescence indicates live cells. Red fluorescence indicates dead cells. **(b)** Representative images of F-actin assay showing elongated cytoskeleton of dental pulps cells (DPCs) on scaffolds surface in different time-points (20x). Red fluorescence indicates actin filaments of cells. Blue

fluorescence indicates nuclei of cells. **(c)** Alamar blue assay. Results are demonstrated in bar graphs as average ± SD. [indicate differences among groups in each period of analysis (ANOVA/Tukey, α=5%).

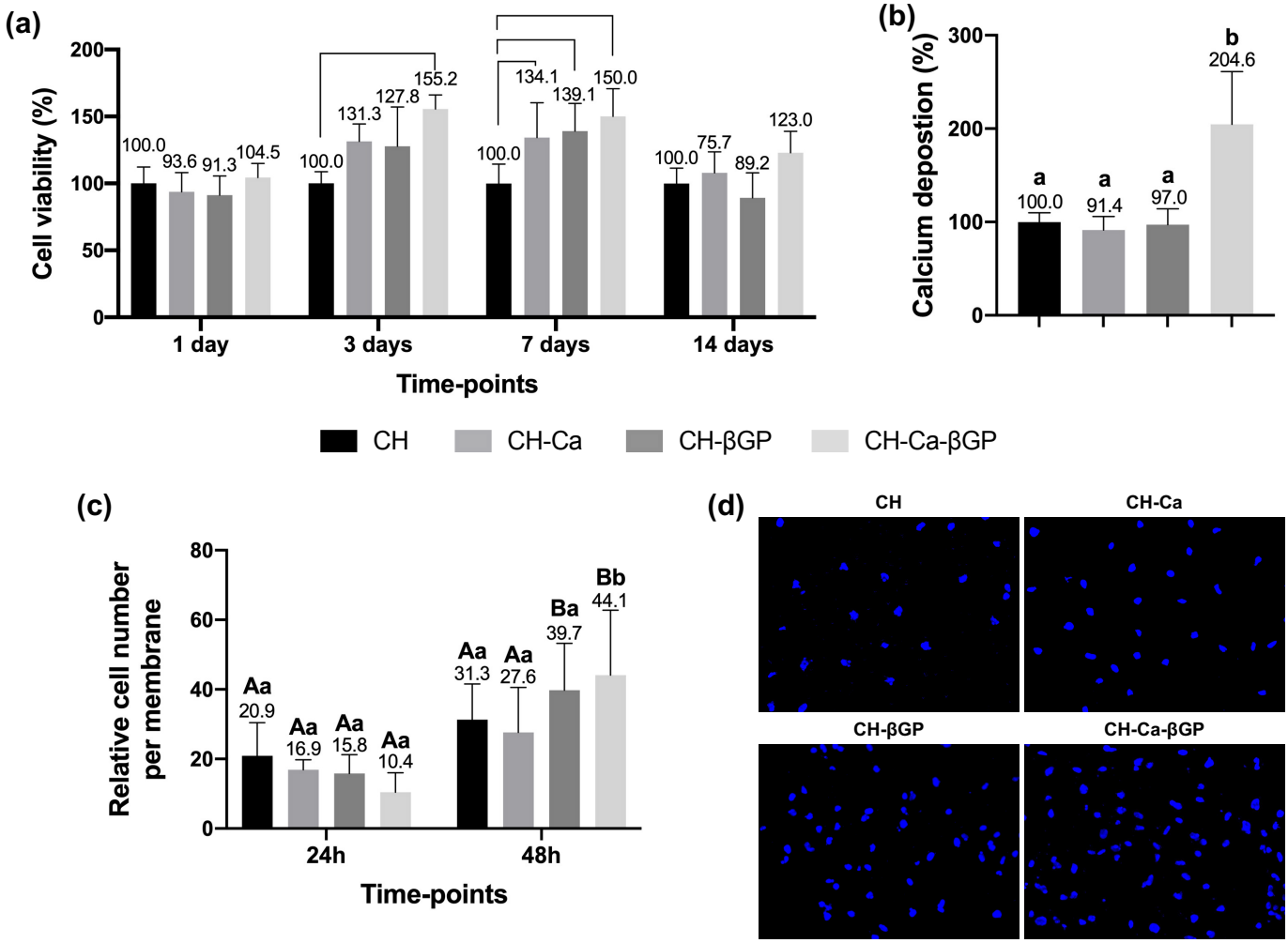

Figure 4. Evaluation of released scaffolds constituents' in cell response. **(a)** Alamar blue assay. Cell viability results are demonstrated in bar graphs as average ± SD. [indicate differences among groups in each time-point (ANOVA/Tukey, α=5%). **(b)** Calcium liquiform assay. The amount of calcium deposited by cells is indicated in representative bar graphs as mean ± SD. Distinct letters indicate statistically significant differences among groups (ANOVA/Tukey, α=5%). **(c)** Transwell assay. Representative bar graphs of mean ± SD demonstrate the chemotactic potential of scaffolds formulation. Upper-case letters allow for comparison among time-points for each group; lower-case letters allow for comparison among groups in each time-point. Different letters indicate statistically significant differences (ANOVA/Tukey, α=5%). **(d)** Representative images of transwell lower surface with cells migrated and stained with DAPI at 48h.

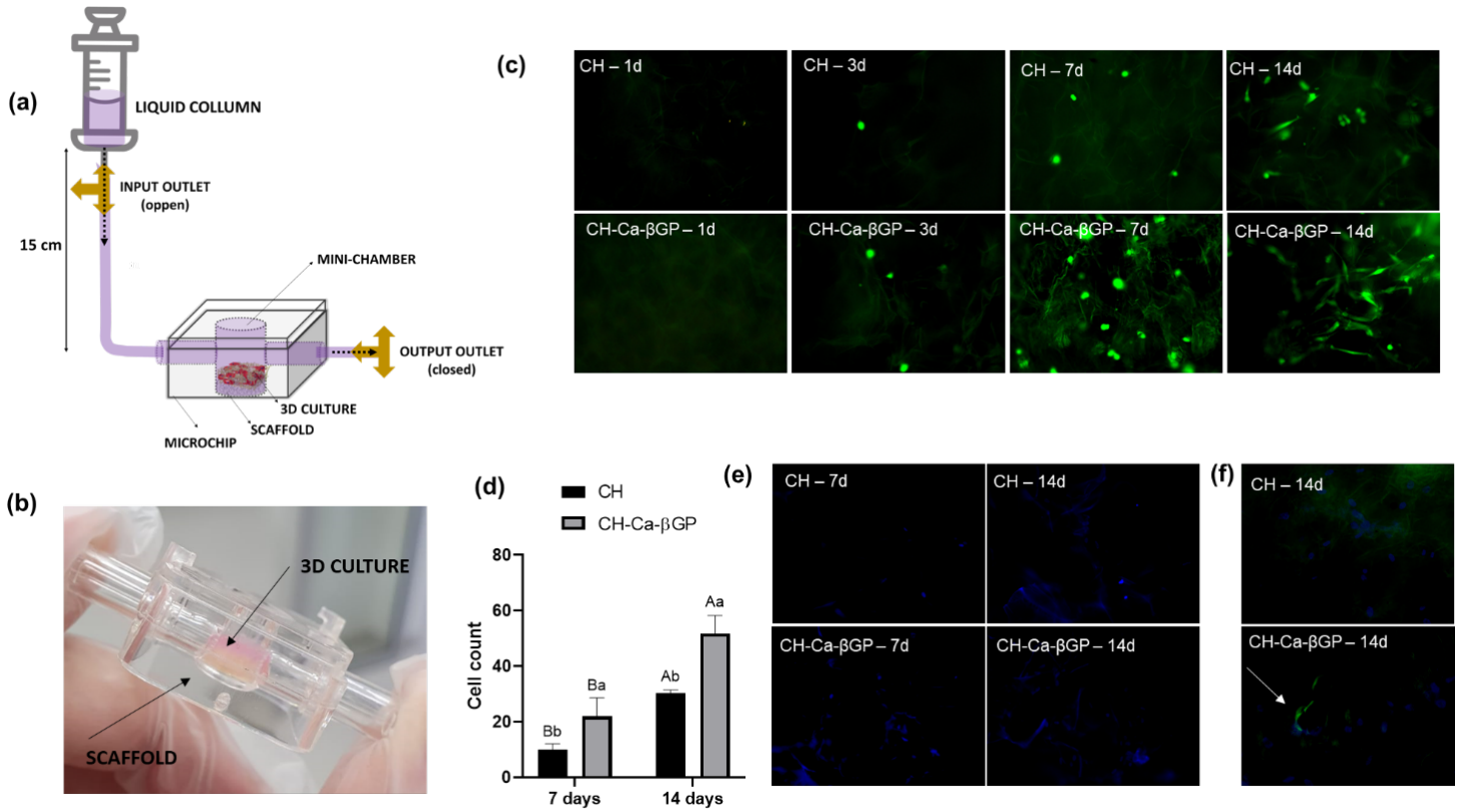

Figure 5. Pulp-in-a-chip assay. **(a)** Schematic representation of the microchip and simulated pulp pressure system. **(b)** Image of microchip and 3D-cell/scaffold interfaces. **(c)** Fluorescence images of Live/dead assay of scaffold surface (20x). Green fluorescence indicates live cells. Red fluorescence indicates dead cells. **(d)** Bar graph of migrating cells at scaffold surface. Upper-case letters allow for comparison among time-points for each group; lower-case letters allow for comparison among groups in each time-point. Different letters indicate statistically significant differences (ANOVA/Tukey, α=5%). **(e)** Representative images of blue fluorescence of migrating cells nuclei (DAPI). (f) Immunofluorescence for DSP at 14 days on scaffold surface (arrow indicate positive cells = green).

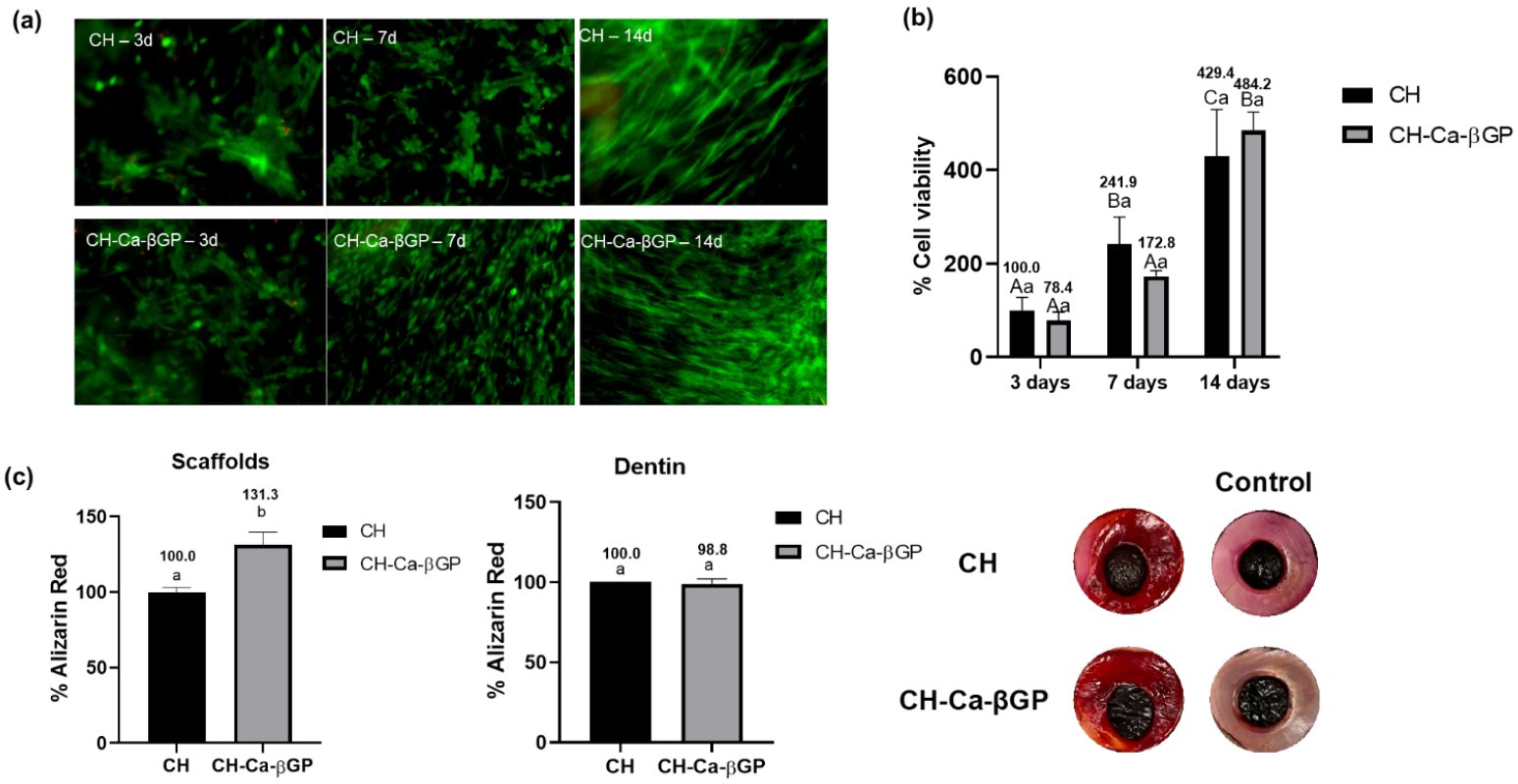

Figure 6. (a) Live/dead assay of 3D culture on pulp-in-a-chip assay. **(b)** Alamar blue assay of 3D culture. Bar graph of cell viability. Results are expressed as mean ± SD. Upper-case letters allow for comparison among time-points for each group; lower-case letters allow for comparison among groups in each time-point. Different letters indicate statistically significant differences (ANOVA/Tukey, α=5%). **(c)** Bar graphs representation of mineral formation around dentin discs and on scaffold surfaces. The values are demonstrated are means ± SD in both graphs. Different letters indicate statistical difference between groups (Student t test, α=5%). Representative images of scaffolds adapted on dentin discs with circular perforations, mimicking the application of biomaterials direct on pulp exposure.

Table 1. Wet mass percentage representative of degradability degree through time on scaffolds submitted or not to cross-linking.

		Periods of analyzes						
Groups	**Cross-linking**	**Baseline**	**1 day**	**7 days**	**14 days**	**21 days**	**28 days**	**35 days**
CH	-	100.0 (±8.15)^{Aa}	47.3 (±9.65)^{Ba}	36.2 (±8.71)^{BCa}	26.0 (±5.41)^{BCa}	15.3 (±6.68)^{BCa}	16.0 (±4.78)^{BCa}	3.61 (±1.12)^{Ca}
CH	+	100.0 (±19.42)^{Aa}	100.8 (±24.12)^{Ab}	115.7 (±15.74)^{Ab}	101.8 (±14.81)^{Ab}	92.9 (±15.54)^{Ab}	104.3 (±15.00)^{Ab}	88.6 (±11.73)^{Ab}
CH-Ca	-	100.0 (±19.65)^{Aa}	36.7 (±17.17)^{Ba}	38.5 (±31.11)^{Ba}	13.5 (±14.25)^{Ba}	6.0 (±5.11)^{Ca}	4.0 (±3.56)^{Cc}	3.8 (±3.74)^{Ca}
CH-Ca	+	100.0 (±24.19)^{Aa}	97.6 (±27.39)^{Ab}	100.7 (±32.83)^{Ab}	95.2 (±24.57)^{Ab}	49.7 (±18.28)^{Bc}	25.2 (±11.30)^{Ba}	9.94 (±5.42)^{Ca}
CH-βGP	-	100.0 (±16.06)^{Aa}	101.2 (±21.87)^{Ab}	104.1 (±22.02)^{Ab}	59.1 (±14.52)^{Bc}	33.9 (±9.14)^{BCd}	18.9 (±5.81)^{CDa}	15.2 (±7.09)^{CDc}
CH-βGP	+	100.0 (±18.56)^{Aa}	106.7 (±32.41)^{Ab}	110.9 (±29.88)^{Ab}	113.8 (±27.20)^{Ab}	63.6 (±32.23)^{Bb}	40.8 (±22.46)^{Bd}	41.3 (±22.65)^{Bd}
CH-Ca-βGP	-	100.0 (±11.24)^{Aa}	96.8 (± 20.63)^{Ab}	76.5 (± 35.30)^{Ab}	39.3 (±19.48)^{Bc}	19.1 (±11.82)^{Bd}	8.7 (±7.58)^{BCa}	4.2 (±4.19)^{Ca}
CH-Ca-βGP	+	100.0 (±16.74)^{Aa}	117.8 (±7.86)^{Ac}	140.3 (±26.27)^{Ab}	130.1 (±39.00)^{Ab}	69.7 (±18.09)^{Bc}	61.5 (±22.11)^{Bd}	23.4 (±4.29)^{Cc}

*Mean percentage values ± standard deviation for biomaterial mass

** Upper-case letters allow for comparison in rows for same group. Lower-case letters allow for comparison in columns for different groups.

*** Different letters indicate statistically significant differences (ANOVA/Tukey, α=5%).

3.2 Publicação 2

Photocrosslinkable Dexamethasone-loaded Hydrogel for Dentin Regeneration Under Pulp Inflammation

Ester A. F. Bordini[a,b], Jessica A. Ferreira[a], Nileshkumar Dubey[a], Juliana S. Ribeiro[a], Carlos A. de Souza Costa[b], Diana G. Soares[c], and Marco C. Bottino[a,d,*]

[a] Department of Cariology, Restorative Sciences, and Endodontics, School of Dentistry, University of Michigan, Ann Arbor, MI USA.

[b] Department of Physiology and Pathology, Universidade Estadual Paulista – UNESP, Araraquara School of Dentistry, Araraquara, SP, Brazil.

[c] Department of Operative Dentistry, Endodontics and Dental Materials, São Paulo University – USP, Bauru School of Dentistry, Bauru, SP, Brazil.

[d] Department of Biomedical Engineering, College of Engineering, University of Michigan, Ann Arbor, MI USA.

***Corresponding author:**

Marco C. Bottino, DDS, MSc, PhD, FADM

Associate Professor

Director, Regenerative Dentistry

University of Michigan School of Dentistry

Department of Cariology, Restorative Sciences and Endodontics

1011 N. University (Room 5223), Ann Arbor, MI - 48109, USA.

Tel: +1-734.763.2206 Fax: +1-734.936.1597.

E-mail: mbottino@umich.edu

Artigo em Revisão na Acta Biomaterialia. Bordini EAF, Ferreira JA, Dubey N, Ribeiro JS, de Souza Costa CA, Soares DG, Bottino MC. Photocrosslinkable Dexamethasone-loaded Hydrogel for Dentin Regeneration Under Pulp Inflammation. Acta Biomater. 2021. (Under review). APÊNDICE A. ANEXO B.

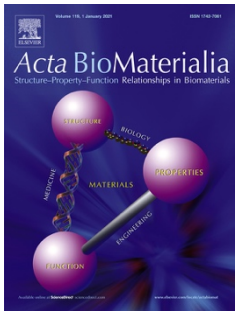

* Artigo formatado segundo as normas da Acta Biomaterialia.

Abstract

The development of multifunctional drug delivery systems capable of amplifying the regenerative capacity of endogenous progenitor cells under pulpal tissue inflammation is central to translating clinically effective strategies for dentin regeneration. Here, we successfully loaded dexamethasone (DEX), a pleotropic drug with anti-inflammatory and mineralizing abilities, into aluminosilicate clay nanotubes (HNTs) to engineer an injectable multifunctional drug delivery system based on photocrosslinkable gelatin methacryloyl (GelMA) hydrogel. In detail, a series of hydrogels based on GelMA formulations containing distinct amounts of DEX-loaded nanotubes were analyzed for physicochemical and mechanical properties, kinetics of DEX release, as well as cytocompatibility in stem cells from human exfoliated deciduous teeth (SHEDs). The anti-inflammatory response and mineralization potential of the injectable drug delivery systems were determined both *in vitro* and *in vivo*. The incorporation of DEX-loaded nanotubes increased the mechanical strength of GelMA with no effect on its degradation and swelling ratio. The controlled release of DEX restored the expression of alkaline phosphatase and mineralization in LPS-stimulated SHEDs *in vitro*. Importantly, *in vivo* data revealed that DEX-loaded nanotube-modified GelMA led to enhanced bone formation compared to DEX-free GelMA formulations with minimum localized inflammatory responses. Altogether, our findings show that the engineered DEX-loaded nanotube-modified hydrogel can be considered a promising therapeutic strategy for applications in mineralized tissue regeneration under inflammation.

Keywords: Dexamethasone, gelatin methacryloyl, GelMA, hydrogel, dentin regeneration, dental

Statement of significance

Knowing that inflammation plays a crucial role in dentin regeneration, it is rational to devise a drug delivery system with anti-inflammatory and mineralizing abilities. Here, we report on the development of an injectable dexamethasone-loaded (DEX) nanotube-modified gelatin methacryloyl (GelMA) hydrogel as a potential strategy to amplify dentin regeneration by resident pulp stem cells under inflammatory conditions. DEX-loaded nanotube-modified GelMA showed a sustained drug release pattern and suitable physicochemical and biomechanical properties. *In vitro*, DEX-loaded nanotube-modified GelMA upregulated the mineralization of SHEDs under proinflammatory stimulus. *In vivo* assays validated the biocompatibility of the DEX-loaded hydrogel and its ability to promote mineralized tissue regeneration. Altogether, the proposed multifunctional hydrogel has the potential to trigger *in situ* mineralized tissue regeneration under inflammatory conditions.

GRAPHICAL ABSTRACT

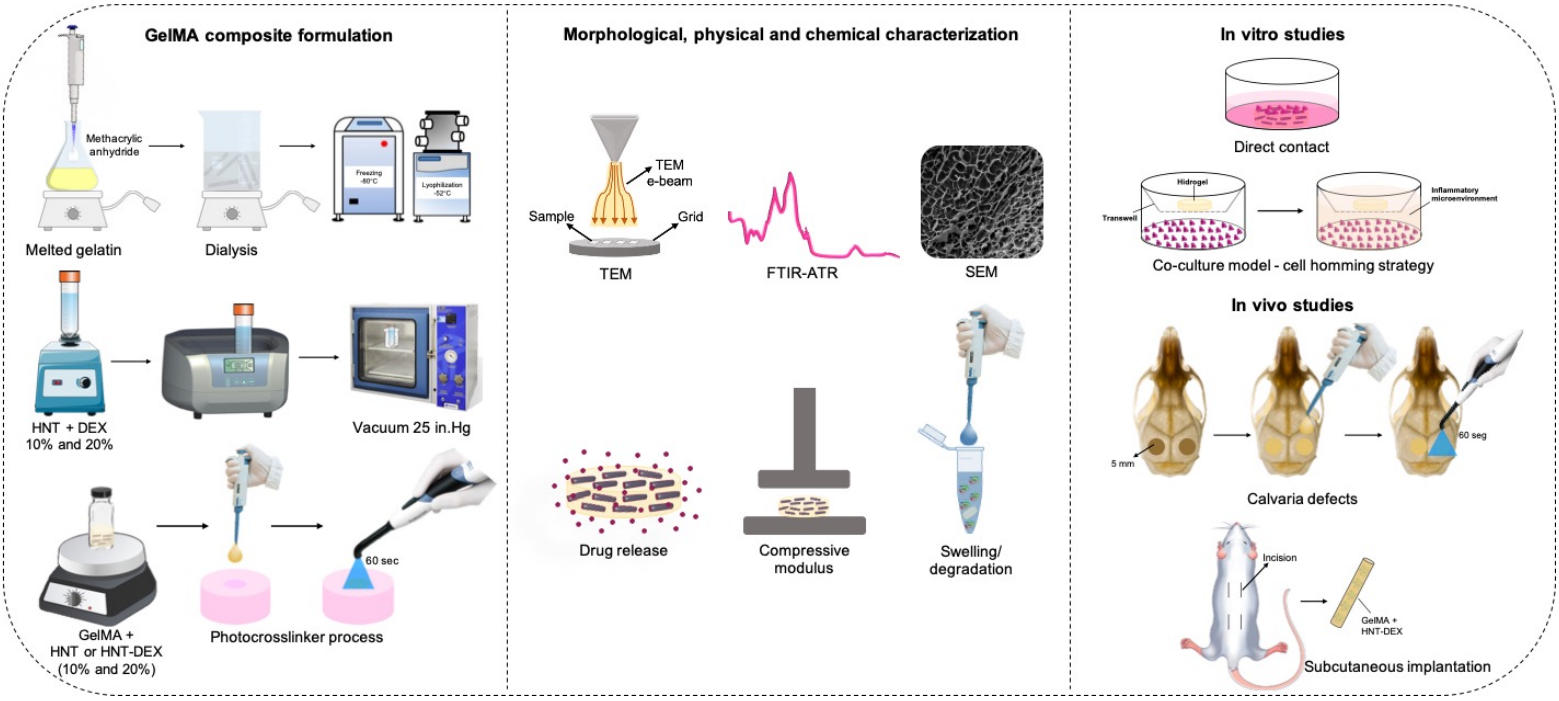

1. Introduction

According to the World Health Organization (WHO), dental caries or tooth decay is one of the world's primary disorders affecting 60-90% of children and most adults [1, 2]. Dental caries is defined as a biofilm-mediated, sugar-driven, multifactorial, dynamic disease that results in the release of acids that gradually destroy mineralized dental tissues [3]. Clinically speaking, if not properly handled, it may lead to the invasion of bacteria, such as *Streptococci* and *Lactobacilli*, and their byproducts toward the pulp. Importantly, if the early-stage dentin infection is appropriately managed, pulp tissue inflammation will recede, and tissue healing, by means of tertiary dentin formation, should ensue, protecting the pulp from further infection. Nonetheless, the success of the therapy depends on the innate regenerative ability of resident pulp cells, the intensity of inflammation generated on the pulp, and the presence of bacterial contamination in the pulp [4, 5].

Calcium hydroxide [$Ca(OH)_2$] cement is widely used clinically when exposed pulp tissue is under reversible inflammation and is free of infection. Pulp tissue in contact with $Ca(OH)_2$ results in the formation of a mineralized barrier capable of sealing pulp exposure. Worth noting, this mineralized tissue comprises a coagulation necrosis area resulting from intense localized toxicity due to the highly alkaline pH of the cement and a disorganized layer of dentin deposited by newly differentiated odontoblast-like cells [4]. This toxicity raises inflammation on the pulp, which may disturb the regenerative potential of resident cells [4]. Therefore, a cell-friendly biomaterial capable of ablating inflammation and promoting odontogenic differentiation of resident pulp stem cells would be a significant advancement to the field of minimally invasive regenerative dentistry. As a result, hydrogels are being investigated due to their injectability and capacity to cater multifunctionality through precise modification with biological cues and/or inorganic nanocontainers that can function as a carrier for therapeutic agents [6]. Additionally, hydrogels offer adjustable biodegradation, good biocompatibility, and a tunable 3D porous polymeric network that plays a crucial role in cell adhesion, proliferation, and phenotype expression [7].

Gelatin methacryloyl (GelMA) is considered an excellent hydrogel candidate for dentin regeneration, as it can be perfectly injected into small, irregular areas, acquiring suitable mechanical properties upon *in situ* photocrosslinking [8]. Of great importance and highly pertinent to the present work, our group recently reported on

the positive modification of GelMA with aluminosilicate clay nanotubes (Halloysite®) to serve as a localized drug delivery system. Precisely, an injectable chlorhexidine-loaded nanotube-modified GelMA hydrogel was synthesized and revealed to be biocompatible, degradable, and provided controlled and sustained release of chlorhexidine, a broad-spectrum antimicrobial for oral and dental infection ablation [9].

Knowing that inflammation plays a crucial role in dentin regeneration, it is extremely rational to devise a drug delivery system with anti-inflammatory action. Therefore, pleiotropic drugs capable of amplifying the odontogenic differentiation ability of pulp stem cells under inflammatory conditions have been deemed a suitable approach to creating drug delivery systems and/or biomaterials for dentin regeneration [10]. For example, dexamethasone (DEX), a synthetic glucocorticoid commonly utilized to treat inflammation [11] has been shown to positively stimulate differentiation of mesenchymal stem cells (MSCs) into odonto/osteogenic phenotypes. Nonetheless, local administration of DEX may induce toxic effects, depending on its concentration, thus impairing the aforesaid differentiation ability [11, 12]. In this work, we postulate that devising a drug delivery system leveraging the proven pleiotropic capacity of DEX with the well demonstrated biocompatibility of GelMA and the controlled release benefits of drug loading into Halloysite® could pave the way towards innovative therapeutic strategy to amplify dentin by resident pulp stem cells under inflammatory environments. To the best of our knowledge, this work is the first to report the fabrication of an injectable, GelMA-based drug delivery system capable of augmenting the odontogenic differentiation of resident cells under pulpal tissue inflammation as potential therapeutics for dentin regeneration.

1. Materials and methods

2.1. Materials and chemicals

Methacrylic anhydride, type A gelatin from porcine skin with ~ 300 g bloom strength, L-ascorbic acid, Triton X-100, cetylpyridinium chloride, β-glycerophosphate disodium salt hydrate, Alizarin red S, and poly(vinylpyrrolidone)-iodine complex were procured from Sigma-Aldrich (St. Louis, MO, USA). Dialysis tube membrane, phosphate-buffered saline (PBS), absolute-200 proof ethanol, fetal bovine serum (FBS), L-glutamine (200 mM), penicillin-streptomycin (5,000 U/mL), alpha-modified

Eagle's medium (α-MEM), and ethanol anhydrous were procured from Thermo Fisher Scientific, Inc. (Waltham, MA, USA). Aluminosilicate clay nanotubes (HNT, Halloysite®, Dragonite HP) were kindly given by Applied Minerals Inc. (New York, NY, USA). Dexamethasone (TCI America, Inc., Portland, OR, USA), SensoLyte® pNPP alkaline phosphatase assay kit (AnaSpec Inc., Fremont, CA, USA), collagenase A (Hoffman La-Roche AG, Basel, Switzerland), CellTiter 96 AQueous One Solution Reagent (Promega Corporation, Madison, WI, USA), isoflurane (Piramal Critical Care, Inc., Bethlehem, PA, USA), Dulbecco's phosphate-buffered saline (DPBS, Gibco Invitrogen Corporation, Grand Island, NY, USA), lithium phenyl-2,4,6-trimethylbenzoylphosphinate (LAP L0290, TCI Chemicals), and normal saline solution (Baxter International Inc., Deerfield, IL, USA), were purchased from their respective manufacturers.

2.2. Gelatin methacryloyl (GelMA) synthesis

The synthesis of GelMA was performed as previously described [9]. In brief, 10 g (w/v) of gelatin type A from porcine skin was solubilized into 100 mL of DPBS at 50 °C. Following that, gelatin methacrylation was carried out by adding methacrylic anhydride dropwise into the solubilized gelatin solution at a rate of 0.5 mL/min for 1 h under stirring conditions. The reaction was interrupted by diluting with 5´ of warm DPBS, and the resulting solution was dialyzed against deionized (DI) water through dialysis tubing (Spectro/Pot, 12-14 kDa molecular weight) at 45 ± 5 °C for 7 days to remove methacrylic acid and non-reacted anhydride. Of note, throughout the dialysis process, the DI water was changed 2´ a day. Next, the prepared solution was frozen at -80 °C overnight, lyophilized (Labconco FreeZone 2.5 L, Labconco Corporation, Kansas City, MO, USA) for 1 week, and stored at -80 °C until further use.

2.3. DEX-loaded nanotube-modified GelMA formulation and characterization

To verify the morphological characteristics of the Halloysite® nanotubes, transmission electron microscopy (TEM, Tecnai BioTWIN, FEI Company, Hillsboro, OR, USA) was performed. In detail, 10 µL of an aqueous dispersion of sieved (< 45 µm) nanotubes was pipetted onto a holey TEM grid (Cu 200 mesh), permitted to air-dry, and imaged at 80 kV. Next, dexamethasone (DEX) loading into the nanotubes was accomplished as described by our group [9]. DEX in powder form was used to

prepare 10% and 20% DEX solutions (w/v) in ethanol anhydrous. Next, previously sieved (<45 μm) nanotubes (1.25 g) and 5 mL of the respective DEX solutions were centrifuged, vortexed for 20 s, and sonicated for 2 h. Then, the mixture was placed in a vacuum (25 in. Hg) chamber (Hi-Temp Vacuum, Thermo Fisher Scientific, Inc.) for 1 h. Following that, the mixture was vortexed for 1 h and the vacuum reapplied. Finally, the HNT/DEX solutions were washed and centrifuged (3000 rpm) for 10 min and then stored at 37 °C for 1 week until fully dried. The dried mixture was once again sieved at 45 μm prior to further use. DEX-loaded nanotubes were obtained (hereafter referred to as H−D10% and H−D20%, respectively). Fourier transform infrared spectroscopy in the attenuated total reflection mode (ATR-FTIR, Nicolet iS50, Thermo Fisher Scientific Inc.) was carried out to assess the drug's presence. In brief, 64 scans with spectra between 4000 and 400 cm^{-1} at 4 cm^{-1} resolutions were used for DEX powder, pristine HNTs, and DEX-loaded nanotubes.

To obtain DEX-loaded nanotube-modified hydrogels, a 20% (w/v) GelMA solution was prepared by dissolving lyophilized GelMA porous foam in DPBS. Next, two different concentrations (2.5 and 5%, w/v) of pristine, as well as DEX-loaded nanotubes (H-DEX10% and H-DEX20%), were incorporated into the GelMA solution and left under vigorous stirring at 50 °C for 1 h until a homogeneous dispersion of the nanotubes was achieved. Next, 0.05% (w/v) of the photoinitiator (LAP) was added to the GelMA solutions. The following GelMA formulations (GelMA [G], G+2.5%HNT [G+2.5H], G+5.0%HNT [G+5.0H], G+2.5%HNT-DEX10% [G+2.5H-D10], G+5.0%HNT-DEX10% [G+5H-D10], G+2.5%HNT-DEX20% [G+2.5H-D20], and G+5.0%HNT-DEX20% [G+5H-D20]) were made to fabricate hydrogel samples for the various assays reported in this work. Briefly, predetermined volumes ranging from 100 to 150 μL of the distinct solutions were pipetted in custom-made silicone (CutterSil Putty PLUS, Kulzer Dental – North America, South Bend, IN, USA) molds, followed by photocrosslinking for 60 s with a dental light-emitting diode (LED) curing device (Bluephase, Ivoclar-Vivadent, Amherst, NY, USA). For morphological analysis, the internal characteristics (microstructure) of the fabricated GelMA-based hydrogels were assessed using scanning electron microscopy (SEM, JMS-6610V, JEOL, Tokyo, Japan) at an accelerating voltage of 12-15 kV on samples sputter-coated with Au.

2.4. Drug release

To determine the amount of drug released from DEX-loaded nanotube-modified GelMA, the distinct hydrogel samples (n=4/group; 8 mm diameter × 3 mm thick) prepared by incorporating 2.5 and 5% amounts of H-D10% and H-D20% were individually immersed into 1.5 mL DPBS containing 1 U/mL of collagenase type I, followed by incubation at 37 °C up to 14 days. At predetermined timepoints the samples were homogenized and 500 μL of supernatant was collected and frozen at -20 °C. Fresh enzymatic solution was replenished with the same amount collected at each timepoint and every 48 h to maintain the enzyme activity. The amount of drug release was determined using a UV–Vis spectrophotometer (SpectraMax iD3, Molecular Devices, LLC, San Jose, CA, USA) at a 242 nm wavelength. DEX concentrations were determined by comparison with a standard curve plotting with known concentrations of DEX.

2.5. Hydrogel swelling and enzymatic degradation

The swelling rate for all GelMA-based hydrogels (*i.e.*, G, G+2.5H, G+5.0H, G+2.5H-D10, G+5H-D10, G+2.5H-D20, and G+5H-D20) was determined by using the known hydration of the formulated gels. In detail, after sample (n=4/group; 6 mm diameter × 2 mm thick) incubation in DPBS at 37 °C for 24 h, wet samples were gently dried with low-lint content tissue paper (Kimberly-Clark Corporation, Irving, TX, USA) and weighed on an analytical balance to obtain wet weights (W_w). The dry weights (W_d) were determined after sample lyophilization. The swelling rate (%) was calculated using the following equation:

$$Swelling\ rate\ (\%) = \frac{Ww - Wd}{Wd} \times 100$$

For degradation analysis, cylindrical-shaped samples (n=4/group) were individually incubated in glass vials (VWR International, LLC, Radnor, PA, USA) with 5 mL DPBS containing 1 U/mL collagenase type I at 37 °C. At predetermined timepoints up to 28 days, each sample was removed from the solution and washed (2×) with sterile DI water, blot-dried, and weighed on an analytical balance. The collagenase-enriched solutions were replaced with fresh solution every 3 days to

keep enzymatic activity constant. The degradation ratio was calculated using the following formula:

$$Degradation\ ratio\ (\%) = \frac{Wt}{Wo} \times 100$$

where W_t is the residual wet weight at distinct timepoints and W_0 is the initial wet weight.

2.6. Biomechanical characterization

To determine the biomechanical properties (*i.e.*, compressive strength and compressive modulus), cylindrical-shaped (n=5/group; 8 mm diameter × 3 mm thick) samples were made. Briefly, 150 µL of the GelMA-based hydrogels was dispensed into custom-made silicone molds followed by 60 s of photocrosslinking. The samples were incubated in DPBS at 37 °C for 24 h. Next, immediately prior to testing, the samples were gently dried, then subjected to unconfined compression at a strain rate of 2 mm/min (expert 5601, ADMET, Inc., Norwood, MA, USA) at RT. The compressive modulus was calculated as the slope of the linear region of the stress-strain curves corresponding with 0-10% strain.

2.7. In vitro biological studies of the DEX-loaded GelMA hydrogels

MSCs from human exfoliated deciduous teeth (SHEDs) were cultured in α-MEM supplemented with 10% FBS, 1% L-glutαmine, and 1% penicillin-streptomycin in an atmosphere of 95% relative humidity and 5%CO_2 at 37 °C, as previously described. Cells at passages 4-6 were used in all experiments. Two experimental designs were performed, as given below:

2.7.1. Direct contact assay

To analyze the biological compatibility and functionality (*i.e.*, bioactivity – induction of odonto/osteogenic differentiation) of GelMA-based formulations, cell viability, activity of alkaline phosphatase (ALP), and mineralized matrix deposition were performed as described below. SHEDs (1×10^4 cells/sample) were seeded in one drop (15 µL) on top of the hydrogels in sextuplicate, followed by incubation for 30 min at 37 °C and 5% CO_2, corresponding to the cell adhesion period on the hydrogel samples. Subsequently, 500 µL of complete α-MEM was then added and

the cell/hydrogel constructs were cultured for 21 days. Cells seeded directly on 48-well plates (Corning Incorporated, Corning, NY, USA) were used as the negative control (SHEDs) and considered to be 100% of cell parameters. *Cell viability*. At predetermined timepoints (up to 21 days), a total of 60 µL of CellTiter 96® AQueous One Solution Cell Proliferation Assay (MTS assay) was added to each well containing 500 µL of fresh, complete medium, and the plate was incubated for 2 h at 37 °C and 5% CO_2 in a humidified atmosphere. Then, 100 µL from each well was transferred into wells of a 96-well plate in triplicate. The absorbance was determined at 490 nm using a plate reader (SpectraMax iD3, Molecular Devices LLC., San Jose, CA, USA). *ALP activity.* For this assay, cell/hydrogel constructs or cells on plates (n=6) were cultured in osteogenic medium (complete α-MEM, 50 mM ascorbic acid, and 10 mM β-glycerophosphate). At predetermined timepoints (7, 14, and 21 days), the samples were incubated for 10 min at 4 °C with a lysis buffer (Triton X-100). The cell/hydrogel constructs were subjected to manual disruption. The supernatant was collected by centrifugation (10,000 g at 4 °C for 15 min), and ALP activity assay was performed using the SensoLyte® pNPP alkaline phosphatase kit. The total protein was determined by the Pierce™ BCA protein assay kit after incubation of the samples for 30 min with the working reagent and measurement of absorbance at 562 nm. ALP activity was determined by data normalization with the total protein. *Mineralized matrix deposition.* Alizarin red staining was performed at 14 and 21 days of culture in osteogenic medium. The cell/hydrogel constructs or cells on plates (n=6) were fixed in 70% ethanol at 4 °C for 1 h, followed by washing in DI water and incubation for 15 min with Alizarin red staining (40 mM, pH 4.2). The samples were washed 5× in DI water. For cells on plates, images of mineralization nodules were captured (BZ-X 710; Keyence Corporation of America, Itasca, IL, USA). To quantify mineralization, the samples were disrupted in 10% cetylpyridinium chloride and absorbance was read at 570 nm. For cell/hydrogel constructs, hydrogel samples with no cells were used as a background control and supernatant was collected by centrifugation (10,000 g at 4 °C for 15 min).

2.7.2. Drug delivery – co-culture model using the transwell approach

To evaluate the potential of selected GelMA-based hydrogel formulations as a potential drug delivery strategy under an inflammatory environment, SHEDs (1.5×10^4

cells/well) were seeded on the bottom of 24-well plates and cultured for 24 h at 37 °C and 5% CO_2 in complete α-MEM. The medium was then replaced by osteogenic medium supplemented or not with 10 µg/mL of lipopolysaccharide (LPS) from *E. coli*. The aforesaid LPS concentration was carefully selected from a systematic dose-response assay aiming to induce a degenerative stimulus on SHEDs capable of reducing its mineralized matrix deposition to ca. 50% without cell toxicity **(Supplement and Fig. S1A)**. To do this, a 24-well transwell system (8 µm pore size, Corning Incorporated) was adapted in the same plate where the cells were cultured, and GelMA hydrogel samples modified or not with 5%HNT and 5%HNT-DEX10% were individually placed in the upper chamber of the transwells to mimic a direct pulp capping clinical scenario. The sets (SHEDs + transwells + hydrogels) were incubated for 21 days and *in vitro* biological assays were performed to determine cell viability (MTS; 1, 7, 14, and 21 days), ALP activity (SensoLyte,® 7, 14, and 21 days), and mineralized matrix deposition (Alizarin red S, 21 days). Cells cultured in osteogenic medium with and without LPS were used as positive and negative controls, respectively.

2.8. In vivo biocompatibility and bone regeneration studies

All animal experiments in rats were approved by the University of Michigan Institutional Animal Care and Use Committee (IACUC, protocol #PRO00008502).

2.8.1. Biocompatibility – subcutaneous implantation model

Twelve 6-week-old male Fischer 344 rats (300-320 g) were allocated (Envigo RMS, Inc., Oxford, MI, USA) to determine the effects of the engineered GelMA-based hydrogels on inflammatory response and overall *in vivo* biocompatibility. All surgical procedures were carried out under general anesthesia induced with inhalation isoflurane (4-5%) and maintained with isoflurane (1-3%). Implantation of the fabricated GelMA hydrogels modified or not with pristine or DEX-loaded nanotubes in dorsal subcutaneous pockets in the rats (n=4/group) was performed, as recently reported by us [9]. After general anesthesia induction, five small distanced subcutaneous pockets were bluntly prepared through short dorsal skin incisions (ca. 12 mm in length), and each animal received 4 sterile polyethylene tubes (1.5 mm inner diameter x 10 mm length; Braintree Scientific, Inc., Braintree, MA, USA) filled with a different experimental group: GelMA (G), GelMA+5%HNT

(G+5.0H), and GelMA+5%HNT-DEX10% (G+5.0H-D10). Sham (unfilled polyethylene tube) was used as a control. After wound closure, the animals were allowed to recover from anesthesia. After 7 days, the animals were euthanized by CO_2 inhalation, and the implants, including adjacent tissue, were retrieved and conventionally processed for histological analysis. Briefly, the explanted samples were fixed overnight in 10% buffered formalin, embedded in paraffin, and cut into 6 µm-thick sections. The histological sections were then stained with Hematoxylin and Eosin (H&E) to investigate for the presence of luminal structures containing red blood and inflammatory cells (Nikon E800, Nikon Corporation, Tokyo, Japan) under light microscopy [13, 14].

2.8.2. Bone regeneration – critical size rat calvarial defects

Eight 6-week-old male Fischer 344 rats (Envigo RMS, Inc.) weighing ca. 300-320 g were used to determine the regenerative capacity of the engineered GelMA-based hydrogels modified with DEX-loaded nanotubes. The surgical procedures were performed under general anesthesia as described in the subcutaneous implantation model. The animal's head was shaved and the surgical site was cleaned with povidone-iodine solution. A sagittal incision was made in the midline region using a scalpel; soft tissue and periosteum were then retracted to expose the calvarial bone. For each animal, full-thickness critical-size (*i.e.*, would not spontaneously heal during the lifetime of the animal) bilateral calvarial defects 5-mm in diameter were created using a trephine bur (Trephines 229XL RA; L Size #229XL-050-RAL, 5.0 mm ID/6.0 mm OD, Meisinger USA, LLC, Centennial, CO, USA) attached to a dental handpiece with a micromotor operating at 800 rpm or less. Constant sterile saline (Baxter International Inc., Deerfield, IL, USA) was irrigated to avoid heat-generated injury during surgery. The animals (n=4) were randomly assigned to Sham (defect only, negative control), GelMA (G), G+5.0%HNT (G+5.0H), and G+5.0%HNT-DEX10% (G+5.0H-D10). The three distinct hydrogel formulations were injected into the created defects and photocrosslinked *in situ* for 60 s with an LED curing-light dental device (Bluephase, Ivoclar-Vivadent). The incision was closed with Vicryl® 3-0 (Ethicon, Inc., Somerville, NJ, USA) resorbable sutures. After surgery, the animals were subcutaneously medicated with non-steroidal anti-inflammatory drugs (5 mg/kg Carprofen® base, Pfizer, Inc., New York, NY, USA). The animals were euthanized 6 weeks post-implantation by conventional CO_2 protocol and the skulls were collected.

Next, skin and muscle tissue were removed, followed by immersion of bone/hydrogel in a 4% paraformaldehyde solution for further assessment of bone regeneration that first included micro-computed tomography (micro-CT), followed by histological analyses by hematoxylin and eosin (H&E) and Masson's trichrome (MT) staining.

Micro-CT (Scanco μCT 100 Medical AG, Scanco Medical AG, Brüttisellen, Switzerland) analysis of the newly formed bone at the artificially created defects was performed as previously described [13, 14]. In brief, samples were scanned with pieces in 360° rotation using 70 kV, 114 μA monochromatic x-rays and 25 μm voxel sizes. The exposure time was kept at an average of 3 frames per 500 ms. The accompanying software (Scanco Medical AG) was utilized for image reconstruction. The reconstructed 3D image was then traced to the circumference of the original defect, which hereafter is referred to as the region of interest (ROI). The ROI of each specimen around the defect was analyzed for tissue volume (TV), bone volume (BV), and bone volume fraction (BVF, BV/TV). Next, following decalcification, the samples were embedded in paraffin, cut into 5-μm thick sections, stained using (H&E to evaluate for the presence of luminal structures containing red blood and inflammatory cells, and MT staining to identify osteoid (red) and mineralized bone tissue (blue). Photomicrographs were taken using a digital camera coupled to the light microscope.

2.9. Statistical analysis

Data collected from two independent experiments were analyzed by one- or two-way ANOVA, followed by Tukey's multiple post-hoc test. A *p*-value of less than 0.05 was considered to be statistically significant.

3. Results and discussion

Our findings confirm the of a controlled release delivery system for dexamethasone from an injectable GelMA-based nanotube-modified hydrogel, demonstrating the potential of this system for mineralized tissue regeneration. Overall, DEX-loaded nanotube-modified GelMA hydrogel, more specifically, the G+5H-D10 formulation (GelMA+5.0%HNT-DEX10%), showed suitable mechanical properties, biodegradability, cytocompatibility with MSCs (SHEDs), *in vivo* biocompatibility, and it also supported greater bone formation in a critical-size defect model in rats.

3.1. DEX-loaded nanotube-modified GelMA hydrogels

TEM images of the aluminosilicate clay (Halloysite®, HNTs) nanocontainers utilized in the fabrication of DEX-loaded nanotube-modified hydrogels are shown in **Fig. 1A-B**. A typical tubular morphology with a defined open lumen measuring around 150 nm to 500 nm in length and approximately 35 nm to 75 nm in diameter can be seen **(Fig. 1A)**. According to the literature, at a pH below 8.5, HNTs exhibit a positively-charged lumen surface and negatively charged outer surface, making negatively charged drugs, such as DEX, to be preferentially loaded inside the lumen [15]. Here, to obtain DEX-loaded nanotubes, DEX was dissolved in 100% ethanol, since it has been demonstrated that DEX loading is greater at higher ethanol-to-water ratio, as DEX solubility increases. DEX loading/impregnation into the nanotubes was assessed by FTIR. Analysis of pristine HNTs revealed peaks at 3750 cm^{-1} associated with Al_2-OH stretching vibration and an asymmetrical strong peak at 1100 cm^{-1}, corresponding to Si-O bond. DEX powder exhibited a smooth band at 3387 cm^{-1} relative to stretch vibrations of -OH and -NH_2, as well as at 1100 cm^{-1} and 1200 cm^{-1} related to C-C and C-O-C bonds, respectively. When evaluating DEX-loaded nanotubes (HNT-DEX10% and HNT-DEX20%), small peaks at 1660 and 1670 cm^{-1} attributed to the amide I band, suggest DEX conjugation with nanotubes **(Fig. 1B)**.

HNTs have proven to be a suitable strategy for promoting sustained drug release when associated with GelMA, since they can be fairly homogeneously dispersed into the hydrogel structure and do not interfere with the overall hydrogel porous microstructure [9]. In **Fig. 2A**, the SEM images demonstrate that the porous architecture of GelMA was not drastically affected by HNT-DEX10% incorporation, regardless of the loading amount (2.5% vs. 5%). On the other hand, GelMA modified with HNT-DEX20% revealed a heterogenous porous matrix. High magnification SEM images suggest the presence of HNTs dispersed throughout the hydrogel surface **(Fig. 2A)**. Veerabadran et al. first described the encapsulation of DEX into HNTs, and demonstrated 75´ times longer release of HNT-DEX compared to DEX microcrystals, when the samples were immersed in water at pH 7.4 [15]. In the present study, two DEX solution concentrations (10% and 20%) were used to load DEX into HNTs prior to DEX-loaded nanotube incorporation at two distinct amounts

(2.5 and 5%) into GelMA to refine the most promising drug delivery candidate for pre-clinical *in vivo* analyses in rat models of biocompatibility and mineralized tissue regeneration. Overall, DEX release occurred in a dose-dependent manner. **Fig. 2B** shows the release profiles of DEX-loaded nanotube-modified GelMA formulations. A steady increase in DEX release was observed for all groups up to 15 h, which was then sustained for G+5.0H-D20 and G+2.5H-D20 groups till day 7, followed by a significant reduction of DEX liberation by day 14. Meanwhile, the G+2.5H-D10 and G+5.0H-D10 formulations experienced a sustained reduction in the amount of DEX release up to day 7, with minimal release by day 14. Taken together, the initial fast release of DEX might be related to its bounded presence at the outer surface of incomplete rolled nanotubes, which leads to exposure of some inner alumina layer [15].

3.2. Degradation, swelling, and biomechanical analyses of DEX-loaded nanotube-modified GelMA

Besides biological functionalities, the design of hydrogels to act as drug delivery systems should also consider biomaterials' parameters, such as degradation, swelling, and biomechanical properties compatible with the intended clinical application. Indeed, the gradual degradation of biomaterials is key to supporting the differentiation of stem cells and should match the rate of new tissue formation [16]. In this study, the effect of DEX-loaded nanotube incorporated into GelMA hydrogel was investigated by mass loss and swelling experiments. The degradation profile of the engineered hydrogels was assessed up to 28 days in an incubation medium containing collagenase. Our GelMA formulation (20%, w/v) featured a controlled degradation rate (G), even under enzymatic challenge, with a mass loss of 24.6%, 30.5%, and 38.5% at 14, 21, and 28 d, respectively **(Fig. 3A)**. This is an important feature, since a previous study in our group demonstrated that GelMA at 15% started to degrade immediately after incubation in a similar enzymatic challenge, with total mass loss detected after 21 days [9]. Thus, the more stable degradation profile seems to be related to GelMA concentration, agreeing with previous studies [9]. Overall, nanotube incorporation, regardless of DEX presence, increased GelMA degradability in a dose-dependent manner. The greater degradability values were associated with groups modified with 5%HNT (*i.e.*, G+5H, G+5H-10D, and G+5H-20D). Nonetheless, it is important to note that all groups remained stable up to 7

days, with a mass loss varying from 13% to 30% at 14 days **(Fig. 3A)**. Cidonio et al. found that clay nanoparticles (Laponite) interfered with GelMA's degradation, where increased soluble fraction was observed [17]. The authors demonstrated that 5%, 7.5%, and 10% GelMA concentrations featured an intense degradation profile after the incorporation of 0.5 to 1% wt.% Laponite. Enhanced soluble fraction occurred regardless of Laponite concentration and increased swelling ratio. Indeed, Ribeiro et al. detected an increased swelling ratio for 15% GelMA after incorporation of 1-5% wt.% HNTs [9]. Meanwhile, in the present study, 20% GelMA modified with nanotubes revealed no significant alteration on swelling ratio, irrespective of HNT concentration and DEX presence **(Fig. 3B)**. This indicates that the original structure of GelMA was maintained, with no alteration in the polymer network after interaction between the hydroxyl groups present on HNTs surface with the hydroxyl groups of GelMA [18, 19]. Therefore, one may conclude that GelMA at 20% seems to be an adequate drug delivery platform when using nanotubes as the carrier, since it displayed a suitable degradation profile over 28 days, with formulations containing DEX showing nearly 80% mass loss, which, in turn, could be of significant importance to support mineralized tissue regeneration *in vivo*.

Recent studies have reported that the incorporation of optimal amounts of nanoparticles into hydrogels' composition represents a viable approach to enhance compressive modulus [20-22]. According to **Fig. 3C**, the incorporation of nanotubes modified or not with DEX significantly increased the compressive modulus of GelMA-based hydrogels, except for G+2.5H, which featured no differences from unmodified GelMA (G). Thus, the formulations tested maintained a constant degree of methacrylation, even with the incorporation of HNTs into the hydrogel structure, without intervening negatively in the mechanical behavior **(Fig. 3D)**.

3.3. Biological characterization of GelMA HNT-DEX composite

To assess the cytocompatibility and bioactive potential of GelMA formulations, MSCs from pulp tissue (SHEDs) were seeded onto photocrosslinked hydrogels. Cells seeded directly onto the plates were used as negative control for all *in vitro* experiments. An MTS-based cell viability assay demonstrated that nanotube incorporation with or without DEX did not lead to cell toxicity over 21 days **(Fig. 4A)**. Importantly, at 21 days, a significant increase in the percentage of cell viability was observed for all groups in comparison to the control. It seems that the cell interaction

mediated by GelMA is a consequence of its composition, since gelatin presents RGD sequences that favor cell attachment and proliferation [23, 24]. Moreover, the compatibility and increased proliferative potential of fibroblasts, osteoblasts, and pulp cells on GelMA have been demonstrated [23, 24].

To assess the odonto/osteogenic potential of the DEX-loaded nanotube-modified hydrogels, SHEDs were cultured on the different formulations and assayed for ALP activity and mineralized matrix formation. Analysis of ALP expression has been used to determine cell differentiation, since ALP is an enzyme deposited by cells with osteo/odontoblastic phenotype in the early stages of mineralized tissue formation [25]. In this study, when SHEDs were cultured in direct contact with G+5H, G+2.5H-D10, and G+5H-D10, a significantly higher ALP activity was observed in comparison with the control groups (cells only and unmodified GelMA, G) at 14 days **(Fig. 4B)**. Enhanced mineralized matrix deposition occurred at 14 and 21 days for cells cultured on G+2.5H-D10 and G+5H-D10, with a significant difference in comparison to the control and G groups. The highest mineralized matrix deposition was seen at 21 days for SHEDs cultured on G+2.5H-D10 and G+5H-D10 **(Fig. 4C)**. The osteogenic potential of DEX-loaded nanotube-modified hydrogels at the lowest DEX concentration (*i.e.*, 2.5H-D10 and 5.0H-D10) may be explained by the lower amount of DEX release in comparison to groups containing nanotubes modified with DEX20% – 2.5H-D20 and 5.0H-D20. According to the literature, depending on the DEX concentration, MSCs can undergo adipogenic, chondrogenic, or myogenic differentiation [26]. A gradual and sustained liberation of low doses of DEX through different drug release systems has proven to be key in promoting osteogenic differentiation of MSCs by upregulating RUNX2, COL-1, BMP-2, OCN, and ALP gene expression [27].

3.4. DEX-loaded nanotube-modified hydrogel as a multifunctional drug delivery strategy

In the clinical scenario, exposed pulps are often under inflammatory conditions, since odontoblasts recognize bacterial components diffused through dentin tubules to elicit innate immune tissue response by triggering the Toll-like receptor 2 and 4 (TLR2 and TLR4) [28]. This process leads to pro-inflammatory mediators' expression, such as IL-1β and TNF-α cytokines, which are rapidly released in

infected or injured tissues [29]; nevertheless, these cytokines at high concentration can suppress the stem cells' regenerative capability since they down-regulate the expression of odontoblastic phenotype, reducing or even impairing mineralized matrix deposition [30-33].

To assess potential of the most promising DEX-loaded nanotube-modified GelMA formulation (*i.e.*, G+5.0-D10) as a multifunctional therapeutic platform to amplify dentin regeneration under an inflammatory microenvironment, we performed an *in vitro* indirect contact assay using a transwell to house the hydrogel while assessing the effects of DEX release on LPS-treated SHEDs cultured on the bottom of the tissue culture plate. Recent studies have demonstrated the relevance of low intensity pulp inflammation on activation of MSCs-mediated tissue regeneration. The authors reinforced the efficient *in vitro* LPS treatment to mimic the *in vivo* damage in cells to stimulate self-repair [34, 35]. Therefore, based on our pilot studies, we performed the aforementioned assay using an optimized LPS concentration capable of reducing the odonto/osteogenic differentiation of SHEDs without negatively interfering with cell viability (Supplement). According to **Fig. S1A**, all LPS concentrations tested were not cytotoxic; a slight reduction in cell viability by 13.6% and 16% was observed in those groups treated with 10 μg/mL of LPS at 14 days and 0.025 μg/mL of LPS at 21 days, respectively. LPS concentrations of 0.1 μg/mL, 1.0 μg/mL, and 10 μg/mL significantly decreased the differentiation capacity of SHEDs, according to the data from the Alizarin red assay **(Supplement, Fig. S1B-C)**.

The positive effect of G+5H-D10 on SHEDs was observed on day 1, when cell viability increased by 37% in comparison to the control (LPS-). A lack of significant differences was observed for the other groups at all timepoints, demonstrating that LPS treatment did not influence cell viability in the presence of GelMA-based hydrogels **(Fig. 5A)**. According to our data, DEX-loaded nanotube-modified GelMA (*i.e.*, G+5.0H-D10) increased the odonto/osteogenic potential of SHEDs when cultured in the presence of the proposed drug delivery system. In detail, significant increases in ALP activity were detected at 14 and 21 days for the G+5.0H-D10 group in comparison to all other groups, irrespective of LPS treatment. This positive effect was also observed for Alizarin red assay, with an increase in mineralized matrix deposition in comparison to the control of ~ 50.5% in the absence of LPS. A more intense effect was detected for LPS-treated cells, with an increase of 119.4% in comparison to the control (LPS+). When we compared these groups with plain

GelMA (G), we detected a 70.5% and 83.8% increase for G+5H-D10 in the absence and presence of LPS, respectively. As expected, LPS treatment promoted a significant reduction in differentiation capacity of SHEDs seeded on the bottom of the tissue culture plate (control), validating the experimental model used. In the control (LPS+), a significant reduction of 32% and 65% on ALP activity **(Fig. 5B)** and mineralized matrix deposition **(Fig. 5C-D)**, respectively, was observed in comparison to the control (LPS-) at 21 days. Nevertheless, it is interesting to note that in the presence of GelMA, irrespective of nanotube incorporation, LPS had no significant effect on ALP activity and mineralized matrix deposition, as no significant differences were observed between the LPS+ and LPS- homologous groups. Therefore, it seems that GelMA had a protective effect on LPS-stimulated SHEDs *in vitro*, which is probably due to RGD sequences' release from its structure that positively modulates cell behavior [36-40]. The RGD motifs remain active and available to interact with cells after reaction of methacrylic anhydride in gelatin [41], and these sequences can be released into the culture medium as GelMA suffers hydrolysis [9]. Biomaterials prepared with ECM proteins, such as GelMA, have recently mimicked the natural regulatory role of the matrix in the immune system, favoring the longevity and functionality of implants. According to a recent study, digested soluble ECM fragments are capable of modulating cell behavior and exhibiting immunomodulatory function during tissue remodeling, thus playing a role in homeostatic control [42]. In the present study, the engineered DEX-loaded nanotube-modified hydrogel (G+5.0H-10D) demonstrated a positive effect on LPS-treated cells likely due to the release pattern mediate by the aforementioned hydrogel formulation, where higher DEX amounts were release initially, followed by a gradual decrease in DEX concentration over time **(Fig. 2B)**. Qi et al. (2018) [43] demonstrated that a two-stage release pattern of DEX obtained by gelatin nanoparticles was essential to promote TNFα downregulation on RAW 264.7 cells, along with osteogenesis induction on MC3T3-E1 cells, by up-regulating the expression levels of RUNX2, COL-1, OCN, ALP, and increasing calcium deposition. From a clinical standpoint, others have found that DEX improves mineralized dentin bridge deposition in cases of pulp exposure *in vivo* with the maintenance of pulp vitality without the presence of inflamed tissue [44-46].

3.5. In vivo biocompatibility and bone regeneration

To evaluate the biocompatibility of DEX-loaded nanotube-modified GelMA, polyethylene (PE) tubes filled with GelMA (G), GelMA+5.0%HNT (G+5.0H), or GelMA+5.0%HNT-DEX10% (G+5.0H-D10) were subcutaneously implanted in rats **(Fig. 6A)**. After 7 days, host tissue response at the tubes' opening was evaluated in comparison to SHAM (*i.e.*, implantation of unfilled PE tubes). Representative images of H&E-stained sections of the explants are shown in **Fig. 6B**. Minimal inflammatory cell infiltration, mainly restricted to the borders of the PE tubes, were detected for G+5.0H and G+5.0H-D10 hydrogels. Of note, a thin fibrous capsule was observed between the hydrogel and the adjacent connective tissue, which exhibited several dilated and congested blood vessels and a few mononuclear inflammatory cells. Such as shown in the control group (PE), in G+5.0H, connective tissue with large areas of edema, a few inflammatory cells, and blood vessels were observed adjacent to the thin, fibrous capsule formed in contact with the G+5.0H inserted into the tube. Also, an ingrowth of blood vessels was observed at sparse locations around the borders of both the G+5.0H and G+5.0H-D10 groups, indicating material biocompatibility with angiogenesis. The findings of this work are in agreement with previous studies that have supported GelMA biocompatibility *in vivo* [5, 47].

To determine *in vivo* the regenerative capacity of DEX-loaded nanotube-modified hydrogel (*i.e.*, G+5.0H-D10), the same GelMA-based formulations implanted subcutaneously were selected for implantation in surgically created critical-size cranial defects in rats **(Fig. 7)**. Micro-CT analysis shows a statistically significant increase in total bone volume for both nanotube-modified GelMA groups when compared to the SHAM and unmodified GelMA (G) controls **(Fig. 8A-B)**. However, the highest bone volume occurred in the GelMA hydrogel containing dexamethasone (G+5.0H-D10). When total bone volume was normalized by total volume, it was determined that G, G+5.0H, and G+5.0H-D10 presented values greater than the SHAM group, with the latter featuring the highest volume. For histological examination, the defects were cut perpendicular at the central line of the defect area and the cut slide section were stained using H&E and Masson's trichrome (MT). The defect area in the negative control (sham) was filled with fibrous connective tissue and a very small amount of bone was formed near the edges **(Fig. 8A and Fig. 9)**. The early phase of new bone formation was observed at the margin of the calvarial defect in the unmodified GelMA (G) and nanotube-modified hydrogels; however, in

the GelMA hydrogel, inflammatory cells and collagen fibers were more frequently observed. Meanwhile, in defects treated with G+5.0H and G+5.0H-D10, newly formed bone was well integrated from the original edges of the defect and small osseous islands were also observed. Cidonio et al. demonstrated that GelMA containing aluminosilicate clay nanoparticles enhanced the mineralization potential of bone marrow stem cells, and this effect was improved by DEX supplementation in the culture medium [17]. The positive osteogenic effect of DEX-free nanotube-modified GelMA (G+5.0H) may be attributed to the increased hydrogel compressive modulus upon HNTs' incorporation **(Fig. 3C)**, thus agreeing with previous studies that assessed the role of hydrogel stiffness on cell behavior; while stiffer hydrogels increased cell spreading and osteogenic differentiation, softer hydrogels were prone to form cell aggregates that resulted in adipogenic differentiation [48].

In the present study, lithium acylphosphinate salt (LAP) was selected as the photoinitiator for GelMA, since it is capable of absorbing light in the visible region [49]. This biomaterial was injected into bone defects and then photocrosslinked with a light-emitting diode (LED) curing-light device. The interesting data obtained using this *in vivo* protocol demonstrated the biocompatibility and possible clinical applicability of the proposed DEX-loaded nanotube-modified GelMA hydrogel. Moreover, mineralized tissue was present in the center of bone defects filled with G+5%HNT and G+5%HNT-DEX **(Fig. 8 and Fig. 9)**, demonstrating that cells from surrounding tissue were able to migrate to the material surface and infiltrating deeply into the GelMA porous architecture. This feature is essential for the success of tissue engineering strategies, since the biomaterial should act as a permeable template to provide a temporary ECM for neotissue formation [50, 51]. Therefore, the engineered drug delivery system composed by GelMA containing HNTs loaded with 10% DEX seemed to be a very promising alternative for dentin tissue regeneration, since it recruited adjacent cells and induced their proliferation, differentiation, and local maturation.

4. Conclusions

In this study, a cytocompatible, biodegradable, DEX-loaded nanotube-modified GelMA hydrogel was formulated for sustained release of DEX for mineralized tissue regeneration under inflammation. Taking into consideration that DEX release led to

similar ALP expression and mineralized nodule formation in LPS-stimulated and non-stimulated SHEDs, this indicates that DEX exerted the protective role against inflammation. The proposed hydrogel induced a favorable tissue response marked by small presence of inflammatory cells in subcutaneous implantation and demonstrated enhanced mineralized tissue regeneration in a critically-sized defect model. Altogether, our findings show that the proposed injectable DEX-loaded nanotube-modified multifunctional hydrogel is considered a promising drug delivery system for potential applications in mineralized tissue regeneration under inflammation.

Declaration of Competing Interest

The authors declare no competing financial interest or with respect to the authorship and/or publication of this article.

Acknowledgements

M.C.B. acknowledges the National Institutes of Health (NIH)/National Institute of Dental and Craniofacial Research (Grants K08DE023552 and R01DE026578), the OsteoScience Foundation (Peter Geistlich Research Award), the International Association for Dental Research (IADR-GSK Innovation in Oral Care Award), and the American Academy of Implant Dentistry Foundation (AAIDF). The first author was supported by a Scholarship from the São Paulo State Research Foundation – FAPESP (grants # 2016/15674-5 and 2018/14257-7).

Declaration of Competing Interest

The authors declare no competing financial interest or with respect to the authorship and/or publication of this article.

References

[1] P.E. Petersen, M.A. Lennon, Effective use of fluorides for the prevention of dental caries in the 21st century: the WHO approach, Community Dent Oral Epidemiol 32(5) (2004) 319-21.

[2] A.J. Fleming E, Prevalence of Total and Untreated Dental Caries Among Youth: United States, 2015–2016, Hyattsville, MD: National Center for Health Statistics MD: National Center for Health Statistics, 2018.

[3] N.B. Pitts, D.T. Zero, P.D. Marsh, K. Ekstrand, J.A. Weintraub, F. Ramos-Gomez, J. Tagami, S. Twetman, G. Tsakos, A. Ismail, Dental caries, Nat Rev Dis Primers 3 (2017) 17030.

[4] C.A. de Souza Costa, J. Hebling, D.L. Scheffel, D.G. Soares, F.G. Basso, A.P. Ribeiro, Methods to evaluate and strategies to improve the biocompatibility of dental materials and operative techniques, Dent Mater 30(7) (2014) 769-84.

[5] A.B. Paula, M. Laranjo, C.M. Marto, S. Paulo, A.M. Abrantes, B. Fernandes, J. Casalta-Lopes, M. Marques-Ferreira, M.F. Botelho, E. Carrilho, Evaluation of dentinogenesis inducer biomaterials: an in vivo study, J Appl Oral Sci 28 (2020) e20190023.

[6] J.M. Campos, A.C. Sousa, A.R. Caseiro, S.S. Pedrosa, P.O. Pinto, M.V. Branquinho, I. Amorim, J.D. Santos, T. Pereira, C.M. Mendonça, A. Afonso, L.M. Atayde, A.C. Maurício, Dental pulp stem cells and Bonelike, Regen Biomater 6(1) (2019) 49-59.

[7] M. Kouhi, J. Varshosaz, B. Hashemibeni, A. Sarmadi, Injectable gellan gum/lignocellulose nanofibrils hydrogels enriched with melatonin loaded forsterite nanoparticles for cartilage tissue engineering: Fabrication, characterization and cell culture studies, Mater Sci Eng C Mater Biol Appl 115 (2020) 111114.

[8] C.H. Lin, J.J. Su, S.Y. Lee, Y.M. Lin, Stiffness modification of photopolymerizable gelatin-methacrylate hydrogels influences endothelial differentiation of human mesenchymal stem cells, J Tissue Eng Regen Med 12(10) (2018) 2099-2111.

[9] J.S. Ribeiro, E.A.F. Bordini, J.A. Ferreira, L. Mei, N. Dubey, J.C. Fenno, E. Piva, R.G. Lund, A. Schwendeman, M.C. Bottino, Injectable MMP-Responsive Nanotube-Modified Gelatin Hydrogel for Dental Infection Ablation, ACS Appl Mater Interfaces 12(14) (2020) 16006-16017.

[10] D.G. Soares, Z. Zhang, F. Mohamed, T.W. Eyster, C.A. de Souza Costa, P.X. Ma, Simvastatin and nanofibrous poly(l-lactic acid) scaffolds to promote the odontogenic potential of dental pulp cells in an inflammatory environment, Acta Biomater 68 (2018) 190-203.

[11] H.C. Lim, O.H. Nam, M.J. Kim, A. El-Fiqi, H.M. Yun, Y.M. Lee, G.Z. Jin, H.H. Lee, H.W. Kim, E.C. Kim, Delivery of dexamethasone from bioactive nanofiber matrices stimulates odontogenesis of human dental pulp cells through integrin/BMP/mTOR signaling pathways, Int J Nanomedicine 11 (2016) 2557-67.

[12] A. Daghrery, Z. Aytac, N. Dubey, L. Mei, A. Schwendeman, M.C. Bottino, Electrospinning of dexamethasone/cyclodextrin inclusion complex polymer fibers for dental pulp therapy, Colloids and Surfaces B: Biointerfaces 191 (2020) 111011.

[13] N. Dubey, J.A. Ferreira, A. Daghrery, Z. Aytac, J. Malda, S.B. Bhaduri, M.C. Bottino, Highly tunable bioactive fiber-reinforced hydrogel for guided bone regeneration, Acta Biomater (2020).

[14] N. Dubey, J.A. Ferreira, J. Malda, S.B. Bhaduri, M.C. Bottino, Extracellular Matrix/Amorphous Magnesium Phosphate Bioink for 3D Bioprinting of Craniomaxillofacial Bone Tissue, ACS Appl Mater Interfaces 12(21) (2020) 23752-23763.

[15] N.G. Veerabadran, P.L. Goli, S.S. Stewart-Clark, Y.M. Lvov, D.K. Mills, Nanoencapsulation of stem cells within polyelectrolyte multilayer shells, Macromol Biosci 7(7) (2007) 877-82.

[16] M. Nakashima, A. Akamine, The application of tissue engineering to regeneration of pulp and dentin in endodontics, J Endod 31(10) (2005) 711-8.

[17] G. Cidonio, C.R. Alcala-Orozco, K.S. Lim, M. Glinka, I. Mutreja, Y.H. Kim, J.I. Dawson, T.B.F. Woodfield, R.O.C. Oreffo, Osteogenic and angiogenic tissue formation in high fidelity nanocomposite Laponite-gelatin bioinks, Biofabrication 11(3) (2019) 035027.

[18] H. Wang, L. Zhou, J. Liao, Y. Tan, K. Ouyang, C. Ning, G. Ni, G. Tan, Cell-laden photocrosslinked GelMA-DexMA copolymer hydrogels with tunable mechanical properties for tissue engineering, J Mater Sci Mater Med 25(9) (2014) 2173-83.

[19] H.A. MJ Saif , M Naveed, Properties and modification methods of halloysite nanotubes: a state-of-The-art review, Journal of the Chilean Chemical Society 63 (2018).

[20] S. Pacelli, R. Maloney, A.R. Chakravarti, J. Whitlow, S. Basu, S. Modaresi, S. Gehrke, A. Paul, Controlling Adult Stem Cell Behavior Using Nanodiamond-Reinforced Hydrogel: Implication in Bone Regeneration Therapy, Sci Rep 7(1) (2017) 6577.

[21] M. Zhuang, Z. Liu, Y. Ding, G.L. Xu, Y. Li, A. Tyagi, X. Zhang, C.J. Sun, Y. Ren, X. Ou, H. Wong, Y. Cai, R. Wu, I.H. Abidi, Q. Zhang, F. Xu, K. Amine, Z. Luo, Methacrylated gelatin-embedded fabrication of 3D graphene-supported Co, Nanoscale 11(14) (2019) 6866-6875.

[22] L. Qu, N. Dubey, J.S. Ribeiro, E.A.F. Bordini, J.A. Ferreira, J. Xu, R.M. Castilho, M.C. Bottino, Metformin-loaded nanospheres laden photocrosslinkable gelatin hydrogel for bone tissue engineering, Journal of the Mechanical Behavior of Biomedical Materials (2020) 104293.

[23] L.E. Bertassoni, J.C. Cardoso, V. Manoharan, A.L. Cristino, N.S. Bhise, W.A. Araujo, P. Zorlutuna, N.E. Vrana, A.M. Ghaemmaghami, M.R. Dokmeci, A. Khademhosseini, Direct-write bioprinting of cell-laden methacrylated gelatin hydrogels, Biofabrication 6(2) (2014) 024105.

[24] M. Ha, A. Athirasala, A. Tahayeri, P.P. Menezes, L.E. Bertassoni, Micropatterned hydrogels and cell alignment enhance the odontogenic potential of stem cells from apical papilla in-vitro, Dent Mater 36(1) (2020) 88-96.

[25] J. Jensen, D.C. Kraft, H. Lysdahl, C.B. Foldager, M. Chen, A.A. Kristiansen, J.H. Rölfing, C.E. Bünger, Functionalization of polycaprolactone scaffolds with hyaluronic acid and β-TCP facilitates migration and osteogenic differentiation of human dental pulp stem cells in vitro, Tissue Eng Part A 21(3-4) (2015) 729-39.

[26] N.A. Nguyen, C.C. Bowland, A.K. Naskar, A general method to improve 3D-printability and inter-layer adhesion in lignin-based composites, Applied Materials Today 12 (2018) 138-152.

[27] M. Qi, J. Hu, J. Li, J. Li, W. Dong, X. Feng, J. Yu, Effect of zoledronate acid treatment on osseointegration and fixation of implants in autologous iliac bone grafts in ovariectomized rabbits, Bone 50(1) (2012) 119-27.

[28] A.-L.B. Farges JC, Renard E, Ducret M, Gaudin A, Smith AJ, Cooper PR., Dental pulp defense and repair mechanisms in dental caries. , Mediators Inflamm 2015:230251. (2015).

[29] T. Lawrence, The nuclear factor NF-kappaB pathway in inflammation, Cold Spring Harb Perspect Biol 1(6) (2009) a001651.

[30] G. Spoto, M. Fioroni, C. Rubini, D. Tripodi, M. Di Stilio, A. Piattelli, Alkaline phosphatase activity in normal and inflamed dental pulps, J Endod 27(3) (2001) 180-2.

[31] K.S. Min, Y.Y. Kwon, H.J. Lee, S.K. Lee, K.H. Kang, E.C. Kim, Effects of proinflammatory cytokines on the expression of mineralization markers and heme oxygenase-1 in human pulp cells, J Endod 32(1) (2006) 39-43.

[32] F.W. Paula-Silva, A. Ghosh, L.A. Silva, Y.L. Kapila, TNF-alpha promotes an odontoblastic phenotype in dental pulp cells, J Dent Res 88(4) (2009) 339-44.

[33] D.J. Alongi, T. Yamaza, Y. Song, A.F. Fouad, E.E. Romberg, S. Shi, R.S. Tuan, G.T. Huang, Stem/progenitor cells from inflamed human dental pulp retain tissue regeneration potential, Regen Med 5(4) (2010) 617-31.

[34] Y. Gao, X. You, Y. Liu, F. Gao, Y. Zhang, J. Yang, C. Yang, Induction of autophagy protects human dental pulp cells from lipopolysaccharide-induced pyroptotic cell death, Exp Ther Med 19(3) (2020) 2202-2210.

[35] G. Sun, Q. Ren, L. Bai, L. Zhang, Phoenixin-20 suppresses lipopolysaccharide-induced inflammation in dental pulp cells, Chem Biol Interact 318 (2020) 108971.

[36] J. Sottile, D.C. Hocking, K.J. Langenbach, Fibronectin polymerization stimulates cell growth by RGD-dependent and -independent mechanisms, J Cell Sci 113 Pt 23 (2000) 4287-99.

[37] C. Chollet, S. Lazare, F. Guillemot, M.C. Durrieu, Impact of RGD micro-patterns on cell adhesion, Colloids Surf B Biointerfaces 75(1) (2010) 107-14.

[38] A. Lagunas, J. Comelles, E. Martínez, E. Prats-Alfonso, G.A. Acosta, F. Albericio, J. Samitier, Cell adhesion and focal contact formation on linear RGD molecular gradients: study of non-linear concentration dependence effects, Nanomedicine 8(4) (2012) 432-9.

[39] A. Grigore, B. Sarker, B. Fabry, A.R. Boccaccini, R. Detsch, Behavior of encapsulated MG-63 cells in RGD and gelatine-modified alginate hydrogels, Tissue Eng Part A 20(15-16) (2014) 2140-50.

[40] N.N.T. Le, S. Zorn, S.K. Schmitt, P. Gopalan, W.L. Murphy, Hydrogel arrays formed via differential wettability patterning enable combinatorial screening of stem cell behavior, Acta Biomater 34 (2016) 93-103.

[41] K. Yue, G. Trujillo-de Santiago, M.M. Alvarez, A. Tamayol, N. Annabi, A. Khademhosseini, Synthesis, properties, and biomedical applications of gelatin methacryloyl (GelMA) hydrogels, Biomaterials 73 (2015) 254-71.

[42] A.T. Rowley, R.R. Nagalla, S.W. Wang, W.F. Liu, Extracellular Matrix-Based Strategies for Immunomodulatory Biomaterials Engineering, Adv Healthc Mater 8(8) (2019) e1801578.

[43] H. Qi, Q. Chen, H. Ren, X. Wu, X. Liu, T. Lu, Electrophoretic deposition of dexamethasone-loaded gelatin nanospheres/chitosan coating and its dual function in anti-inflammation and osteogenesis, Colloids Surf B Biointerfaces 169 (2018) 249-256.

[44] R.D.C. Moretti, M.T. Duailibi, P.O. Martins, J.A. Dos Santos, S.E. Duailibi, Osteoinductive effects of preoperative dexamethasone in human dental pulp stem cells primary culture, Future Sci OA 3(3) (2017) FSO184.

[45] S.A. Mousavi, J. Ghoddusi, N. Mohtasham, S. Shahnaseri, P. Paymanpour, J. Kinoshita, Human Pulp Response to Direct Pulp Capping and Miniature Pulpotomy with MTA after Application of Topical Dexamethasone: A Randomized Clinical Trial, Iran Endod J 11(2) (2016) 85-90.

[46] M.L. Porter, E.A. Münchow, M.T. Albuquerque, K.J. Spolnik, A.T. Hara, M.C. Bottino, Effects of Novel 3-dimensional Antibiotic-containing Electrospun Scaffolds on Dentin Discoloration, J Endod 42(1) (2016) 106-12.

[47] P. Trongkij, S. Sutimuntanakul, P. Lapthanasupkul, C. Chaimanakarn, R.H. Wong, D. Banomyong, Pulpal responses after direct pulp capping with two calcium-silicate cements in a rat model, Dent Mater J 38(4) (2019) 584-590.

[48] L. Tytgat, M.R. Kollert, L. Van Damme, H. Thienpont, H. Ottevaere, G.N. Duda, S. Geissler, P. Dubruel, S. Van Vlierberghe, T.H. Qazi, Evaluation of 3D Printed Gelatin-Based Scaffolds with Varying Pore Size for MSC-Based Adipose Tissue Engineering, Macromol Biosci 20(4) (2020) e1900364.

[49] N. Monteiro, G. Thrivikraman, A. Athirasala, A. Tahayeri, C.M. França, J.L. Ferracane, L.E. Bertassoni, Photopolymerization of cell-laden gelatin methacryloyl hydrogels using a dental curing light for regenerative dentistry, Dent Mater 34(3) (2018) 389-399.

[50] L. Lisuzzo, G. Cavallaro, P. Pasbakhsh, S. Milioto, G. Lazzara, Why does vacuum drive to the loading of halloysite nanotubes? The key role of water confinement, J Colloid Interface Sci 547 (2019) 361-369.

[51] M. Roozbahani, M. Kharaziha, R. Emadi, pH sensitive dexamethasone encapsulated laponite nanoplatelets: Release mechanism and cytotoxicity, Int J Pharm 518(1-2) (2017) 312-319.

FIGURES

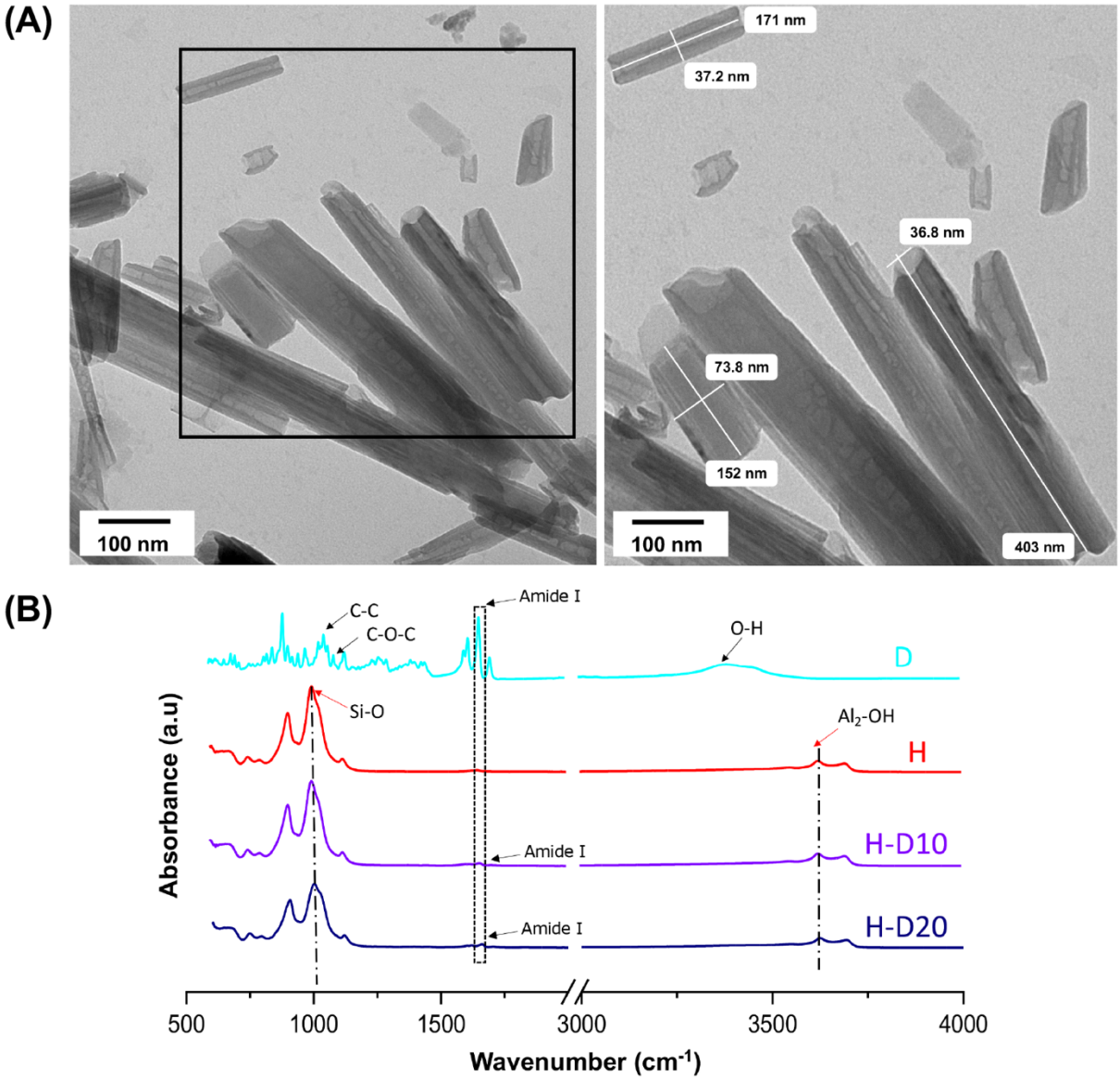

Fig. 1. Morphological and chemical analyses of aluminosilicate clay Halloysite^{Ò} nanotubes (H) loaded or not with dexamethasone (D). (a) Representative TEM micrograph of pristine nanotubes. (b) High magnification TEM micrograph demonstrating the well-defined open lumen and overall morphology of the nanotubes employed in this study (scale bars = 100 nm). (c) FTIR spectrum of nanotubes (H), dexamethasone powder (D), and DEX-loaded nanotubes (H-D10 [10%] and H-D20 [20%]).

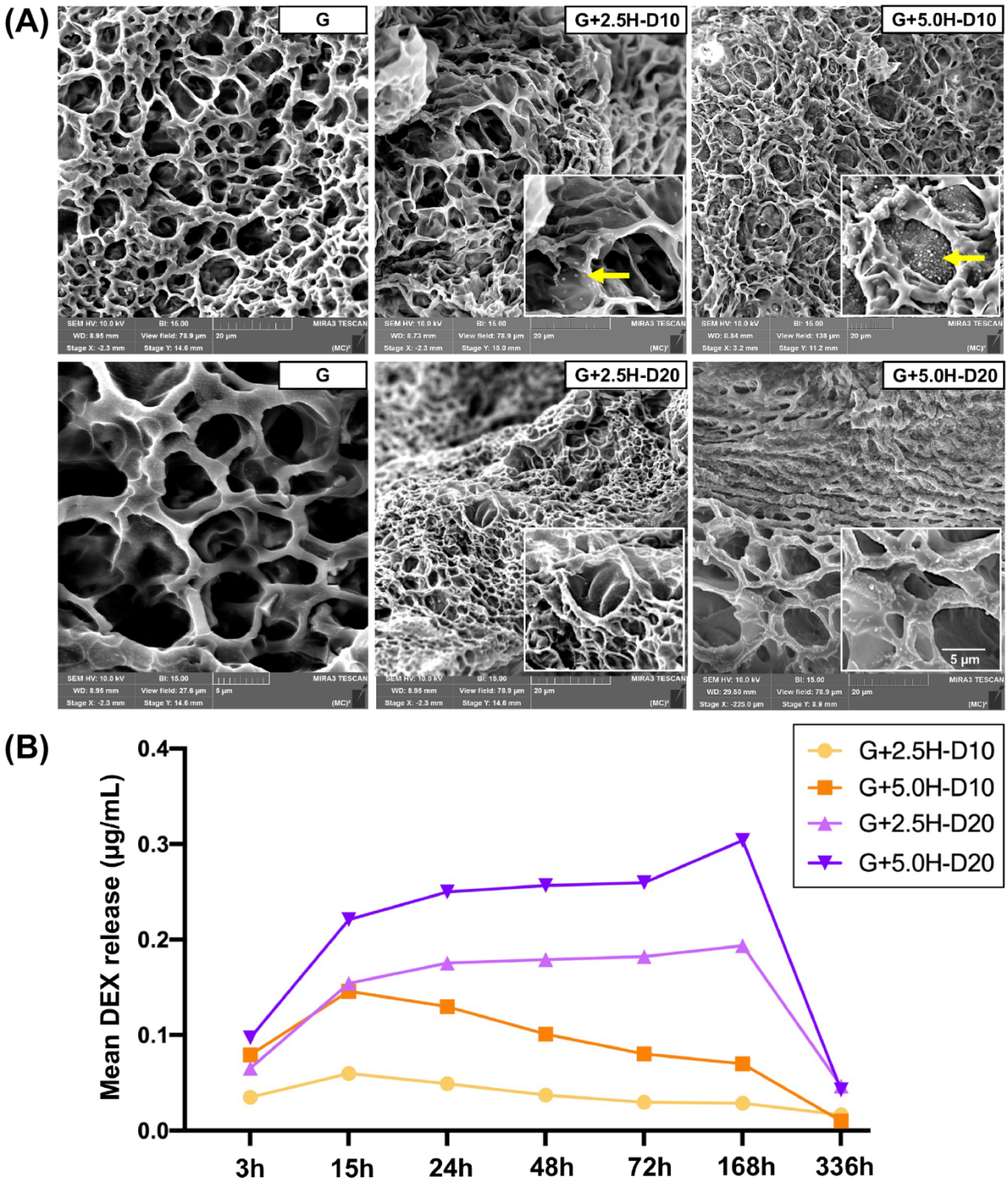

Fig. 2. (a) Morphological characterization of GelMA-based hydrogel formulations. Representative SEM images of hydrogels' cross-sections to reveal the internal microstructure. Note the well-dispersed DEX-loaded nanotubes in the nanotube-modified GelMA-based formulations (yellow arrows). (b) Mean DEX release over 14 days (336 h) for DEX-loaded nanotube-modified hydrogels after incubation at 37 °C with enzymatic solution (PBS + 1U/mL collagenase A). Data represent mean ± SD (n=6).

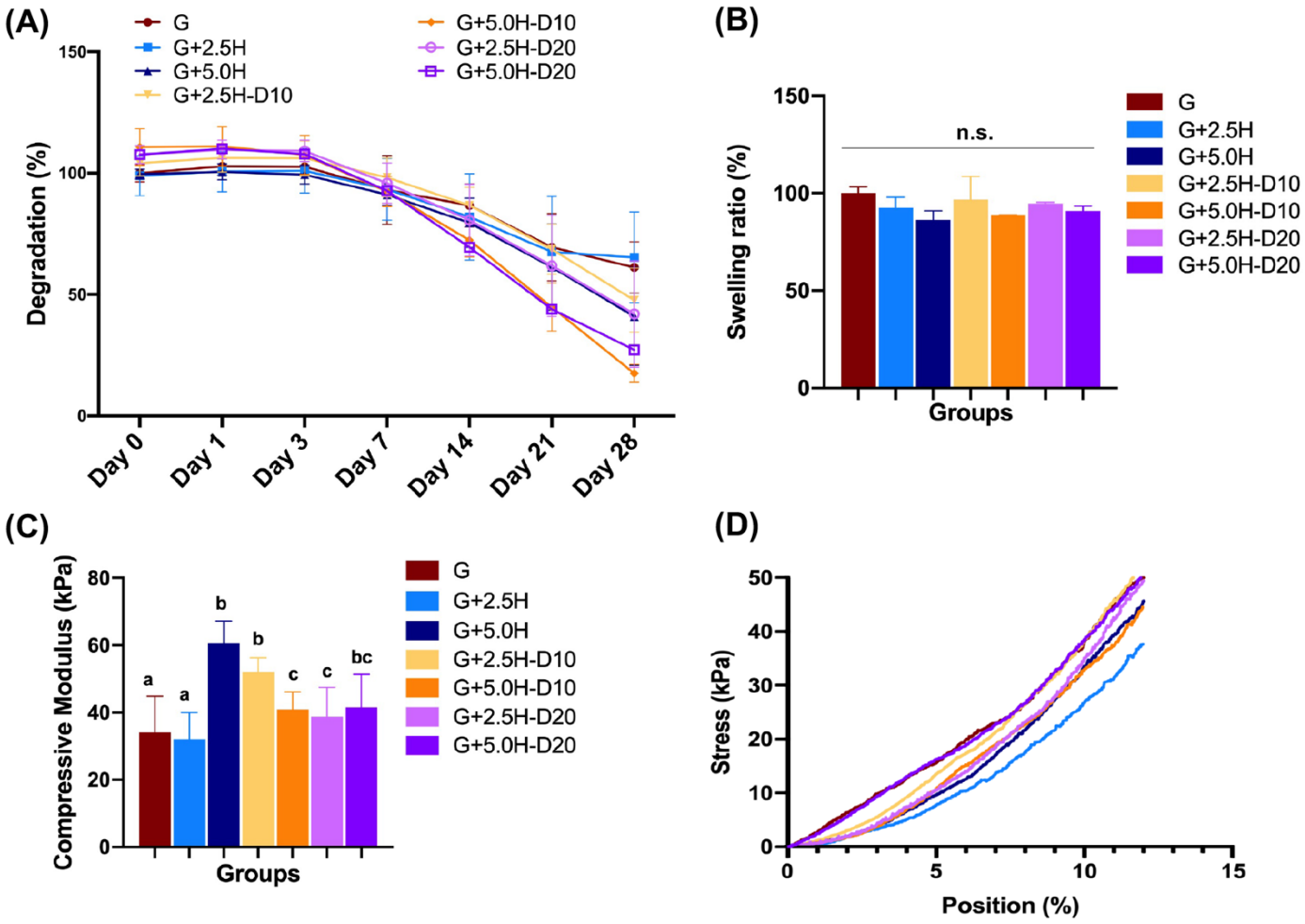

Fig. 3. Enzymatic hydrogel degradation, swelling ratio, and biomechanical properties of the various GelMA-based hydrogels. (a) *In vitro* hydrogel degradation after enzymatic (1U/mL collagenase A at 37 °C) challenge. Mass loss (%) was determined over 28 days. (b) Swelling ratio of the distinct hydrogels was measured upon PBS incubation at 37 °C for 24 h. (c) Compressive modulus (kPa). (d) Representative stress-strain curves for all groups.

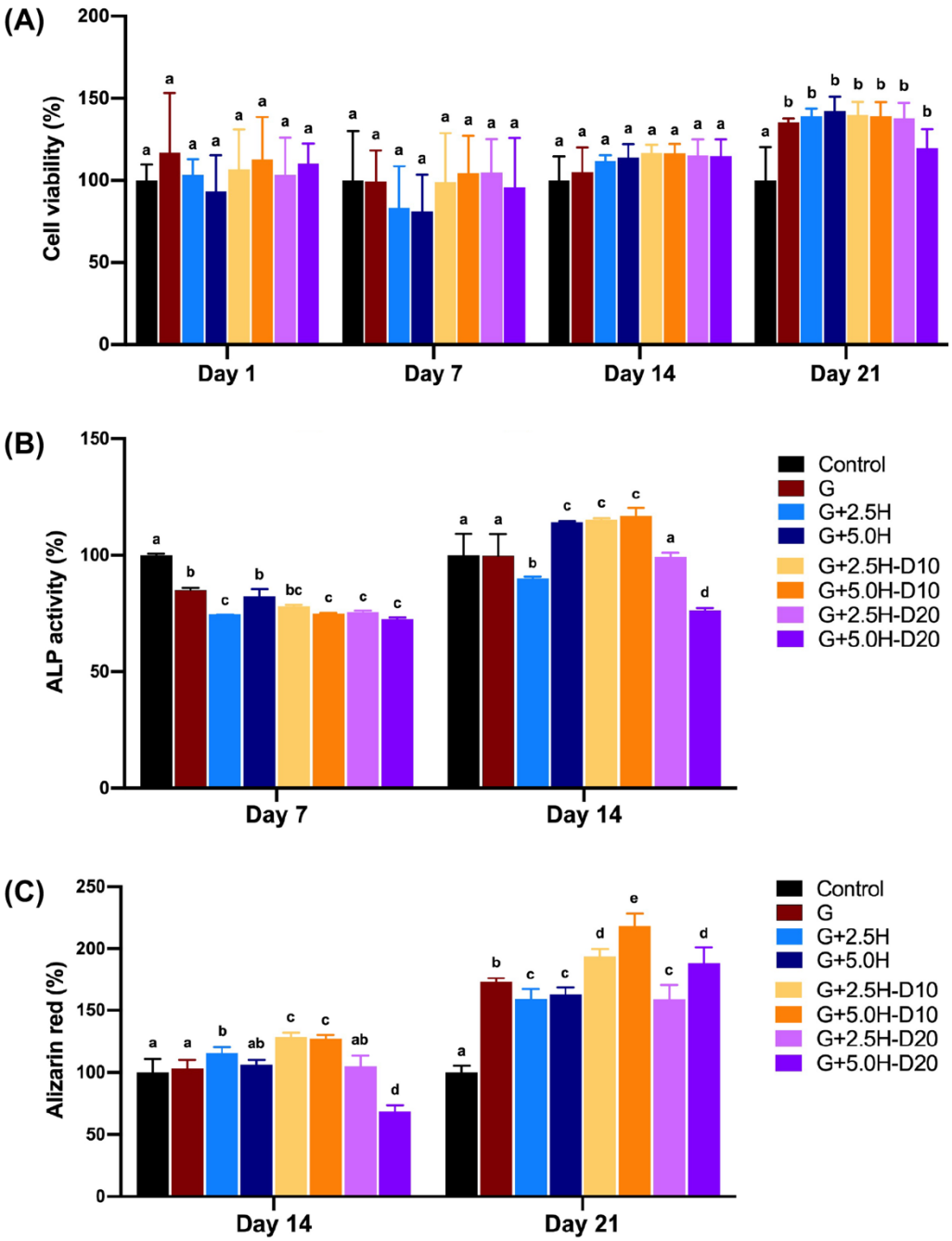

Fig. 4. *In vitro* biological assessment of GelMA-based hydrogel formulations. (a) Cell viability over time of SHEDs seeded on GelMA-based hydrogel samples (MTS assay). The percentage of cell viability was normalized to SHEDs cultured on the plate at day 1 (100%). (b) ALP activity in SHEDs after 7 and 14 days. At day 14, G+5.0H, G+2.5H-10D, and G+5.0H-10D promoted significant upregulation of ALP expression compared to the control. (c) Quantitative Alizarin red staining showing mineralized matrix deposition in SHEDs seeded on the hydrogels at 14 and 21 days. All experimental groups led to higher mineralization compared to the control at day 21. Distinct letters indicate statistically significant differences between the groups when compared with the control (two-way ANOVA, followed by Tukey's test, n=6; α=5%).

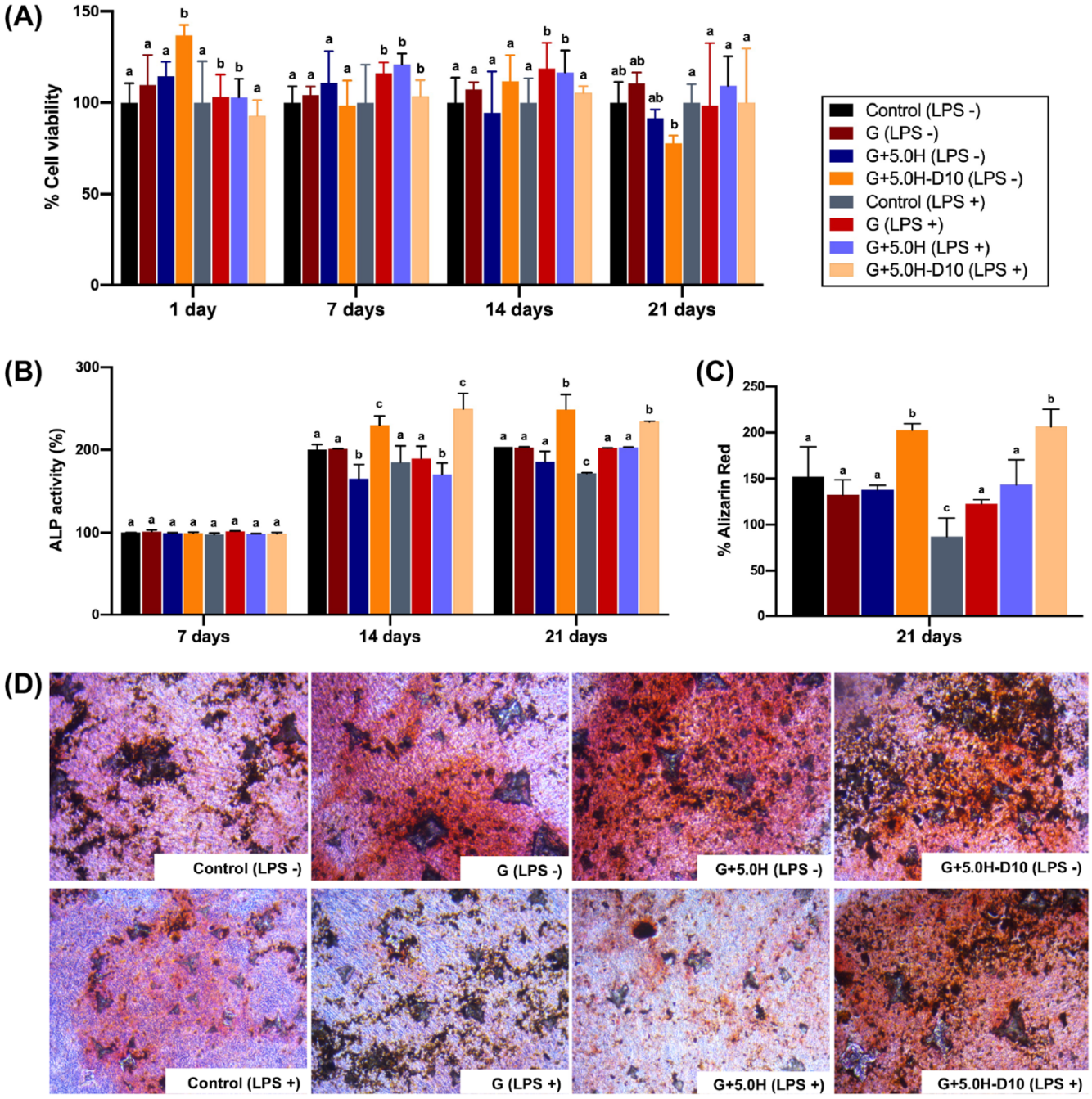

Fig. 5. Cell viability and mineralization capacity of GelMA-based hydrogel formulations on LPS (10 µg/mL)-stimulated SHEDs. The assay was performed by individually placing the formulated hydrogels on a plastic Transwell® insert, with permeable support to allow the facile transport of released drug into the underlying cellular monolayer. (a) Cell viability analysis over 21 days using MTS assay (normalized to SHEDs cultured on the plate at day 1). (b) ALP activity of SHEDs over time presented an increasing trend with G+5.0H-D10 (LPS-) and G+5.0H-D10 (LPS-), showing highest activity at 14 and 21 days. (c-d**)** Qualitative and quantitative Alizarin red staining showing highest mineralization for G+5.0H-D10 (LPS-) and G+5.0H-D10 (LPS-). Distinct letters indicate statistically significant differences between the groups when compared with the control (SHEDs) (two-way ANOVA and Tukey's test, n=6; α=5%).

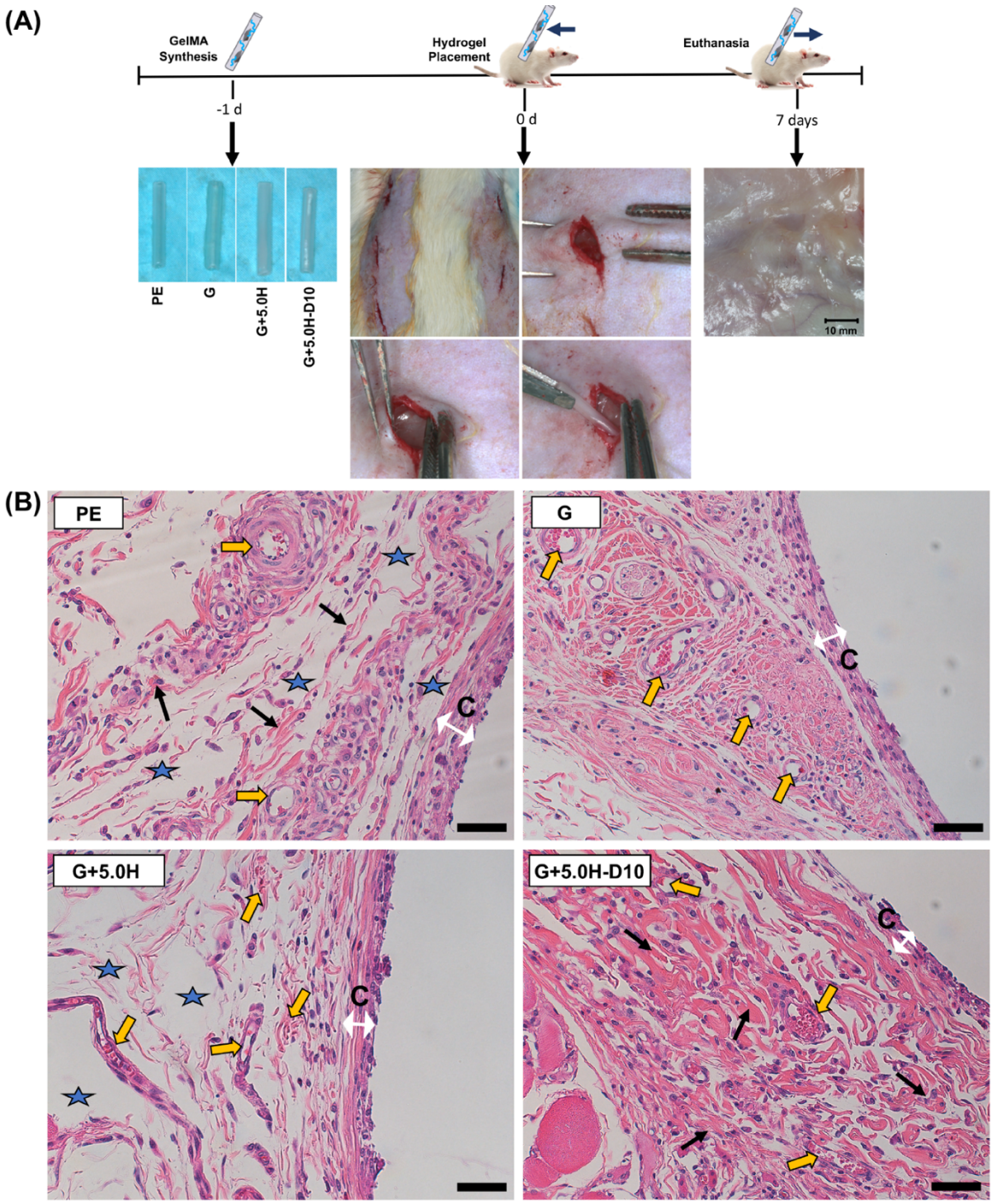

Fig. 6. (a) *In vivo* biocompatibility of GelMA-based hydrogel formulations. Schematic of the surgical procedures involved in the implantation of the engineered GelMA-based hydrogel formulations in dorsal subcutaneous pocket in rats. (b) HE-stained images of the tissue section of implant area at 7 days post-implantation. A thin, fibrous capsule (C) was formed at the polyethylene tube opening with subjacent connective tissue exhibiting small, congested blood vessels (yellow arrows), collagen fibrils (black arrows), areas of edema (stars), and fibroblasts distributed among mononuclear inflammatory cells.

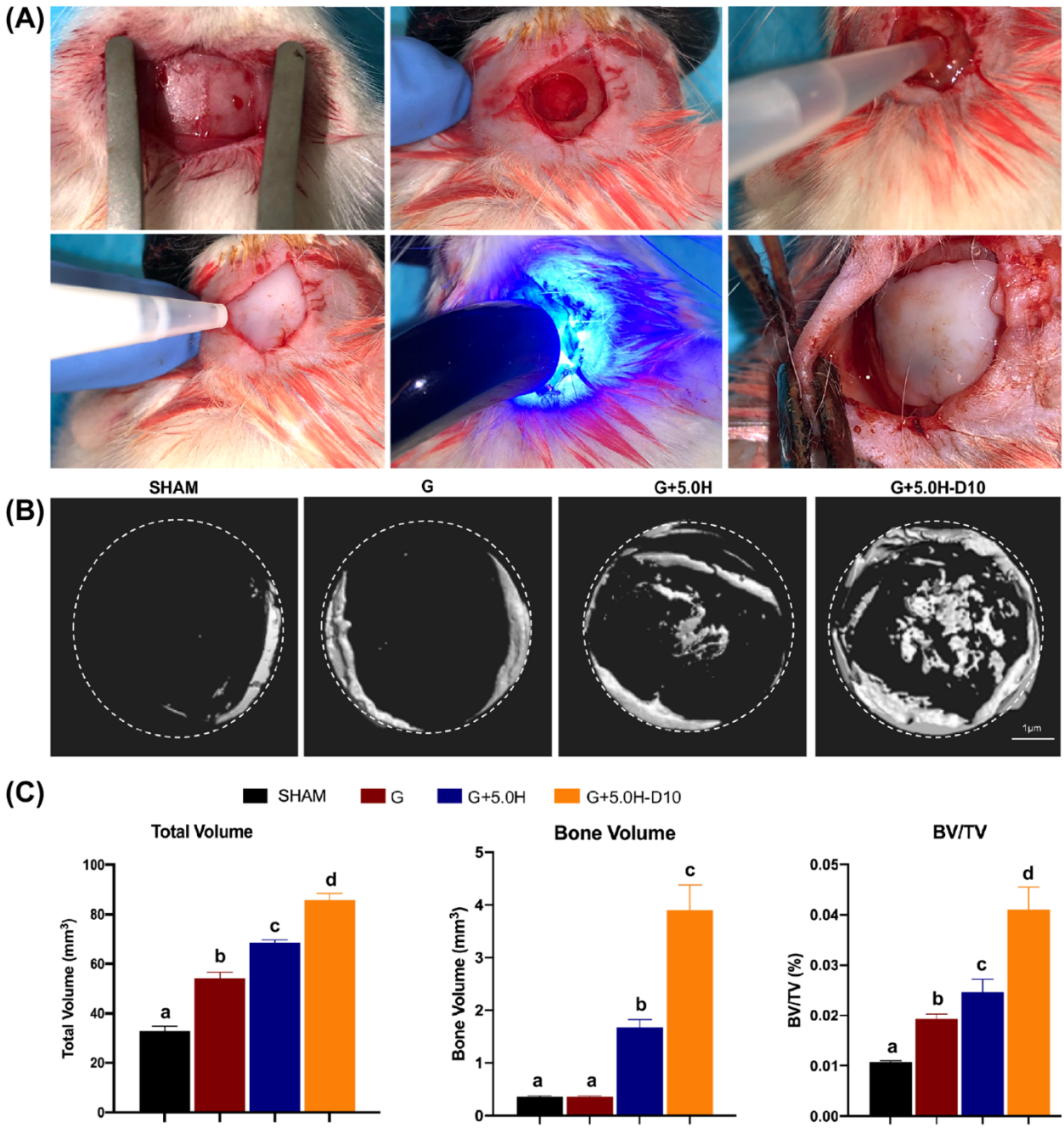

Fig. 7. (a) Representative images of the clinical and surgical procedures employed in the creation of critical size calvaria defects performed in rats; followed by the injection of 150 µL of the GelMA-based formulations (*i.e.*, GelMA [G], GelMA+5.0%HNT [G+5.0H], and GelMA+5.0%HNT-DEX10% [G+5.0H-D10] into the defects and *in situ* photocrosslinking for 60 s with an LED light-curing device. (b) Representative micro-CT images of calvarial defects showing mineralized bone formation 6-weeks post-implantation of the various GelMA-based formulations (scale bar = 1 mm). (c) Quantitative assessment of bone regeneration parameters for each treatment. Of note, G+5.0H-D10 formulation outperformed the other groups in all evaluated parameters (*p<0.05; mean ± SD, n=4).

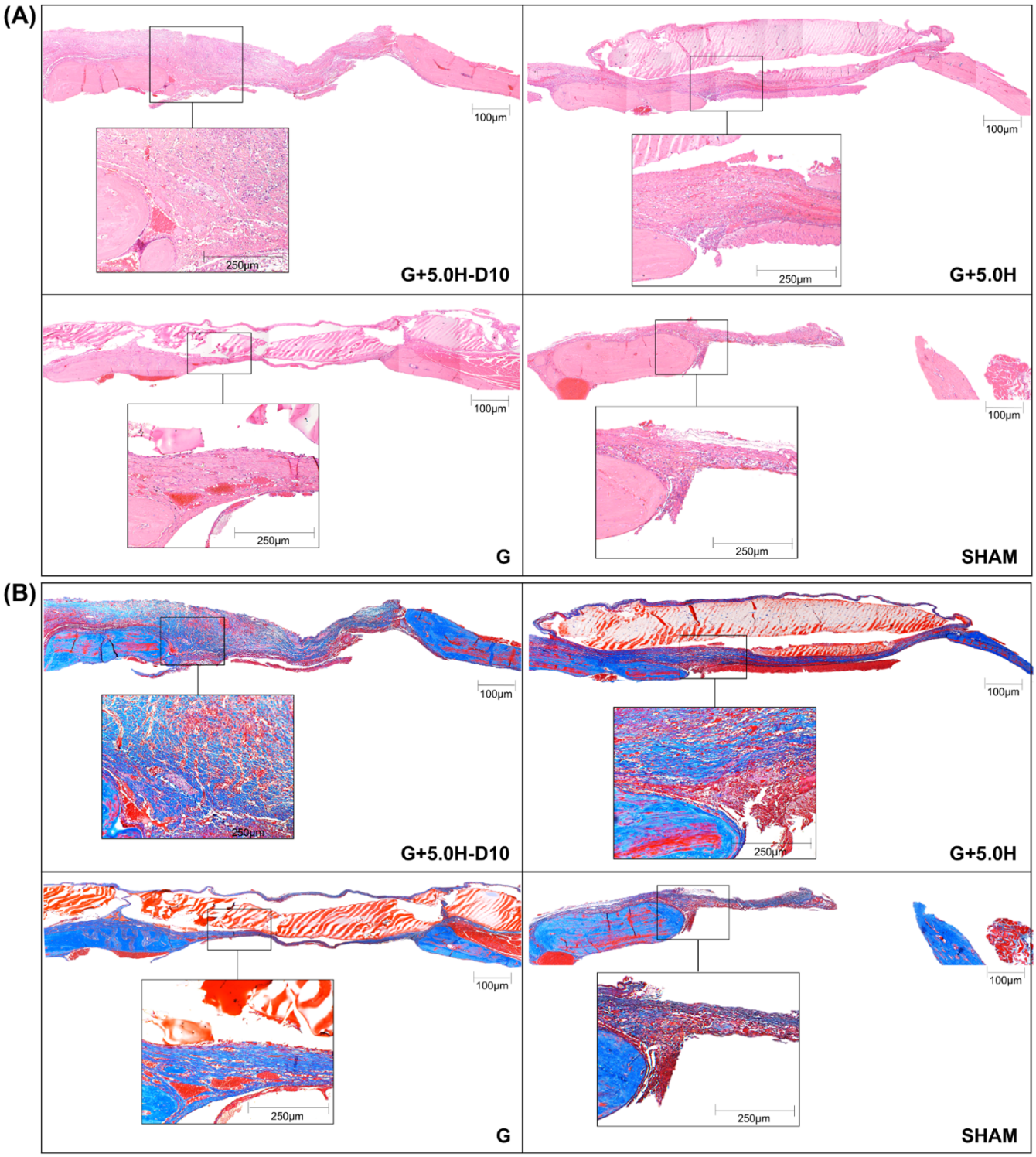

Fig. 8. Histological assessment of the regenerative capacity of the GelMA-based hydrogel formulations. (a) HE-stained images and (b) MT-stained images show bone regeneration response at the defect level in the different experimental groups at 6 weeks post-implantation. The early phase of new bone formation at the margin of the calvarial defect in the G+5.0H-D10 was considerably improved compared to the other groups.

4 CONSIDERAÇÕES FINAIS

Os tratamentos tradicionalmente empregados no cenário clínico para manutenção da vitalidade pulpar envolvem a aplicação de cimentos à base de hidróxido de cálcio, que são conhecidos por seus efeitos tóxicos sobre as células da polpa dental humana (DPCs), induzindo necrose de coagulação associado à inflamação no tecido circundante, retardando o processo de reparo do tecido pulpar.

As técnicas empregadas na Engenharia tecidual permitem o desenvolvimento de scaffolds bioativos com diferentes formulações e topografias de superfície, as quais interferem diretamente no processo de reparo tecidual dentro de um contexto minimamente invasivo. Estes biomateriais buscam otimizar a resposta celular criando um microambiente similar ao da matriz extracelular do tecido alvo que foi perdido, com o intuito de promover alta biocompatibilidade para as interações celulares, favorecendo seu crescimento.

Scaffold poroso de quitosana contendo em sua composição cálcio e solução de beta-glicerofosfato de sódio favorece a proliferação celular e diferenciação odontogênica para DPCs semeadas em contato direto sobre sua estrutura, além de apresentar potencial bioativo a distância sobre as células. Resultados promissores desta formulação, para aplicação em terapias cell-homing foram obtidos quando empregado o modelo de *pulp-in-a-chip*, demonstrando o potencial quimiotático destes scaffolds em estimular a migração de células para sua estrutura, com consequente diferenciação odontogênica determinada pela deposição de matriz rica em cálcio e expressão de DSP.

O desenvolvimento do hidrogel a base de metacrilato de gelatina (GelMA), contendo em sua composição 5% de nanotubos de haloisita carregados com dexametasona 10%, demonstrou excelente potencial bioativo e odontogênico sobre células pulpares humanas de dentes decíduos (SHEDs). A partir da composição deste hidrogel multifuncional foi possível estimular a deposição de matriz mineralizada mesmo em ambiente celular sob estímulo inflamatório. Esta formulação apresentou potencial promissor para aplicação em terapias cell-homing em estratégias de regeneração/reparo dentinário por aumentar consideravelmente a formação óssea em defeitos críticos de calvária, além de apresentar reação inflamatória tecidual mínima.

REFERÊNCIAS*

1. Wataha JC. Predicting clinical biological responses to dental materials. Dent Mater. 2012; 28(1): 23-40.

2. Motamedian SR, Hosseinpour S, Ahsaie MG, Khojasteh A. Smart scaffolds in bone tissue engineering: a systematic review of literature. World J Stem Cells. 2015; 7(3): 657-68.

3. Moreira MS, Diniz IM, Rodrigues MF, de Carvalho RA, de Almeida Carrer FC, Neves II, Gavini G, Marques MM. In vivo experimental model of orthotopic dental pulp regeneration under the influence of photobiomodulation therapy. J Photochem Photobiol B. 2017; 166: 180-6.

4. Ma PX. Biomimetic materials for tissue engineering. Adv Drug Deliv Rev. 2008; 60(2): 184-98.

5. Pearson RG, Bhandari R, Quirk RA, Shakesheff KM. Recent advances in tissue engineering, J Long Term Eff Med Implants. 2017; 27(2-4): 199-231.

6. Eltom A, Zhong G, Muhammad A. Scaffold techniques and designs in tissue engineering functions and purposes: a review. Adv Mater Sci Eng. 2019; 2019: 1-13.

7. Gupte MJ, Ma PX. Nanofibrous scaffolds for dental and craniofacial applications. J Dent Res. 2012; 91(3): 227-34.

8. Rosa V, Della Bona A, Cavalcanti BN, Nör JE. Tissue engineering: from research to dental clinics. Dent Mater. 2012; 28(4): 341-8.

9. Costello BJ, Kumta P, Sfeir CS. Regenerative technologies for craniomaxillofacial surgery. J Oral Maxillofac Surg. 2015; 73(12 Suppl): S116-25.

10. Tollemar V, Collier ZJ, Mohammed MK, Lee MJ, Ameer GA, Reid RR. Stem cells, growth factors and scaffolds in craniofacial regenerative medicine. Genes Dis. 2016; 3(1): 56-71.

11. Galler KM, Eidt A, Schmalz G. Cell-free approaches for dental pulp tissue engineering. J Endod. 2014; 40(4 Suppl): S41-5.

12. Marques MM, Diniz IM, de Cara SP, Pedroni AC, Abe GL, D'Almeida-Couto RS, Lima PL, Tedesco TK, Moreira MS. Photobiomodulation of dental derived mesenchymal stem cells: a systematic review. Photomed Laser Surg. 2016; 34(11): 500-8.

* De acordo com o Guia de Trabalhos Acadêmicos da FOAr, adaptado das Normas Vancouver. Disponível no site da Biblioteca: http://www.foar.unesp.br/Home/Biblioteca/guia-de-normalizacao-atualizado.pdf

13. Soares DG, Zhang Z, Mohamed F, Eyster TW, de Souza Costa CA, Ma PX. Simvastatin and nanofibrous poly(l-lactic acid) scaffolds to promote the odontogenic potential of dental pulp cells in an inflammatory environment. Acta Biomater. 2018a; 68: 190-203.

14. Piva E, Silva AF, Nör JE. Functionalized scaffolds to control dental pulp stem cell fate. J Endod. 2014; 40(4 Suppl): S33-40.

15. Moura-Netto C, Ferreira LS, Maranduba CM, Mello-Moura ACV, Marques MM. Low-intensity laser phototherapy enhances the proliferation of dental pulp stem cells undernutritional deficiency. Braz Oral Res. 2016; 30(1): S1806-83242016000100265.

16. Bertassoni LE. Progress and challenges in microengineering the dental pulp vascular microenvironment. J Endod. 2020; 46(9S): S90-S100.

17. Ha M, Athirasala A, Tahayeri A, Menezes PP, Bertassoni LE. Micropatterned hydrogels and cell alignment enhance the odontogenic potential of stem cells from apical papilla in-vitro. Dent Mater. 2020; 36(1): 88-96.

18. Nakashima M, Akamine A. The application of tissue engineering to regeneration of pulp and dentin in endodontics. J Endod. 2005; 31(10): 711-8.

19. Shah D, Lynd T, Ho D, Chen J, Vines J, Jung HD, Kim JH, Zhang P, Wu H, Jun HW, Cheon K. Pulp-dentin tissue healing response: a discussion of current biomedical approaches. J Clin Med. 2020; 9(2): 434.

20. Soares DG, Bordini EAF, Cassiano FB, Bronze-Uhle ES, Pacheco LE, Zabeo G, Hebling J, Lisboa-Filho PN, Bottino MC, de Souza Costa CA. Characterization of novel calcium hydroxide-mediated highly porous chitosan-calcium scaffolds for potential application in dentin tissue engineering. J Biomed Mater Res B Appl Biomater. 2020; 108(6): 2546-59.

21. Soares DG, Rosseto HL, Basso FG, Scheffel DS, Hebling J, Costa CA. Chitosan-collagen biomembrane embedded with calcium-aluminate enhances dentinogenic potential of pulp cells. Braz Oral Res. 2016; 30(1): e54.

22. Swetha S, Lavanya K, Sruthi R, Selvamurugan N. An insight into cell-laden 3D-printed constructs for bone tissue engineering. J Mater Chem B. 2020; 8(43): 9836-62.

23. Xin T, Mao J, Liu L, Tang J, Wu L, Yu X, Gu Y, Cui W, Chen L. Programmed sustained release of recombinant human bone morphogenetic protein-2 andinorganic ion composite hydrogel as artificial periosteum. ACS Appl Mater Interfaces. 2020; 12(6): 6840-51.

24. Hu D, Lian Z, Xian H, Jiang R, Wang N, Weng Y, Peng X, Wang S, Ouyang X. Adsorption of Pb(II) from aqueous solution by polyacrylic acid grafted magnetic chitosan nanocomposite. Int J Biol Macromol. 2020; 154: 1537-47.

25. Pan J, Deng J, Yu L, Wang Y, Zhang W, Han X, Camargo PHC, Wang J, Liu Y. Investigating the repair of alveolar bone defects by gelatin methacrylate hydrogels-encapsulated human periodontal ligament stem cells. J Mater Sci Mater Med. 2019; 31(1): 3.

26. Kim Y, Lee D, Song D, Kim H, Kim S. Biocompatibility and bioactivity of set direct pulp capping materials on human dental pulp stem cells. Materials (Basel). 2020; 13(18): 3925.

27. Xu HH, Zhao L, Weir MD. Stem cell-calcium phosphate constructs for bone engineering. J Dent Res. 2010; 89(12): 1482-8.

28. Liu H, Peng H, Wu Y, Zhang C, Cai Y, Xu G, Li Q, Chen X, Ji J, Zhang Y, OuYang HW. The promotion of bone regeneration by nanofibrous hydroxyapatite/chitosan scaffolds by effects on integrin-BMP/Smad signaling pathway in BMSCs. Biomaterials. 2013; 34(18): 4404-17.

29. Wang P, Zhao L, Chen W, Liu X, Weir MD, Xu HH. Stem cells and calcium phosphate cement scaffolds for bone regeneration. J Dent Res. 2014; 93(7): 618-25.

30. Emamgholi A, Rahimi M, Kaka G, Sadraie SH, Najafi S. Presentation of a novel model of chitosan- polyethylene oxide-nanohydroxyapatite nanofibers together with bone marrow stromal cells to repair and improve minor bone defects. Iran J Basic Med Sci. 2015; 18(9): 887-93.

31. Roy P, Sailaja RR. Chitosan-nanohydroxyapatite composites: mechanical, thermal and bio-compatibility studies. Int J Biol Macromol. 2015; 73: 170-81.

32. Shalumon KT, Lai GJ, Chen CH, Chen JP. Modulation of bone-specific tissue regeneration by incorporating bone morphogenetic protein and controlling the shell thickness of silk fibroin/chitosan/nanohydroxyapatite core-shell nanofibrous membranes. ACS Appl Mater Interfaces. 2015; 7(38): 21170-81.

33. Bordini EAF, Cassiano FB, Silva ISP, Usberti FR, Anovazzi G, Pacheco LE, Pansani TN, Leite ML, Hebling J, de Souza Costa CA, Soares DG. Synergistic potential of 1α,25-dihydroxyvitamin D3 and calcium-aluminate-chitosan scaffolds with dental pulp cells. Clin Oral Investig. 2020; 24(2): 663-74.

34. Hosseini FS, Enderami SE, Hadian A, Abazari MF, Ardeshirylajimi A, Saburi E, Soleimanifar F, Nazemisalman B. Efficient osteogenic differentiation of the dental pulp stem cells on β-glycerophosphate loaded polycaprolactone/polyethylene oxide blend nanofibers. J Cell Physiol. 2019; 234(8): 13951-58.

35. He Y, Li Q, Ma C, Xie D, Li L, Zhao Y, Shan D, Chomos SK, Dong C, Tierney JW, Sun L, Lu D, Gui L, Yang J. Development of osteopromotive poly (octamethylene citrate glycerophosphate) for enhanced bone regeneration. Acta Biomater. 2019; 93: 180-91.

36. Li D, Zhang K, Shi C, Liu L, Yan G, Liu C, Zhou Y, Hu Y, Sun H, Yang B. Small molecules modified biomimetic gelatin/hydroxyapatite nanofibers constructing an ideal osteogenic microenvironment with significantly enhanced cranial bone formation. Int J Nanomedicine. 2018; 13: 7167-81.

37. Smith EE, Zhang W, Schiele NR, Khademhosseini A, Kuo CK, Yelick PC. Developing a biomimetic tooth bud model. J Tissue Eng Regen Med. 2017; 11(12): 3326-36.

38. Sun H, Tang J, Mou Y, Zhou J, Qu L, Duval K, Huang Z, Lin N, Dai R, Liang C, Chen Z, Tang L, Tian F. Carbon nanotube-composite hydrogels promote intercalated disc assembly in engineered cardiac tissues through β1-integrin mediated FAK and RhoA pathway. Acta Biomater. 2017; 48: 88-99.

39. Rajabi N, Kharaziha M, Emadi R, Zarrabi A, Mokhtari H, Salehi S. An adhesive and injectable nanocomposite hydrogel of thiolated gelatin/gelatin methacrylate/Laponite® as a potential surgical sealant. J Colloid Interface Sci. 2020; 564: 155-69.

40. Dong Z, Yuan Q, Huang K, Xu W, Liu G, Gu Z. Gelatin methacryloyl (GelMA)-based biomaterials for bone regeneration. RSC Adv. 2019; 31: 17737-44.

41. Yue K, Trujillo-de Santiago G, Alvarez MM, Tamayol A, Annabi N, Khademhosseini A. Synthesis, properties, and biomedical applications of gelatin methacryloyl (GelMA) hydrogels. Biomaterials. 2015; 73: 254-71.

42. Chen X, Bai S, Li B, Liu H, Wu G, Liu S, Zhao Y. Fabrication of gelatin methacrylate/nanohydroxyapatite microgel arrays for periodontal tissue regeneration. Int J Nanomedicine. 2016; 11: 4707-18.

43. Qiao Y, Liu X, Zhou X, Zhang H, Zhang W, Xiao W, Pan G, Cui W, Santos HA, Shi Q. Gelatin templated polypeptide co-cross-linked hydrogel for bone regeneration. Adv Health Mater. 2020; 9(1): e1901239.

44. Monteiro N, Smith EE, Angstadt S, Zhang W, Khademhosseini A, Yelick PC. Dental cell sheet biomimetic tooth bud model. Biomaterials. 2016; 106: 167-79.

45. Ha M, Athirasala A, Tahayeri A, Menezes PP, Bertassoni LE. Micropatterned hydrogels and cell alignment enhance the odontogenic potential of stem cells from apical papilla in-vitro. Dent Mater. 2020; 36(1): 88-96.

46. Visser J, Gawlitta D, Benders KE, Toma SM, Pouran B, van Weeren PR, Dhert WJ, Malda J. Endochondral bone formation in gelatin methacrylamide hydrogel with embedded cartilage-derived matrix particles. Biomaterials. 2015; 37: 174-82.

47. Santos AC, Ferreira C, Veiga F, Ribeiro AJ, Panchal A, Lvov Y, Agarwal A. Halloysite clay nanotubes for life sciences applications: From drug encapsulation to bioscaffold. Adv Colloid Interface Sci. 2018; 257: 58-70.

48. Lvov Y, Wang W, Zhang L, Fakhrullin R. Halloysite clay nanotubes for loading and sustained release of functional compounds. Adv Mater. 2016; 28(6): 1227-50.

49. Kurczewska J, Pecyna P, Ratajczak M, Gajęcka M, Schroeder G. Halloysite nanotubes as carriers of vancomycin in alginate-based wound dressing. Saudi Pharm J. 2017; 25(6): 911-20.

50. Satish S, Tharmavaram M, Rawtani D. Halloysite nanotubes as a nature's boon for biomedical applications. Nanobiomedicine (Rij). 2019; 6: 1849543519863625.

51. Cunha DA, Rodrigues NS, Souza LC, Lomonaco D, Rodrigues FP, Degrazia FW, Collares FM, Sauro S, Saboia VPA. Physicochemical and microbiological assessment of an experimental composite doped with triclosan-loaded halloysite nanotubes. Materials (Basel). 2018; 11(7): 1080.

52. Massaro M, Buscemi G, Arista L, Biddeci G, Cavallaro G, D'Anna F, Di Blasi F, Ferrante A, Lazzara G, Rizzo C, Spinelli G, Ullrich T, Riela S. Multifunctional carrier based on halloysite/laponite hybrid hydrogel for kartogenin delivery. ACS Med Chem Lett. 2018; 10(4): 419-24.

53. Yamina AM, Fizir M, Itatahine A, He H, Dramou P. Preparation of multifunctional PEG-graft-halloysite nanotubes for controlled drug release, tumor cell targeting, and bio-imaging. Colloids Surf B Biointerfaces. 2018; 170: 322-9.

54. Jamshidzadeh F, Mohebali A, Abdouss M. Three-ply biocompatible pH-responsive nanocarriers based on HNT sandwiched by chitosan/pectin layers for controlled release of phenytoin sodium. Int J Biol Macromol. 2020; 150: 336-43.

55. Lim HC, Nam OH, Kim MJ, El-Fiqi A, Yun HM, Lee YM, Jin GZ, Lee HH, Kim HW, Kim EC. Delivery of dexamethasone from bioactive nanofiber matrices stimulates odontogenesis of human dental pulp cells through integrin/BMP/mTOR signaling pathways. Int J Nanomedicine. 2016; 11: 2557-67.

56. Moretti RDC, Duailibi MT, Martins PO, dos Santos JA, Duailibi SE. Osteoinductive effects of preoperative dexamethasone in human dental pulp stem cells primary culture. Future Sci OA. 2017; 3(3): FSO184.

57. Chuang YC, Yu Y, Wei MT, Chang CC, Ricotta V, Feng KC, Wang L, Bherwani AK, Ou-Yang HD, Simon M, Zhang L, Rafailovich M. Regulating substrate mechanics to achieve odontogenic differentiation for dental pulp stem cells on TiO_2 filled and unfilled polyisoprene. Acta Biomater. 2019; 89: 60-72.

58. Zhang M, Ni S, Zhang X, Lu J, Gao S, Yang Y, Wang Z, Sun H, Li Y. Dexamethasone-loaded hollow hydroxyapatite microsphere promotes odontogenic differentiation of human dental pulp cells in vitro. Odontology. 2020; 108(2): 222-30.

59. van den Heuvel SAS, van der Wal SEI, Bronkhorst EM, Warlé MC, Ronday M, Plat J, van Alfen N, Joosten LAB, Lerou JGC, Vissers KCP, Steegers MAH. Acute cytokine response during breast cancer surgery: potential role of dexamethasone and lidocaine and relationship with postoperative pain and complications - analysis of three pooled pilot randomized controlled trials. J Pain Res. 2020; 13: 1243-54.

60. Veerabadran NG, Goli PL, Stewart-Clark SS, Lvov YM, Mills DK. Nanoencapsulation of stem cells within polyelectrolyte multilayer shells. Macromol Biosci. 2007; 7(7): 877-82.

APÊNDICE A – SUPPLEMENTARY INFORMATION (PUBLICAÇÃO 2)

Materials and methods

Determination of lipopolysaccharide (LPS) concentration. LPS (*Escherichia coli* O111:B4; Sigma-Aldrich) concentration capable of negatively interfering with SHEDs differentiation was selected. SHEDs ($2.5´10^3$ cells/well) were seeded in 96 well-plates, followed by a 24 h growth period in complete α-MEM. Basal medium was then removed, and the cells cultured for 21 days in osteogenic media (complete α-MEM, 50 mM ascorbic acid, and 10 mM β-glycerophosphate) supplemented with 0.0 µg/mL (negative control), 0.0125 µg/mL, 0.025 µg/mL, 0.05 µg/mL, 0.1 µg/mL, 1 µg/mL, or 10 µg/mL of LPS. The media was changed every 2 days. Cell viability was measured by MTS assay at 7, 14, and 21 days, as previously described, and cells from the negative control were considered as 100% cell viability at day 1. The *in vitro* differentiation of SHEDs was investigated by Alizarin red staining assay at 21 days for quantification of mineralized matrix deposition.

Supplemental Figure

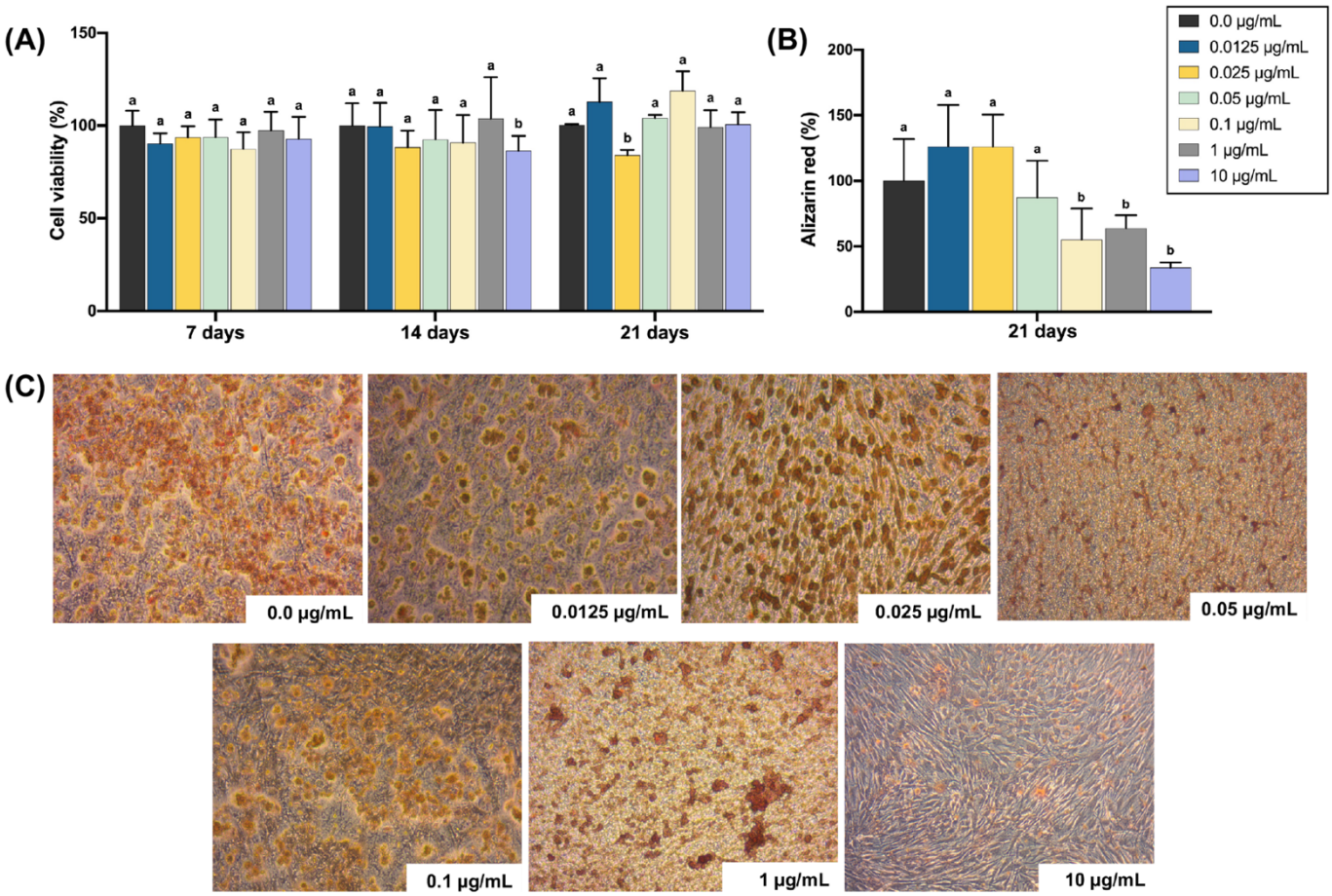

Fig. S1. A carefully defined dose-dependent screening was conducted to determine the most suitable LPS concentration to induce a degenerative stimulus on SHEDs capable of reducing its mineralized matrix deposition to ~ 50% without cell toxicity. (a) Cell viability (%) after SHEDs incubation with different concentrations of LPS up to 21 days (MTS assay). (b) Alizarin red staining assay to quantify mineralized matrix deposition (%) by SHEDs stimulated with distinct LPS concentrations at day 21. Bar graphs (mean ± SD) of the percentage of viable cell and mineralized matrix deposition normalized by control (0 µg/mL) at day 1. Distinct letters indicate statistically significant differences between the groups when compared with the control (two-way ANOVA, followed by Tukey's test, n=6; α=5%). **(C)** Representative images from Alizarin red staining assay for LPS-stimulated SHEDs at day 21.

ANEXO A – COMPROVANTE ARTIGO EM REVISÃO NA DENTAL MATERIALS

Submissions Being Processed for Author Ester Alves Ferreira Bordini, DDS, Ms

Page: 1 of 1 (1 total submissions) Display 10 results per page.

Action	Manuscript Number	Title	Authorship	Initial Date Submitted	Status Date	Current Status
Action Links	DENTMA-D-21-00067	CHITOSAN IN ASSOCIATION WITH OSTEOGENIC FACTORS AS A CELL-HOMING PLATFORM FOR DENTIN REGENERATION: ANALYSIS IN A PULP-IN-A-CHIP MODEL	Other Author	Jan 26, 2021	Feb 10, 2021	Under Review

Page: 1 of 1 (1 total submissions) Display 10 results per page.

<< Author Main Menu

ANEXO B – COMPROVANTE ARTIGO EM REVISÃO NA ACTA BIOMATERIALIA

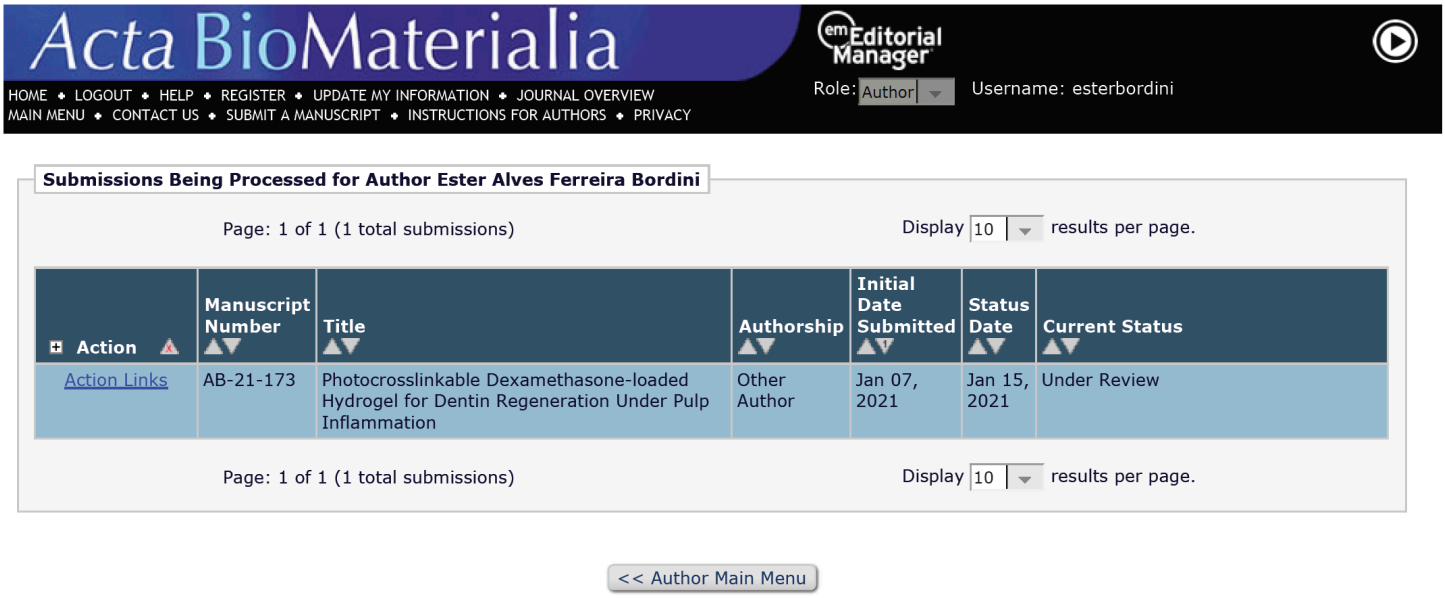

Acta BioMaterialia

Editorial Manager

HOME • LOGOUT • HELP • REGISTER • UPDATE MY INFORMATION • JOURNAL OVERVIEW
MAIN MENU • CONTACT US • SUBMIT A MANUSCRIPT • INSTRUCTIONS FOR AUTHORS • PRIVACY

Role: Author Username: esterbordini

Submissions Being Processed for Author Ester Alves Ferreira Bordini

Page: 1 of 1 (1 total submissions) Display 10 results per page.

Action	Manuscript Number	Title	Authorship	Initial Date Submitted	Status Date	Current Status
Action Links	AB-21-173	Photocrosslinkable Dexamethasone-loaded Hydrogel for Dentin Regeneration Under Pulp Inflammation	Other Author	Jan 07, 2021	Jan 15, 2021	Under Review

Page: 1 of 1 (1 total submissions) Display 10 results per page.

<< Author Main Menu

ANEXO C – COMPROVANTE ARTIGO PUBLICADO CLINICAL ORAL INVESTIGATIONS

Clinical Oral Investigations (2020) 24:663–674
https://doi.org/10.1007/s00784-019-02906-z

ORIGINAL ARTICLE

Synergistic potential of 1α,25-dihydroxyvitamin D3 and calcium–aluminate–chitosan scaffolds with dental pulp cells

Ester Alves Ferreira Bordini[1] · Fernanda Balestrero Cassiano[1] · Isabela Sanches Pompeo Silva[2] · Felipe Rochelle Usberti[1] · Giovana Anovazzi[3] · Leandro Edgar Pacheco[2] · Taísa Nogueira Pansani[1] · Maria Luísa Leite[1] · Josimeri Hebling[3] · Carlos Alberto de Souza Costa[1] · Diana Gabriela Soares[2]

Received: 13 July 2018 / Accepted: 4 April 2019 / Published online: 22 May 2019

Abstract

Objectives This study aimed to develop a porous chitosan–calcium–aluminate scaffold (CH-AlCa) in combination with a bioactive dosage of 1α,25-dihydroxyvitamin D3 (1α,25VD), to be used as a bioactive substrate capable to increase the odontogenic potential of human dental pulp cells (HDPCs).

Materials and methods The porous CH-AlCa was developed by the incorporation of an AlCa suspension into a CH solution under vigorous agitation, followed by phase separation at low temperature. Scaffold architecture, porosity, and calcium release were evaluated. Thereafter, the synergistic potential of CH-AlCa and 1 nM 1α,25VD, selected by a dose–response assay, for HDPCs seeded onto the materials was assessed.

Results The CH-AlCa featured an organized and interconnected pore network, with increased porosity in comparison with that of plain chitosan scaffolds (CH). Increased odontoblastic phenotype expression on the human dental pulp cell (HDPC)/CH and HDPC/CH-AlCa constructs in the presence of 1 nM 1α,25VD was detected, since alkaline phosphatase activity, mineralized matrix deposition, dentin sialophosphoprotein/dentin matrix acidic phosphoprotein 1 mRNA expression, and cell migration were overstimulated. This drug featured a synergistic effect with CH-AlCa, since the highest values of cell migration and odontoblastic markers expression were observed in this experimental condition.

Conclusions The experimental CH-AlCa scaffold increases the chemotaxis and regenerative potential of HDPCs, and the addition of low-dosage 1α,25VD to this scaffold enhances the potential of these cells to express an odontoblastic phenotype.

Clinical relevance Chitosan scaffolds enriched with calcium–aluminate in association with low dosages of 1α,25-dihydroxyvitamin D3 provide a highly bioactive microenvironment for dental pulp cells prone to dentin regeneration, thus providing potential as a cell-free tissue engineering system for direct pulp capping.

Keywords Tissue engineering · Dental pulp · Stem cells · Scaffolds

✉ Diana Gabriela Soares
soares.dg@usp.br

[1] Department of Physiology and Pathology, Araraquara School of Dentistry, Univ. Estadual Paulista – UNESP, Humaita Street, 1680, Araraquara, SP 14801-903, Brazil

[2] Department of Operative Dentistry, Endodontics and Dental Materials, Bauru School of Dentistry-FOB, Sao Paulo University – USP, Al. Dr. Octavio Pinheiro Brizola, 9-75, Bauru, SP 17012-901, Brazil

[3] Department of Orthodontics and Pediatric Dentistry, Araraquara School of Dentistry, Univ. Estadual Paulista – UNESP, Araraquara, SP, Brazil. Humaitá Street, 1680, Araraquara, SP 14801-903, Brazil

Introduction

Mediating dentin regeneration by resident dental pulp stem cells (DSPCs) to maintain the biologic functions of the pulp–dentin complex is the current goal of regenerative dentistry [1–3]. Within this scenario, the development of biocompatible and bioactive porous scaffolds based on the principles of tissue engineering is essential to modulate the chemotaxis, proliferation, and odontoblastic differentiation of DSPCs, culminating in the deposition of a dentin barrier at the pulp exposure site [4–8]. Chitosan-based biomaterials have been shown to allow for mesenchymal stem cell (MSC) adhesion

Araraquara, 02 de fevereiro de 2021.

ESTER ALVES FERREIRA BORDINI